

TECHNISCHE UNIVERSITÄT MÜNCHEN

Lehrstuhl Für Experimentelle Genetik

Quantitative analysis of ciliary protein networks - Characterization of the intraflagellar transport complex B

Yves Stephan Texier, M. Sc.

Vollständiger Abdruck der von der Fakultät Wissenschaftszentrum Weihenstephan für Ernährung, Landnutzung und Umwelt der Technischen Universität München zur Erlangung des akademischen Grades eines

Doktors der Naturwissenschaften

genehmigten Dissertation.

Vorsitzender: Univ.-Prof. Dr. Bernhard Küster

Prüfer der Dissertation:

1. Univ.-Prof. Dr. M Hrabé de Angelis
2. apl. Prof. Dr. J. Adamski
3. Univ.-Prof. Dr. M Ueffing, Eberhard Karls Universität Tübingen

Die Dissertation wurde am 30.04.2013 bei der Technischen Universität München eingereicht und durch die Fakultät Wissenschaftszentrum Weihenstephan für Ernährung, Landnutzung und Umwelt am 02.10.2013 angenommen.

Im Gedenken an meine Oma

Table of contents

Abbreviations	12
Summary	15
Zusammenfassung	16
I. Introduction.....	19
1. The Cilium.....	19
1.1. Structure of the Cilium	21
1.2. The intraflagellar transport (IFT)	22
1.3. Ciliogenesis	27
1.4. The connecting cilium of the photoreceptor cell.....	28
2. Cilia-related disorders - the ciliopathies	29
3. Ciliopathies and the IFT	30
4. Protein complexes	31
4.1. Purification and analysis of native protein complexes.....	32
4.1.1. Affinity purification	33
4.1.1.1. One-step purification	35
4.1.1.2. Two-step purification	35
4.1.2. Sucrose density centrifugation	37
4.2. Quantitative analysis of native protein complexes	38
4.2.1. Mass spectrometry and quantitative protein complex analysis.....	38
4.2.2. Stable isotope labelling by amino acids in cell culture (SILAC)	40
4.2.1. Further stable isotope labelled quantification methods.....	42
4.2.2. Label-free quantification	43
II. Aim of the study.....	44
III. Material and Methods	46
5. Material	46
5.1. Chemicals.....	46

5.2.	General equipment	46
5.3.	Molecular biology	48
5.3.1.	Special equipment.....	48
5.3.2.	Kits and special reagents	48
5.3.1.	Enzymes.....	49
5.3.2.	<i>Escherichia coli</i> strains.....	49
5.3.3.	Oligonucleotides.....	49
5.3.4.	Plasmids and constructs.....	50
5.3.4.1.	DNA constructs	50
5.3.4.2.	DNA plasmids	51
5.3.5.	siRNA sequences.....	52
5.4.	Mammalian cell culture	52
5.4.1.	Special equipment.....	52
5.4.2.	Special reagents.....	53
5.4.3.	Mammalian cell lines	54
5.5.	Protein chemistry	54
5.5.1.	Special equipment.....	54
5.5.2.	Special reagents.....	55
5.6.	Immunocytochemistry	55
5.6.1.	Special equipment.....	55
5.6.2.	Special reagents.....	56
5.6.2.1.	Primary antibodies	56
5.6.2.2.	Secondary antibodies.....	57
5.7.	Mass spectrometry	57
5.7.1.	Special equipment.....	57
5.7.2.	Kits and special reagents	58
5.8.	Software and databases	58

5.8.1.	Software	58
5.8.2.	Databases and online tools	58
6.	Methods	59
6.1.	Molecular biology	59
6.1.1.	<i>Escherichia coli</i> cultures	59
6.1.1.1.	Liquid cultures	59
6.1.1.2.	Plating cultures.....	59
6.1.1.3.	Generation of cryo stocks	60
6.1.1.4.	Chemical transformation of <i>E. coli</i>	60
6.1.2.	Plasmid DNA preparation	60
6.1.1.	Agarose gel electrophoresis	60
6.1.2.	DNA sequencing	61
6.1.1.	Purification of DNA	61
6.1.1.1.	From agarose gels	61
6.1.1.2.	From enzymatic reactions	61
6.1.2.	Polymerase chain reaction (PCR)	61
6.1.3.	Enzymatic treatment of DNA	62
6.1.4.	Gateway cloning	62
6.1.5.	Gene silencing.....	65
6.1.5.1.	Target selection.....	65
6.1.5.2.	siRNA knockdowns	65
6.1.5.3.	Evaluation of knockdown efficiency.....	66
6.1.5.3.1.	Isolation of total RNA.....	66
6.1.5.3.2.	Reverse transcription.....	66
6.1.5.3.3.	Determination of the amplification efficiency.....	67
6.1.5.3.4.	Quantitative analysis of RNA.....	67
6.2.	Mammalian cell culture	68

6.2.1.	Growth and maintenance of mammalian cells.....	68
6.2.2.	Generation of cryo stocks.....	68
6.2.3.	Growth and maintenance of SILAC cultures.....	68
6.2.4.	Growth on coverslips.....	69
6.2.5.	Transient transfection of mammalian cells.....	69
6.2.6.	Generation of stable cell lines.....	70
6.2.7.	Cell harvesting and generation of protein extracts.....	70
6.3.	Protein chemistry.....	70
6.3.1.	Determination of protein concentration by Bradford assay.....	70
6.3.2.	Protein concentration and purification.....	71
6.3.2.1.	Protein concentration using centrifugal units.....	71
6.3.2.2.	Protein precipitation.....	71
6.3.3.	SDS-PAGE.....	72
6.3.3.1.	Staining of SDS-PAGE gels.....	73
6.3.3.1.1.	Coomassie staining.....	74
6.3.3.1.2.	Colloidal Coomassie.....	74
6.3.3.1.3.	Silver staining.....	74
6.3.4.	Western blot analysis.....	75
6.3.4.1.	Semi-dry blotting.....	75
6.3.4.2.	Tank blotting.....	75
6.3.4.3.	Ponceau staining.....	76
6.3.4.4.	Immunodetection.....	76
6.3.4.5.	Stripping of western blots.....	77
6.3.5.	Digitalizing results from SDS-PAGE gels and western blot films....	77
6.4.	Protein complex purification.....	77
6.4.1.	Strep-Tactin affinity purification.....	78
6.4.2.	FLAG affinity purification.....	79

6.4.3.	Tandem affinity purification by SF-TAP	79
6.5.	Analysis of protein complexes	80
6.5.1.	Sucrose density centrifugation	80
6.5.2.	Destabilization of protein complexes by treatment with SDS.....	81
6.6.	Immunohistochemistry	82
6.6.1.	Fixation of cells.....	82
6.6.2.	Staining on cover slips	82
6.6.3.	Operetta screens.....	83
6.6.4.	Microscopy	84
6.7.	Mass spectrometry	85
6.7.1.	Sample preparation	85
6.7.1.1.	Pre-fractionation by SDS-PAGE.....	85
6.7.1.2.	In-gel cleavage.....	86
6.7.1.3.	In-solution cleavage	87
6.7.1.4.	Purification with StageTips.....	87
6.7.2.	LC-MS/MS on the LTQ-Orbitrap XL and LTQ-Orbitrap Velos.....	88
6.7.2.1.	Liquid chromatography.....	91
6.7.2.2.	Mass spectrometry methods	93
6.7.2.3.	Database searching	94
6.7.3.	Data analysis using Scaffold	94
6.7.4.	SILAC quantification using MaxQuant.....	95
6.7.5.	Label-free Quantification using MaxQuant and correlation profiling	96
IV.	Results.....	98
1.	Establishment and optimization of the SDS-affinity purification (SDS-AP) using the interactome of Lebercilin	98
1.1.	Optimization of the concentrations for SDS destabilization	99
1.2.	Destabilization of the Lebercilin complex by SDS-AP.....	101

2.	The intraflagellar transport complex B	105
2.1.	Determination of the components of the IFT complex B	105
2.1.1.	Detection of the IFT-B by transient overexpression of IFT88-SF-TAP in HEK293-T	105
2.1.2.	Detection of the IFT-B by stable expression of IFT88-SF-TAP in HEK293.....	106
2.2.	Determination of the substructure of the IFT complex B.....	107
2.2.1.	Transient overexpression of several IFT proteins in HEK293-T ...	107
2.2.2.	Sucrose density centrifugation	108
2.3.	Analysis of functional differences between the IFT-B sub-complexes B1 and B2	110
2.4.	Predicted network of the IFT complex B	115
3.	The centrosomal protein 170 is associated with the IFT-B	116
3.1.	Analysis of the interactome of SF-TAP-tagged CEP170 in HEK293-T cells 117	
3.2.	CEP170 localizes to the basal body of the cilium in hTERT cells	122
3.3.	CEP170 co-localizes with TRAF3IP1 during ciliogenesis	123
3.4.	Knockdown of <i>Cep170</i> in IMCD3 cells.....	124
V.	Discussion	127
1.	The SDS-AP - a fast and easy method to analyse protein complexes.....	127
2.	Analysis of the IFT complex B	131
3.	Characterization of CEP170 and its association to the IFT-B	136
4.	Perspectives	138
VI.	References	141
VII.	Annex.....	154
1.	Figure index	154
2.	Table index	155
3.	Publications and poster presentations	156

3.1. Peer-reviewed publications.....	156
3.2. Poster presentations.....	156
4. Acknowledgements.....	157
5. Curriculum vitae.....	160

Abbreviations

ACN	Acetonitrile
Amp	Ampicillin
AP	Affinity purification
APS	Ammonium persulfate
AQUA	Absolute quantification
ATP	Adenosine 5'-triphosphate
BB	Basal body
BBS	Bardet Biedl Syndrome
bp	Base pairs
BSA	Bovine serum albumin
Ca	Calcium
CBD	Chitin binding domain
CBP	Calmodulin binding peptide
CC	Connecting cilium
cDNA	Complementary DNA
CID	Collision induced dissociation
CO ₂	Carbon dioxide
C _T	Threshold cycle
CTLH	C-terminal to LisH
CV	Ciliary vesicle
CY3	Indocarbocyanin
Da	Dalton
DAPI	4',6-diamidino-2-phenylindole
ddH ₂ O	Ultra pure water
dH ₂ O	De-ionized water
DMEM	Dulbecco's modified eagle medium
DMSO	Dimethylsulfoxide
DNA	Deoxyribonucleic acid
dNTP	Deoxynucleotide triphosphate
DPBS	Dulbecco's phosphate buffered saline
dsDNA	Double stranded DNA
DTT	Dithiothreitol
ECL	Enhanced chemiluminescence
<i>E. coli</i>	<i>Escherichia coli</i>
EDTA	Ethylenediaminetetraacetic acid
ER	Endoplasmatic reticulum
Exp	Experiment
FBS	Fetal bovine serum
FDR	False discovery rate
FT	Fourier transformation

gsp	Gene specific primer
GST	Glutathion-S-transferase
HA	Hemagglutinin
HCD	Higher-energy collision dissociation
HCl	Hydrochloric acid
HEK	Human embryonic kidney
His	Histidine
HPLC	High-performance liquid chromatography
Hrp	Horseradish peroxidase
hTERT	Human telomerase reverse transcriptase
ICPL	Isotope coded protein labelling
IFT	Intraflagellar transport
IFT-A	Intraflagellar transport complex A
IFT-B	Intraflagellar transport complex B
IgG	Immunoglobulin G
IMCD	Inner Medullary Collecting Duct
IP	Immunoprecipitation
IS	Inner segment
IT	Ion trap
iTRAQ	Isobaric Tag for Relative and Absolute Quantitation
JATD	Jeune (asphyxiating thoracic dystrophy) syndrome
JBTS	Joubert syndrome
Kan	Kanamycin
kd	Knockdown
LB	Luria-Bertani
LC	Liquid chromatography
LCA	Leber congenital amaurosis
LFQ	Label-free quantification
LisH	Lissencephaly type-1-like homology
LIT	Linear ion trap
M-MLV RT	Moloney murine leukemia virus reverse transcriptase
m/z	Mass over charge ratio
MBP	Maltose binding protein
MKKS	McKusick-Kaufman syndrome
MKS	Meckel-Gruber syndrome
MQ	Max Quant
MS	Mass spectrometry
MS/MS	Tandem mass spectrometry
MW	Molecular weight
NaCl	Sodium chloride
NP-40	Nonidet P-40
NPH	Nephronophthisis

Abbreviations

OFD1	Orofaciodigital syndrome
OS	Outer segment
PAGE	Polyacrylamide gel electrophoresis
PBS	Phosphate buffered saline
PCP	Protein correlation profiling
PCR	Polymerase chain reaction
PEI	Polyethylenimine
PEP	Posterior error probability
PFA	Paraformaldehyde
POI	Protein of interest
ProtA	Protein A
PTM	Posttranslational modification
PVDF	Polyvinylidene difluoride
qPCR	Quantitative PCR
RNA	Ribonucleic acid
RNAi	RNA interference
RPE	Retinal pigmentary epithelium
RT	Reverse transcription
SBP	Streptavidin-Binding Peptide
SDS	Sodium dodecyl sulfate
SDS-AP	Sodium dodecyl sulfate affinity purification
SF-TAP	Strep-FLAG-tandem affinity purification
SILAC	Stable isotope labelling by amino acids in cell culture
siRNA	Short interfering RNA
SLS	Senior-Loken syndrome
SRM	Single reaction monitoring
TAP	Tandem affinity purification
TBS	Tris-buffered saline
TEMED	N,N,N',N'-tetramethylethylene-diamine
TEV	Tobacco etch virus
TFA	Trifluoroacetic acid
TFs	Transition fibers
T _m	Melting temperature
Tris	Tris(hydroxymethyl)aminomethane
TZ	Transition zone
U	Units
UHPLC	Ultra-high pressure liquid chromatography
UV	Ultraviolet
v/v	Volume per volume
w/v	Weight per volume

Summary

Cilia are ancient organelles protruding from the surfaces of virtually all cell types within the human body. The intraflagellar transport (IFT) machinery transports cargo along the axoneme of the cilium. The cargo binds to the IFT particle, a large multi-protein complex consisting of IFT-A, IFT-B modules and the motor proteins. Diseases affecting the ciliary function, the ciliopathies, can affect single organs or occur as multi-organ disorders. In many cases the ciliopathies are caused by mutations in ciliary genes, which have an effect on the IFT and therefore on the formation and the function of the cilium. Although the field of ciliary research is increasing steadily the exact mechanism of the IFT remains elusive.

Protein complex analysis by affinity purification coupled to mass spectrometry is a common method to analyse the composition of molecular machines, large protein networks and to determine functional modules within those networks. Interaction data from these experiments can be used for the prediction of biological pathways or disease mechanisms that these proteins are involved in. Still, these analyses result in a mixture of co-purified proteins and it is in most cases impossible to determine how these assemble in the cell. This prevents the accurate description of the analysed protein complexes. Approaches for the determination of sub-modules are therefore of great interest to improve the method of purification to maximize the output of the experiment.

A novel workflow, combining mild destabilization of protein complexes by SDS with quantitative mass spectrometry and protein correlation profiling (PCP), was developed to determine the sub-structure of protein complexes, using Lebercilin as proof of principle. The protein complex of SF-TAP-tagged Lebercilin was purified using FLAG-affinity purification. Subsequent, the protein complexes were destabilized on beads by application of an SDS-gradient. The sequentially eluted fractions were processed by quantitative label-free mass spectrometry by using the software MaxQuant and PCP. The results of this experiment showed that the complex of Lebercilin consists of at least five different sub-modules. Additionally, using PCP it was possible to detect a novel component of the IFT-A, Tubby-like protein 3 (TULP3) and a protein that is likely to be associated to the IFT-B, centrosomal protein 170 (CEP170). This new combination of methods is a powerful

tool to analyse the sub-structure of partially known protein complexes and even detect new components of those.

The IFT-B was characterized in detail by the affinity purification strategy SF-TAP and by sucrose density centrifugation in combination with label-free quantitative mass spectrometry. The results of these experiments revealed that many of the proteins that were thought to be associated to the IFT-B are stably attached to the complex. Furthermore, the analysis of the sub-structure of the IFT-B showed that the complex consists of two distinct sub-modules. Knockdown studies in IMCD3 cells, using siRNA, were performed to analyse the importance of selected components of the IFT-B. These experiments resulted in malformation and/or shortening of the cilia by the knockdown of *Ift52*, *Ift88*, *Ttc30a1*, *Ttc30b* and *Ar13b*. Taking together the resulting data, it was possible to generate a predicted network for the IFT-B indicating the two sub-complexes and the possible central role of IFT52 and IFT88 within the complex.

Following the detailed characterization of the IFT-B, the association of the protein CEP170 to the complex was analysed by different means. Interaction of CEP170 with the IFT-B could be shown by data from SF-TAP purification, SILAC combined with one-step affinity purification coupled to quantitative mass spectrometry and western blot. Immunofluorescence experiments showed the localization of CEP170 to the base of the cilium in hTERT-RPE1 cells. Furthermore, co-localization of CEP170 with the IFT-B during certain stages of ciliogenesis could be shown. Knockdown of CEP170 in IMCD3 cells prevented IFT localization to the cilium while the phenotype of the formed cilia appeared normal. However, the number of cells bearing a single cilium was reduced when CEP170 was knocked down. These results indicate an essential role of CEP170 for the function of the IFT.

Zusammenfassung

Zilien sind sehr alte Organellen, die aus der Zelloberfläche fast aller humanen Zelltypen hervorragen. Die intraflagellare Transport (IFT) -maschinerie transportiert 'Ladung' entlang des Axonems des Ziliums. Die Ladung bindet an den IFT-Partikel, einen großen Multi-Proteinkomplex, welcher aus den IFT-A und IFT-B Modulen sowie den Motorproteinen besteht. Erkrankungen, welche die ziliäre Funktion

beeinträchtigen, die Ziliopathien, können einzelne Organe betreffen oder als Multiorgan-Erkrankungen auftreten. In vielen Fällen werden Ziliopathien durch Mutationen in ziliären Genen hervorgerufen, welche einen Einfluss auf den IFT und, hierdurch bedingt, einen Effekt auf die Funktion und Bildung des Ziliums haben. Obwohl das Forschungsgebiet der Zilien stetig wächst, ist die genaue Funktion des IFT bisher nicht bekannt.

Die Proteinkomplexanalyse mittels Affinitätsaufreinigung in Kombination mit Massenspektrometrie ist eine gängige Methode zur Analyse der Zusammensetzung molekularer Maschinen, großer Proteinnetzwerke und zur Bestimmung funktionaler Einheiten in diesen Netzwerken. Interaktionsdaten dieser Experimente können zur Vorhersage biologischer Signalwege oder von Krankheitsmechanismen, an denen diese Proteine beteiligt sind, verwendet werden. Das Ergebnis dieser Analysen ist eine Mischung aufgereinigter Proteine. In den meisten Fällen ist es allerdings nicht möglich zu bestimmen, wie diese Proteine in der Zelle miteinander interagieren, was die exakte Beschreibung der analysierten Proteinkomplexe verhindert. Ansätze zur Bestimmung von Komplex-Untereinheiten sind daher von großem Interesse, um die Aufreinigung zu verbessern und die Aussagekraft der Experimente zu erhöhen.

Es wurde ein neuer Arbeitsablauf entwickelt, bei welchem die milde Destabilisierung von Proteinkomplexen mittels SDS mit quantitativer Massenspektrometrie und Korrelation von Proteinprofilen (protein correlation profiling, PCP) kombiniert wurde. Unter Verwendung dieser Methode kann die Substruktur von Proteinkomplexen bestimmt werden, was anhand des Proteinkomplexes von Lebercilin exemplarisch gezeigt wurde. Der Proteinkomplex von SF-TAP markiertem Lebercilin wurde mittels FLAG-Affinitätsaufreinigung isoliert. Im Anschluss wurden die an Kunstharz immobilisierten Proteinkomplexe mittels eines SDS-Gradienten destabilisiert. Die sequenziell eluierten Fraktionen wurden mittels markierungsloser, quantitativer Massenspektrometrie unter Verwendung des Programms MaxQuant und der Methode PCP prozessiert. Die Ergebnisse dieses Experiments haben gezeigt, dass der Proteinkomplex von Lebercilin aus mindestens fünf Untereinheiten besteht. Des Weiteren war es möglich, durch die Verwendung von PCP ein neues Mitglied des IFT-A, Tubby-like protein 3 (TULP3), sowie ein Protein, welches wahrscheinlich an den IFT-B assoziiert ist, centrosomal protein 170 (CEP170), zu identifizieren. Diese neue Kombination von Methoden stellt ein leistungsfähiges Werkzeug zur Analyse

der Untereinheiten partiell bekannter Proteinkomplexe dar und ermöglicht sogar die Detektion neuer Komponenten dieser Proteinkomplexe.

Der IFT-B wurde im Detail mittels der Affinitätsaufreinigungsmethode SF-TAP und Saccharosegradientenzentrifugation, kombiniert mit markierungsloser, quantitativer Massenspektrometrie, charakterisiert. Die Ergebnisse dieser Experimente haben gezeigt, dass viele der am IFT-B assoziiert geglaubten Proteine stabil mit dem IFT-B interagieren. Ferner hat die Analyse der Substruktur des IFT-B gezeigt, dass der Komplex aus zwei unterschiedlichen Untereinheiten besteht. Es wurden Studien zur Reduktion der Genexpression mittels siRNA in IMCD3 Zellen durchgeführt, um die Bedeutung ausgewählter Komponenten des IFT-B zu analysieren. Die Herabsetzung der Genexpressionsraten von *Ift52*, *Ift88*, *Ttc30a1*, *Ttc30b* und *Arl13b* führten zu einer Fehlbildung und/oder einer Verkürzung der Zilien. Die Verwendung der erhobenen Daten erlaubte die Erstellung eines Netzwerkes des IFT-B, welches seine beiden Untereinheiten sowie eine mögliche zentrale Rolle von IFT52 und IFT88 vorhersagt.

Im Anschluss an die detaillierte Charakterisierung des IFT-B wurde die Assoziation des Proteins CEP170 an den IFT-B unter Verwendung verschiedener Methoden untersucht. Die Interaktion von CEP170 und dem IFT-B konnte anhand von SF-TAP-Aufreinigung, SILAC in Kombination mit quantitativer Massenspektrometrie, sowie Western Blot Analyse gezeigt werden. Immunfluoreszenz-Experimente zeigten die Lokalisation von CEP170 am Basalkörper des Ziliums in hTERT-RPE1 Zellen. Des Weiteren konnte eine Co-Lokalisation von CEP170 mit dem IFT-B zu einem bestimmten Zeitpunkt der Ziliogenese gezeigt werden. Die Herabsetzung der Genexpression von CEP170 in IMCD3 Zellen verhinderte die Lokalisation von IFT-B zum Zilium, während die gebildeten Zilien normal ausgebildet wurden. Jedoch war die Anzahl der Zellen mit einem einzelnen Zilium während dieses Experiments reduziert. Diese Ergebnisse weisen auf eine entscheidende Rolle von CEP170 bei der Funktion des Ziliums hin.

I. Introduction

1. The Cilium

Cilia have a very long history in research and were firstly described as ‘thin little feet, or little legs’ on ciliated protozoa by Antoni van Leeuwenhoek in 1677 (1). In the year 1835 W. Sharpey hypothesized that flagella are active organelles that are moved by contractile material along their length rather than being passively moved by the cytoplasmic flow or other contractile activity within the cell body (2).

At the end of the 19th century Zimmermann described a second type of cilia, the central flagellum (German: Zentralgeissel) and distinguished them from cilia on multi-ciliated cells by their association with a pair of centrioles (3). This single immotile cilium was termed primary cilium by Sorokin in 1968 since occurring prior to motile cilia during the pulmonary development (4).

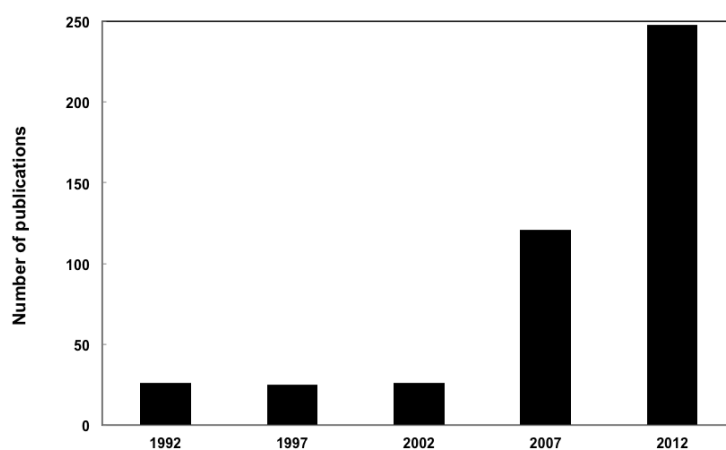


Figure 1: Number of publications on primary cilia.

This figure shows the number of publication registered at PubMed per year for the last decade. (Source: PubMed, search-term: 'primary AND (cilia OR cilium)')

However, the biological importance of cilia remained neglected until their recent association with a number of human genetic diseases (5). The number of publications describing links between cilia and morphogen pathways steadily increased in the last decade, expanding the field of cilia biology very fast (Figure 1, (6).

Cilia are ancient subcellular structures that were probably present in the ancestral eukaryote (7). Flagella are essential to locomotion in free living protozoa and to

feeding in sessile protozoa (8). The structure and function of cilia is very similar to eukaryotic flagella, therefore motility was their only assigned function for several decades (9). Nowadays it is clear that cilia are highly conserved, hair-like microtubular organelles with a big variety of functions in the human body. They can be grouped into two distinct categories: motile cilia and non-motile (primary) cilia.

The main function of motile cilia is to propel cells through aqueous solutions or to move liquids over cell surfaces (10). Unlike primary cilia, motile cilia therefore are restricted to a small number of tissues and cell types, including the respiratory tract, brain ventricles and the oviducts (11). Motile cilia in most cases are present as clusters on multi-ciliated cells, that can consist of up to 200-300 cilia, where they beat in wave-like concerted motion (12).

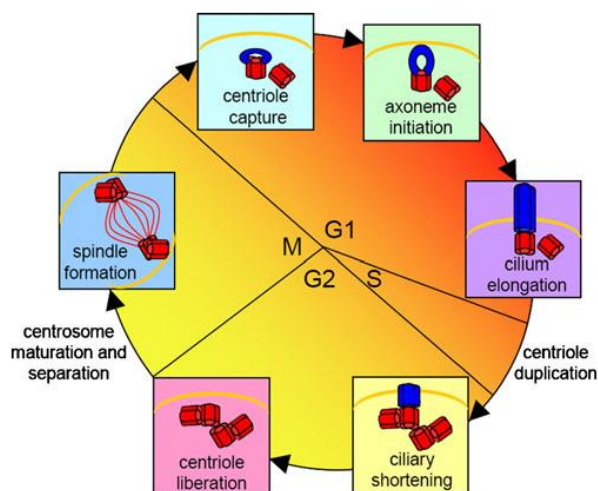


Figure 2: Formation and resorption of the primary cilium.

The formation of the primary cilium starts when the cell exits the cell cycle to growth arrest. The mother centriole is translocated to the plasma membrane and the cilium is formed. When the cell re-enters the cell cycle the cilium is resorbed and the centrosome duplicates during mitosis. Abbreviations: G1: G1-phase, S: S-phase, G2: G2-phase, M: mitosis. This figure is reprinted from Gate et al. (13) with friendly permission of Springer.

In contrast, non-motile cilia occur as single primary cilia with different functions on virtually all polarized cells, as for example signalling, transport and mechanosensation. Mechanosensation of cilia for example can have a great effect on cilia structure, it has been shown that it can affect the ciliary length and also results in a difference of ionic currents (14). Another example for such a mechanism is described in two studies from Praetorius et al. (15, 16) which show the function of the cilium as a flow sensors that induce Ca^{2+} -influx.

Primary cilia are dynamic structures and their formation and resorption is closely correlated with the cell cycle (17, 18). Formation of primary cilia only appears when the cell exits mitosis and, conversely, the cilia are resorbed when the cell re-enters the cell cycle (Figure 2, (19)). Primary cilia arise from the distal end of the mother centriole of the centrosome that is translocated to the cell surface (20).

1.1. Structure of the Cilium

The structure of the cilium can be divided into sub-compartments, namely the basal body, the transition zone, the axoneme, the cilia membrane, and the cilia tip ((21) Figure 3).

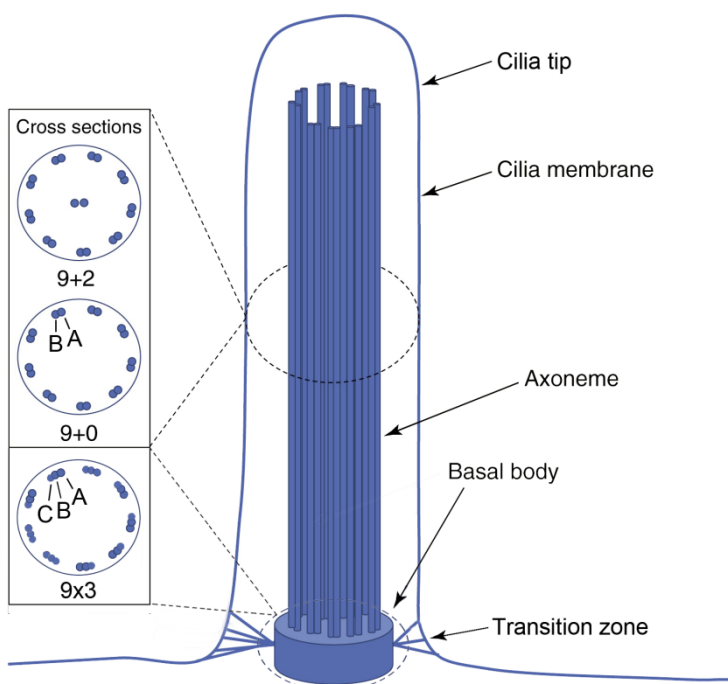


Figure 3: Structure of the cilium.

The cilium can be divided into structural units: The basal body, the transition zone, the axoneme, the cilia membrane and the cilia tip. The cross section of the cilium shows the different types of cilia, '9+2' (motile) and the '9+0' (non-motile, primary cilia). Nine microtubule pairs, consisting of an A tubule and a B tubule, are arranged circular and surround an additional pair of microtubules in the case of the '9+2' structure. In the basal body the cilium has a nine times three microtubule structure (9x3), consisting of A, B and C tubules. Y-shaped transition fibers connect the basal body to the ciliary membrane. This figure was adapted from Berbari et al. (21) with friendly permission of Elsevier Limited.

The basal body is the part from which the cilium arises and it derives from the mature centriole. The junction of the basal body and the axoneme is called the transition zone. At the transition zone, Y-shaped transition fibers project from the basal body to

the ciliary membrane. The transition fibers are thought to be part of the ciliary pore complex which is thought to act as a barrier to restrict the access to the ciliary compartment to certain proteins (22).

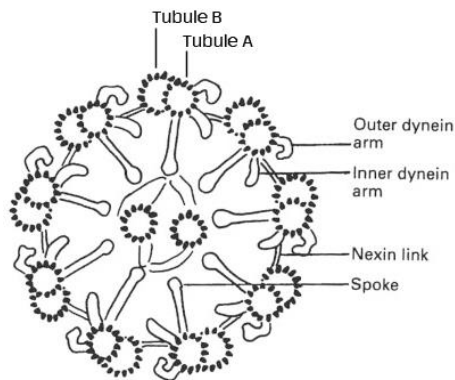


Figure 4: Cross section of the cilium.

Cross section of a 9+2 cilium showing the arrangement of the microtubule doublets. The structure is stabilized by Nexin links and radial spokes. The movement (bending) of the cilium is achieved by dynein motor units attached to the Tubule A that move on the back of the neighbouring doublets (Tubule B). This figure is reproduced from Afzelius et al. (23) with friendly permission of John Wiley and Sons.

The axoneme of all cilia is composed of nine microtubule doublets (heterodimers of tubulin A and B, Figure 3 and Figure 4, (24)). The so-called '9+2' cilia contain a central pair of microtubules and are mainly motile whereas the '9+0' or primary cilia have no microtubules in the center and are, in most cases immotile (25, 26). Recent studies revealed that this rough classification is not accurate enough, for example a new type of cilia was found that has a '9+4' structure (27), still this nomenclature is widely used to describe cilia in literature.

The microtubules of '9+2' cilia additionally are connected via nexin links, that together with the radial spokes increase the resistance of the cilium to bending (Figure 4, (28)) The movement of the cilia is achieved by two rows of dynein motor units (Figure 4, outer and inner dynein arm), extending from the A tubules. The dynein motor units are able to move along the back of the B tubules of the neighbouring microtubule doublet by an ATP-dependent process (29, 30).

1.2. The intraflagellar transport (IFT)

Protein synthesis is restricted to the cytoplasm, therefore a selective transport system is required to bring proteins and other cargo to the tip of the cilium as well as to return

turnover products to the cell body (31). This molecular machinery, which is powered by motor proteins, is called the intraflagellar transport (IFT). The IFT was first described by Kozminski et al. in 1993 who described the transport system in the green algae *Chlamydomonas reinhardtii* (32). Studies on the IFT from its discovery until present show that this process is highly conserved and essential for the assembly and function of cilia (33).

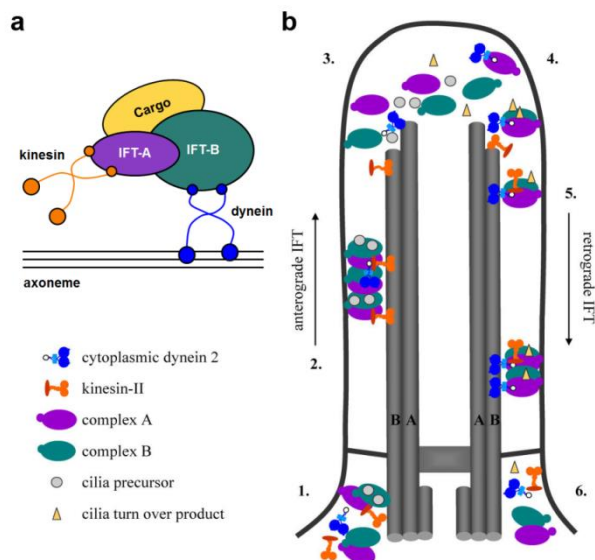


Figure 5: Schematic illustration of the IFT and its components.

a The IFT particle: The IFT complex A (IFT-A) is coupled to a kinesin motor unit and the IFT complex B (IFT-B) to a dynein motor unit. Each of the motor units is able to move along the axoneme of the cilium in an ATP-dependent manner to transport the cargo along the ciliary axoneme. **b** The IFT can be described by the following points. 1. Localization of the components of the IFT particle and the cargo proteins to the peri-ciliary region. Assembly of the IFT-particle and binding of the cargo to the IFT-particle. 2. During the anterograde IFT, kinesin motor units drive the transport of the cargo from the base of the cilium to the tip. 3. The cargo is released at the ciliary tip, the IFT particle dissociates. 4. The IFT particle is re-assembled, turnover products or other cargo is bound to the IFT particle. 5. The cargo is transported from the ciliary tip to the cell body. In the retrograde direction dynein motor units mediate the IFT. 6. The IFT particle re-enters the cell body, the cargo is released and the IFT particle disassembles. This figure was adapted from Pedersen et al. (34) with friendly permission of John Wiley and Sons.

The IFT is a bidirectional process. The transport of cargo from the ciliary base to the tip is called anterograde IFT and the transport from the tip to the base of the cilium is named the retrograde IFT (32). These two processes are mediated by different motor proteins, the anterograde transport is mediated by kinesin, whereas the retrograde transport is enabled by dynein as motor protein. The IFT involves a large multi-protein complex that builds the connection between cargo and the motor proteins, the

IFT particle. The IFT particle consists of at least 20 proteins and is divided into two distinct complexes, the IFT complex A (IFT-A) and the IFT complex B (IFT-B, Figure 5, Table 1). The combination of the motor units with these complexes defines the direction of the IFT. The IFT-B together with a kinesin-2 motor mediates the transport from the ciliary base to the tip (anterograde transport). In contrast, the transport from the ciliary tip back to the cell body (retrograde transport) is mediated by the interplay of the IFT-A with a dynein-1b unit (35, 36).

Phylogenetic studies between different organisms showed that IFT components are highly conserved within ciliated eukaryotes but are missing completely in species lacking cilia, like plants or yeasts (37). Studies on homology between IFT proteins and components of coat protein I (COPI) and clathrin-coated vesicles raised the hypothesis that the IFT evolved as a specialized form of the coated vesicle transport from a protocoatomer complex (38, 39). The knockout of IFT genes has severe influence on the accurate formation of cilia or flagella indicating the essential role of the IFT components. Furthermore, the fact that no null mutation in any IFT gene was ever reported, indicates that the IFT proteins presumably are necessary for life (40-43).

Most ciliary studies have focussed on functionality whereas little is known about the exact structure of the IFT (44). Studies of the IFT particle in *Chlamydomonas* firstly showed that it dissociates into two complexes (IFT-A and IFT-B) by the use of ionic strength (35). Biochemical studies showed that the IFT-B consists of a core complex with peripheral proteins, that dissociate when increasing the ionic strength further (Figure 6, (45)). Table 1 shows an overview of the components of the IFT particle indicating their affiliation to the particular machineries.

The IFT particle is a protein complex that is highly interconnected. There are multiple studies analysing the crystal structure of parts of the IFT complex or its internal interactions (46-48). Still, the exact structure of the IFT itself or the selection and interaction of cargo with the latter remains elusive.

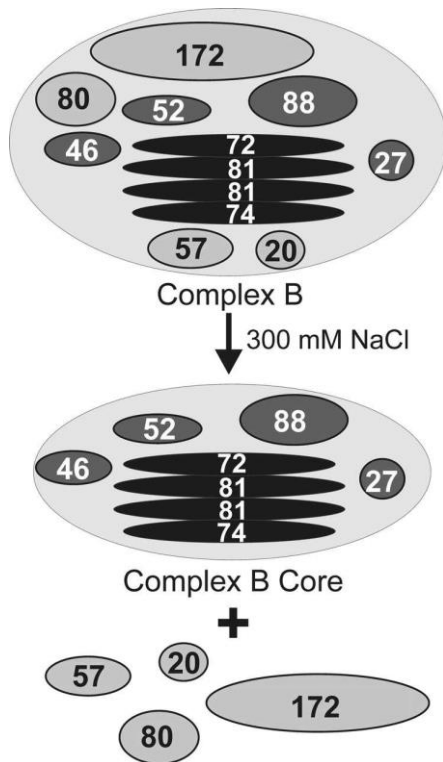


Figure 6: Dissociation of the IFT-B by ionic strength.

The IFT-B of *Chlamydomonas* dissociates when applying high ionic strength (300 mM NaCl). It disassembles into a core complex (IFT27, IFT46, IFT52, IFT72, IFT74, IFT81 and IFT88) and also frees some components (IFT20, IFT57, IFT80 and IFT172). IFT81 forms a higher order oligomer with IFT72 and IFT74 in form of a tetramer. This figure is reprinted from Lucker et al. (45) with friendly permission of the American Society for Biochemistry and Molecular Biology.

Table 1: Overview of the components of the IFT particle.

This table shows the components of the IFT particle. The information were combined from Blacque et al 2008 (49) and Boldt et al. 2011 (50). In case of missing information the homologue's gene names were identified by BLAST-search with the corresponding protein sequences from Uniprot.

IFT component	Protein	Uniprot	Gene Name	homologue C. elegans	homologue D. rerio	homologue C. reinhardtii	homologue M. musculus	Reference
Transport associated Microtubule motor proteins	Lebercilin	Q86VQ0	LCA5	-	si:dkey-241o6.2	-	Lca5	Boldt et al. 2012
	Dynein light chain 1, cytoplasmic	P63167	DYNLL	-	dynll1	DYL1	Dynll1	Boldt et al. 2012
	Dynein light chain 2, cytoplasmic	Q96FJ2	DYNLL	dlc-1	dynll2a, dynll2b	DYL1	Dynll2	Boldt et al. 2012
	Cytoplasmic dynein 2 heavy chain 1	Q8NCM8	DHC2	che-3	LOC100332402	DHC1B	Dync2h1	Blacque et al. 2008
	Cytoplasmic dynein 2 light intermediate chain 1	Q8TCX1	DYNC2	xbx-1	dync2li1	D1bLIC	Dync2li1	Blacque et al. 2008
	Kinesin-like protein KIF3A	Q9Y496	KIF3A	klp-20	kif3a	FLA8	Kif3a	Blacque et al. 2008
	Kinesin-like protein KIF3B	O15066	KIF3B	klp-11	kif3b	FLA10	Kif3b	Blacque et al. 2008
	Kinesin-like protein KIF17	Q9P2E2	KIF17	osm-3	kif17	-	Kif17	Blacque et al. 2008
	Kinesin-associated protein 3	Q92845	KIFAP	kap-1	kifap3a	FLA3	Kifap3	Blacque et al. 2008
	Kinesin-like protein KIF7	Q2M1P5	KIF7	-	kif7	-	Kif7	Boldt et al. 2012
Intraflagellar transport complex B	Intraflagellar transport protein 20 homolog	Q8IY31	IFT20	Y110A7A.2	ift20	IFT20	ift20	Blacque et al. 2008, Boldt et al. 2012
	Intraflagellar transport protein 27 homolog	Q9BW83	IFT27	-	ift27	IFT27	ift27	Blacque et al. 2008, Boldt et al. 2012
	Intraflagellar transport protein 46 homolog	Q9NQC8	IFT46	dyf-6	ift46	IFT46	ift46	Blacque et al. 2008, Boldt et al. 2012
	Intraflagellar transport protein 52 homolog	Q9Y366	IFT52	osm-6	ift52	BLD1	ift52	Blacque et al. 2008, Boldt et al. 2012
	Intraflagellar transport protein 57 homolog	Q9NWB7	IFT57	che-13	ift57	IFT57/55	ift57	Blacque et al. 2008, Boldt et al. 2012
	Intraflagellar transport protein 74 homolog	Q96LB3	IFT74	ift-74	zgc:92052	IFT74/72	ift74	Blacque et al. 2008, Boldt et al. 2012
	Intraflagellar transport protein 80 homolog	Q9P2H3	IFT80	che-2	ift80	IFT80	ift80	Blacque et al. 2008, Boldt et al. 2012
	Intraflagellar transport protein 81 homolog	Q8WYA0	IFT81	ift-81	ift81	IFT81	ift81	Blacque et al. 2008, Boldt et al. 2012
	Intraflagellar transport protein 88 homolog	Q13099	IFT88	osm-5	ift88	IFT88	ift88	Blacque et al. 2008, Boldt et al. 2012
	Intraflagellar transport protein 172 homolog	Q9UG01	IFT172	osm-1	ift172	IFT172	ift172	Blacque et al. 2008, Boldt et al. 2012
Intraflagellar transport complex B-associated	Clusterin-associated protein 1	Q96AJ1	CLUAP	dyf-3	cluap1	FAP22	Cuap1	Blacque et al. 2008, Boldt et al. 2012
	Rab-like protein 5	Q9H7X7	RABL5	-	rabl5	IFT22	Rabl5	Blacque et al. 2008, Boldt et al. 2012
	Intraflagellar transport protein 25 homolog	Q9Y547	HSPB1	-	zgc:158640	IFT25	Hspb11	Blacque et al. 2008, Boldt et al. 2012
	Intraflagellar transport protein 54 homolog	Q8TDR0	TRAF3	dyf-11	traf3ip1	FAP116	Traf3ip1	Blacque et al. 2008, Boldt et al. 2012
	Tetratricopeptide repeat protein 26	A0AVF1	TTC26	dyf-13	ttc26	DYF13	Ttc26	Blacque et al. 2008, Boldt et al. 2012
	Tetratricopeptide repeat protein 30A	Q86WT1	TTC30	-	ttc30a	-	Ttc30a1	Blacque et al. 2008, Boldt et al. 2012
Intraflagellar transport complex A	Tetratricopeptide repeat protein 30B	Q8N4P2	TTC30	dyf-1	flr	FAP259	Ttc30b	Blacque et al. 2008, Boldt et al. 2012
	Intraflagellar transport protein 43 homolog	Q96FT9	IFT43	-	-	IFT43	ift43	Blacque et al. 2008, Boldt et al. 2012
	WD repeat-containing protein 35	Q9P2L0	WDR3	ifta-1	wdr35	IFT121	Wdr35	Blacque et al. 2008, Boldt et al. 2012
	Intraflagellar transport protein 122 homolog	Q9HBG6	IFT122	daf-10	ift122	IFT122	ift122	Blacque et al. 2008, Boldt et al. 2012
	Tetratricopeptide repeat protein 21B	Q7Z4L5	TTC21	ZK328.7	ttc21b	IFT139	Ttc21b	Blacque et al. 2008, Boldt et al. 2012
	Intraflagellar transport protein 140 homolog	Q96RY7	IFT140	che-11	ift140	IFT140	ift140	Blacque et al. 2008, Boldt et al. 2012
	WD repeat-containing protein 19	Q8NEZ3	WDR1	dyf-2	si:dkey-	IFT144	Wdr19	Blacque et al. 2008, Boldt et al. 2012

1.3. Ciliogenesis

The formation of the cilium, the ciliogenesis, only takes place during the G1 phase of the cell cycle of proliferating cells or in G0 of post-mitotic cells which have exited the cell cycle (Figure 2, (51)) Therefore, for example over-proliferative cancer cell lines lack cilia and their ciliogenesis is impaired (52). Ciliogenesis starts when the cell exits mitosis and is divided into several stages (Figure 7).

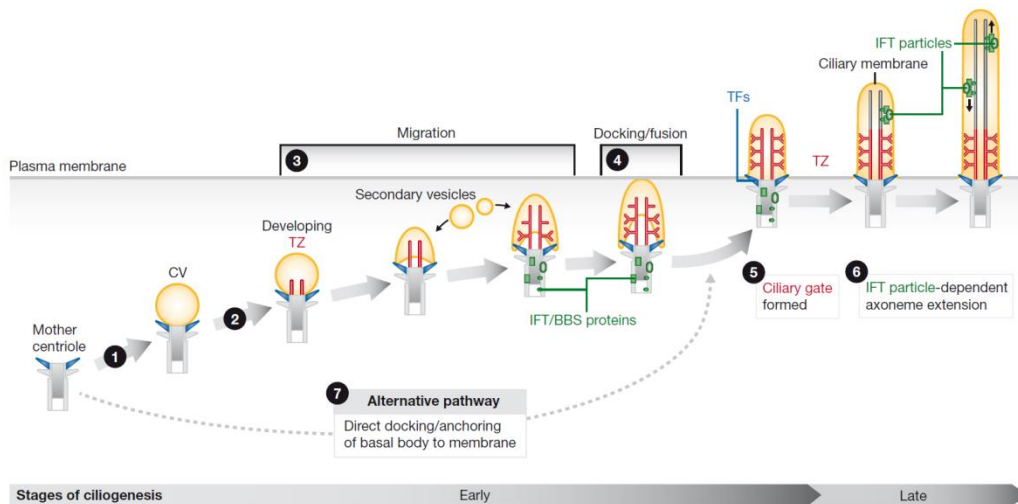


Figure 7: Ciliogenesis.

In this figure the formation of the primary cilium is shown schematically. The mature centriole forms the basal body and fuses together with ciliary vesicles to the plasma membrane. During this process the transition zone is formed and the elongation of the axoneme by the intraflagellar transport starts. Abbreviations: CV: ciliary vesicle, TZ: transition zone, IFT: intraflagellar transport, BBS: bardet biedl syndrome, TFs: transition fibers. This figure is reprinted from Reiter et al. (53) with friendly permission of Nature Publishing Group.

The cells must exit the mitosis to release the mother centriole from its centrosomal role (54). The earliest step observed during ciliogenesis in mammalian cells is the migration of the mother centriole to the apical cell surface. This is followed by fusion of a ciliary vesicle to the mother centriole (55). This process is mediated by the transition fibers when they are associated with the cilium (56). The centriole then differentiates into a basal body enabling its anchoring to the plasma membrane (57). Afterwards, the transition zone is developed by elongation of the axonemes. The ciliary vesicle is flattened by the elongation process and fuses with nearby secondary ciliary vesicles to extend the ciliary membrane (55). Subsequent, the membrane-bound axonemes reach the plasma membrane, fuse with the plasma membrane and the ciliary neck is developed (58). Within the cilium there is no protein synthesis

and therefore the IFT (section 1.2) has to deliver axonemal components to the tip of the cilium for the further elongation of the cilium.

Before the cell can re-enter the cell cycle the cilium must be resorbed (19, 59). The destabilization of the axoneme and the basal body is mediated by Aurora A kinase that activates the tubulin deacetylase HDAC6. The resorption of the cilium releases the centriole, enabling it to function as an organization center for the mitotic spindle. The ciliogenesis and cilia resorption thus is highly correlated with the process of cell division (60).

1.4. The connecting cilium of the photoreceptor cell

There are two classes of photoreceptor cells in the retina, the rods and the cones, whose detailed structure and function has been described very elegantly in the literature (61, 62). The photoreceptor cell is divided into an inner (IS) and an outer segment (OS, Figure 8, (63)). The inner segments have an elongated cell body which contains the nucleus and forms a synaptic junction with the retinal bipolar cells. The IS contains all of the main cell organelles including numerous mitochondria in the distal region, Golgi and ER in the proximal region as well as the basal body (BB, (64)). From the BB the so-called connecting cilium (CC) protrudes and connects the IS and the OS (65). The CC has a 9+0 axoneme which extends as microtubule singlets up to half-way along the OS. The OS are composed of stacks of disks that are assembled from the base of the ciliary membrane at the bottom of the CC and which contain the visual pigment molecules (40).

Photoreceptors are the most active neurons within the human body, the OS have a renewal rate of about 10% per day (66). Membrane is constantly shed from the distal end of the OS to prevent the accumulation of toxic bi-products of the visual cycle. In the OS there is no biomolecule synthesis, requiring the supply of protein and lipids as well as the removal of turnover products by a suitable mechanism (67). This function is performed by the abovementioned IFT (section 1.2) along the CC and implicates a massive traffic along the CC (68). Although the function of the CC is far from being resolved, it seem to play an essential role within the photoreceptor cell and the visual process of the retina (69).

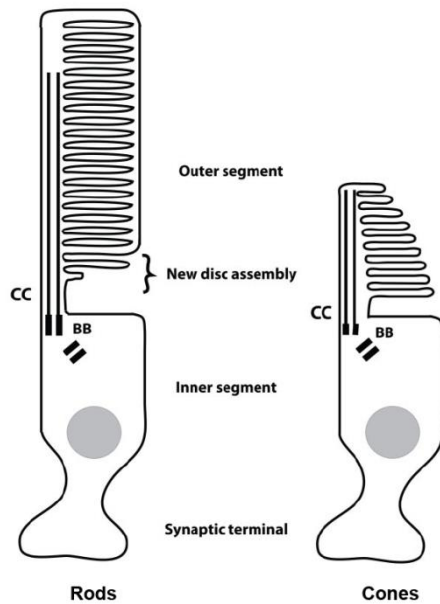


Figure 8: Schematic overview of the retinal photoreceptor cell.

On the left a rod photoreceptor cell is depicted and on the right a cone photoreceptor cell. In both cases the inner and the outer segment are connected by the connecting cilium (CC) which arises from the basal body (BB). The outer segment is composed of a stack of disks that initiate from the ciliary membrane at the base of the cilium. The inner segment includes the nucleus and a short axon that ends in a synapse. This figure is adapted from Insinna et al. (70) with friendly permission of John Wiley and Sons.

2. Cilia-related disorders - the ciliopathies

Cilia are present on virtually any polarized cell type in the human body, therefore cilia-related disorders - the so-called ciliopathies - can affect many organ systems. Ciliopathies can not only affect single organs but show variable and overlapping phenotypes as multi-systemic disorders (71). Figure 9 shows an overview of selected ciliopathies and their corresponding phenotypes. Additionally, there might also be some diseases and syndromes that are related to ciliary defects but are not assigned to the field of ciliopathies yet.

The most frequent cause of congenital blindness in infants and children is the disease Leber congenital amaurosis (LCA, (72)). One form of LCA can be caused by defects in connecting cilia and the disease phenotype is restricted to the eye. In contrast, defects in cilia may affect many organs with symptoms including obesity, retinal degeneration and polycystic kidneys in Bardet-Biedl syndrome (BBS (73)). The progress in research on BBS revealed similarities between the phenotype of BBS and the phenotypes of traditionally discrete clinical disorders such as

nephronophthisis (NPH), Joubert syndrome (JBTS) and Meckel-Gruber syndrome (MKS). This understanding offered the awareness that insight into the mechanism of some ciliopathies might illuminate the etiopathology of other ciliopathies (74, 75). Indeed, it is now known that cilia dysfunction is the cause of all of these developmental conditions.

Clinical phenotypes associated with ciliopathies

	MKS	BBS	JBTS	JATD	OFD1	MKKS	SLS	NPH	LCA
Retinopathy	+	+	+	-	-	-	+	+	+
Polydactyly	+	+	+	-	+	+	-	-	-
Kidney disease	+	+	+	+	+	-	+	+	-
Situs inversus	+	+	+	-	-	-	+	-	-
Mental retardation/developmental delay	+	+	+	-	+	-	-	+	+
Hypoplasia of cerebellum	+	+	+	-	+	-	-	+	-
Hydrometrocolpos	-	+	-	-	-	+	-	-	-
Obesity	-	+	+	-	-	-	-	-	-
Hepatic dysfunction	+	+	+	-	-	-	+	+	-

JATD, Jeune syndrome; OFD1, orofacioidigital syndrome 1; MKKS, McKusick-Kaufman syndrome; SLS, Senior-Loken syndrome.

Figure 9: Clinical phenotypes associated with ciliopathies.

This Figure is reprinted from Zaghoul et al. (74) with friendly permission of the American Society for Clinical Investigation. Abbreviations: MKS: Meckel-Gruber syndrome, BBS: Bardet Bardet-Biedl syndrome, JBTS: Joubert syndrome, NPH: Nephronophthisis, LCA: Leber congenital amaurosis.

Ciliary proteins are organized in large protein complexes and networks that are dynamically assembled in a cell- and context-specific manner (49). Spatio-temporal patterns and compositions, generated by differential gene expression, alternative splicing, post-transcriptional regulation via micro RNAs as well as post-translational regulatory mechanisms such as protein modifications and compartmentalization result in complex dependent protein compositions, complexes and organelles (76-80). Therefore cilia present in different organs and tissues have developed specific functional properties due to specific protein repertoires and regulatory circuits (81, 82)). This in turn might explain why some cilia with specific functions but not others are sensitive to certain perturbations, inducing disease-associated phenotypes in distinct tissues harbouring a specific type of cilia (83).

3. Ciliopathies and the IFT

The characterization of the gene *LCA5* and Lebercilin, the protein encoded by *LCA5* showed the association of Lebercilin to the transport machinery of the cilium (72). In a further study of the interactome of Lebercilin we were able to determine the interaction of Lebercilin with the IFT, further strengthening the hypothesis of it being involved in the ciliary transport machinery (50).

The connection of Lebercilin to the IFT was lost due to LCA-associated mutations. This resulted in the hypothesis that the loss of connectivity of Lebercilin to the IFT is the mechanism by which these mutations cause LCA. The generation of a *Lca5* knockout mouse showed a disturbed architecture of photoreceptor outer segments. The localization of IFT proteins to the connecting cilium was normal, but rhodopsin and opsin transport to the outer segments was disrupted. The light-induced translocation of arrestin and transducin was clearly impaired within this mouse model. This study demonstrated the importance of Lebercilin for the IFT along the connecting cilium of the photoreceptor. The mislocalization of visual pigments to the OS suggests severely impaired IFT in the photoreceptors in the absence of wild-type Lebercilin, indicating the severity of the loss of a single protein for the organelle. The IFT seems to be an essential component during the ciliogenesis and in the photoreceptors connecting cilium also during the process of vision.

4. Protein complexes

During the first decades of the last century the perception of proteins interactions within a cell was based on diffusion of single molecules interacting randomly by collision (84). Today we know that proteins exist in discrete modules that consist of many different types of molecules and differ from other modules by their function (85). Within these modules, the so-called (multi-) protein complexes, single proteins bearing structural domains interact dynamically with one or more other proteins by various biophysical processes (86). There is a big variety of protein complexes that can be classified for example by their stability (transient or stable complexes) but also by their stoichiometry (homo- or hetero-oligomers) or their function (87).

Protein complexes are in general only functional when all components are assembled in a certain composition. This is widely used as regulatory mechanism, where the complex is pre-assembled and is activated by the binding of the regulatory component or by depletion of inhibitory ones (88). The localization of protein complexes can also be an important factor for their regulation and a different localization can result in a different or modified function (89, 90). Furthermore, the function of protein complexes can vary in time due to conformational changes of proteins (91, 92). Still, these regulatory mechanisms cannot only be concerted by spatio-temporal differences but also by posttranslational modifications like

phosphorylation of proteins (93, 94). Other mechanisms like induced binding by conformational change, oligomerization or mutation of one or more of the involved proteins also play an important role for the function of protein complexes (95, 96). One example for the loss of function by mutation within a protein complex is the already mentioned IFT particle. The truncation of the protein Lebercilin by a mutation leads to the loss of interaction between the IFT's motor unit and the IFT complex A and B. This leads to an impaired IFT and therefore to the degeneration of the photoreceptor outer segments (50).

4.1. Purification and analysis of native protein complexes

Proteins and their complexes play an essential role within the cell, for basic processes like metabolism, signalling, transport and structural organization (97). Proteins are organized in large assemblies of several proteins that work in a concerted manner like molecular machines. The components of these complexes interact by stable and/or transient interactions and transduce a wide variety of signals within different compartments of the cell (98). While most critical biological processes are fulfilled by networks of large protein complexes, our global knowledge about those complexes remains limited (99). Figure 10 shows the historical timeline of protein interaction research to summarize the most important steps of the last century. One can clearly see that most of the major technical inventions in the field are followed by milestones in protein research. This indicates the importance of newly invented methods and techniques within the field of protein sciences.

Protein complex analysis has been proven to be a highly valuable tool for the identification of biological processes and disease mechanisms (100). In recent years the analysis and generation of large protein maps and networks have become an irreplaceable tool to describe and interpret data from protein interaction studies (101). A great example that shows the importance of those networks is the work of Kiel and co-workers (102). In this study the authors characterized the signal transduction network of rod photoreceptor cells around the central protein rhodopsin by a systems biology approach, integrating experimental data from protein complex analysis, data from literature and structural information. The combination of those data allowed valuing of the interactions and establishing sub-networks and functional units within this cellular compartment. This in turn, led to the definition of molecular machines giving insight into the underlying signalling mechanisms. New insights into the

happen by recognition of an epitope of the protein itself or by the capture of a small tag fused to the protein of interest (POI).

Table 2: Overview of commonly used affinity tags for protein purification.

Abbreviations: CBP: calmodulin binding peptide, His: histidine, FLAG: short polypeptide (108), HA: hemagglutinin, Myc: polypeptide from the c-myc gene product, V5: Peptide sequence of the simian virus 5, Strep: Streptavidin, SBP: Streptavidin-Binding Peptide, CBD: chitin binding domain, GST: Glutathion-S-transferase, MBP: maltose binding protein. This table is reproduced from Li et al. (109) with friendly permission of Portland Press Ltd.

Affinity tag	Sequence or size (kDa)	Affinity matrix	Elution strategy
Z domain*	VDNKFNKEQQNAFYELHLPNLNEEQRNAFI QSLKDDPSQSANLLAEAKKLNDQAQPK	IgG	IgG or low pH
CBP	KRRWKKNFIAVSAANRFKKISSGAL	Calmodulin	2 mM EGTA
His tag	HHHHHH	Ni ²⁺ , Co ²⁺	150–500 mM imidazole
FLAG	DYKDDDDK	Antibody	FLAG peptide or low pH
HA	YPYDVPDYA	Antibody	HA peptide or low pH
Myc	EQKLISEEDL	Antibody	Low pH
V5	GKPIPNPLLGLDST	Antibody	V5 peptide or low pH
Strep II	WSHPQFEK	StrepTactin	2.5–5 mM desthiobiotin
SBP	MDEKTTGWRGGHVVVEGLAGELEQLRARLEH HPQGQREP	Streptavidin	2 mM biotin
S-peptide	KETAALKFERQHMDS	S-protein	Denaturant or low pH
CBD	TNPGVSAWQVNTAYTAGQLVYNGKTYKCL QPHTSLAGWEPSNVPALWQLQ	Chitin	Thiol reagents or pH and temperature shift (when fused with intein)
GST	26	Glutathione	10 mM reduced glutathione
MBP	40	Maltose	10 mM maltose

*Z domain is a synthetic Fc-region-binding domain derived from the B domain of ProtA.

The isolation of protein complexes by fusion tags is achieved by the genetic modification of the POI. This can only be achieved using an organism in which the modified POI can be exogenously expressed, as for example in bacteria or human cell lines. The choice of the organism used depends on the requirements on the produced protein concerning, for example, posttranslational modifications or protein amount, which differ in prokaryotes and eukaryotes. For the expression of a protein, the POI is cloned into a DNA expression vector, downstream of an appropriate promoter (often strong promoters for overexpression) and a fusion tag is introduced at the N- or C-terminus of the POI. In most cases a certain number of amino acids is additionally introduced to act as a spacer, reducing steric inhibition of the tag to the proteins function (110). The additional amino acids not only can function as a spacer but can contain specific cleavage sites to remove the tag enzymatically after purification of the protein. In some cases the function and/or the ability of the fusion protein to bind its interaction partners depends on the position of the tag (N- or C-terminal). There is a wide variety of commonly used tags that can be used to generate fusion proteins for affinity purification (Table 2). The available tags differ in their size, specificity and avidity as well as in the extent of non-specific binding (111).

The amount of non-specific binding is also dependent on the immobilisation resin used and the capturing reagent for the affinity tag.

4.1.1.1. One-step purification

The one-step affinity purification can either be used to isolate native proteins and their complexes by the use of antibodies against an epitope of the protein or by the use of an affinity tag. This method only implements one affinity purification step, where the protein is captured and enriched from a crude lysate. This enables the purification of a native protein including its interaction partners. The advantage of the one-step purification compared to a two-step purification strategy is that transient interaction partners are co-purified with the complex. On the other hand, due to the purification by a single affinity epitope, a lot of non-specific interactions will lead to a great number of isolated proteins.

4.1.1.2. Two-step purification

The two step purification is a method whereby two different affinity tags are used consecutively. This method was first published in 1999 and was called tandem affinity purification (TAP, (112)). The method was applied to isolate proteins from yeast and was later adapted to other organisms. TAP involves the fusion of the so-called TAP-tag to the POI, that is then introduced to a host cell to trap the endogenous interacting partners of the POI (109). The original TAP-tag consisted of two IgG binding domains of *Staphylococcus aureus* protein A (ProtA) and a calmodulin binding peptide (CBP) which were separated by a TEV protease cleavage site (113). In this classical approach, the POI is captured by the ProtA epitope of the TAP-tag, subsequently cleaved off by TEV protease and then captured again by CBP. This allows the isolation of stable native protein complexes at high purity.

Since then, the TAP-tag has been modified by various groups and has been adapted to different experimental requirements (114). In this study the so-called SF-TAP-tag and the corresponding method from Gloeckner et al. 2007 was applied (115). Figure 11 schematically shows the principle of the SF-TAP purification. The SF-TAP tag consists of a double Strep II and a single FLAG tag and can be used on the N- and C-terminal end of the POI. The optimization of the original TAP tag led to a reduced size of the tag (~5 kDa) and the removal of the cleavage process after the first binding step. In the first purification step the POI, fused to the SF-TAP-tag, is bound

to Strep-tactin by the Strep II tag. After elution with desthiobiotin, the eluate is incubated with anti-FLAG-M2 agarose to further enrich the native protein complexes. The final elution is then performed by incubation with FLAG peptide.

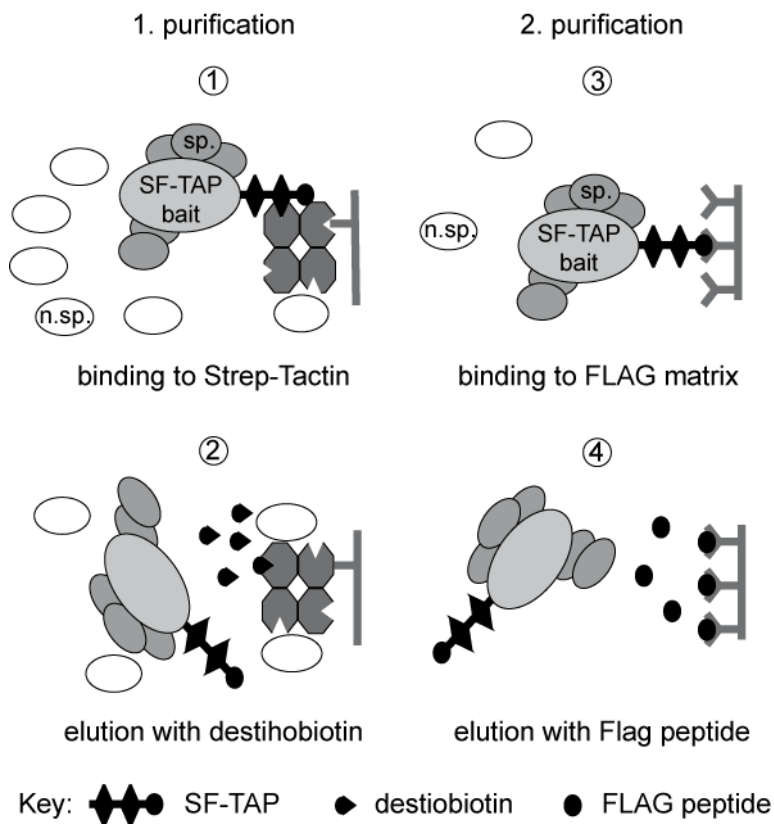


Figure 11: SF-TAP workflow.

1) Purification by the Strep-tag II tag: binding to Strep-Tactin matrix followed by elution with desthiobiotin. 2) Purification by the FLAG-tag: binding to anti-FLAG M2 agarose by elution with FLAG peptide. Abbreviations: sp: specific interactors, n.sp: nonspecific proteins. This figure is reprinted from Gloeckner et al. (116) with friendly permission of John Wiley and Sons.

There are clear differences between TAP and one-step affinity purification. The major advantage of SF-TAP, or similar TAP approaches, is the quick detection of stable complexes. Thereby these methods can be applied for medium to high throughput studies. The stringent isolation of the POI by sequential purification with two different epitopes only allows the enrichment of stable complexes, which at the same time is the main disadvantage of this method. In contrast, the one-step affinity purification allows a more sensitive detection of interaction partners compared to TAP. The identification of more labile and transient complex components can be the result. However, the sensitivity and purification of transient interaction partners is accompanied by the co-purification of hundreds to thousands of non-specific

contaminants. The choice of the right method depends on the needs of the experimental setup and has to be well considered.

4.1.2. Sucrose density centrifugation

Density centrifugation is a common method to separate cells, subcellular compartments and protein complexes (117-120). There are a lot of different solutions available for these gradients but the principle is the same. Particles are separated according to their size and/or their density by application of centrifugational force in viscous solutions (121). Due to the high toxicity of some of the formerly used chemicals, the most commonly used solutions for density centrifugation nowadays are sucrose, polysucrose (Filcoll) or polyvinylpyrrolidone-coated colloidal silica (Percoll). Low molecular weight molecules like sucrose, caesium chloride (CsCl) or sodium bromide (NaBr) have the disadvantage of a high osmolality, causing problems with cells or subcellular particles sensitive to osmosis. Filcoll and Percoll in contrast, have a much lower osmolality and are therefore much more suitable for those purposes.

There are two different methods of gradient centrifugation. Differential centrifugation by equilibrium (isopycnic centrifugation) is a method where the particles separate due to their density. The analytes attain a certain position within the gradient, where the density of the surrounding solution equals their own density. The particles will remain at their equilibrium independent of the centrifugation time, which is rather long and takes usually between 8 to 16 hours. Differential centrifugation by velocity (rate-zonal centrifugation) separates the analytes by their shape and size. Using rate-zonal centrifugation the molecules are separated in a relatively short time period (1-3 hours). The centrifugation time defines the separation state and no equilibrium within the gradient is reached. Therefore the centrifugation has to be stopped before the first particles reach the bottom of the centrifugation tube. Usually soluble protein complexes have similar densities which makes the rate-zonal centrifugation the method of choice for their separation (122).

Additionally, the separation of protein complexes by ultracentrifugation can be classified by the use of different gradients: continuous and discontinuous gradients. In continuous gradients the concentration of the solution increases steadily whereas discontinuous gradients are formed by layers of different concentrations. The use of

the different gradients depends on the needs of the application. Continuous gradients provide a better resolution than discontinuous gradients, which can result in higher purity of the resulting fractions (123). Nevertheless, discontinuous gradients are much easier to handle and more reproducible than the continuous gradients.

It also needs to be mentioned that for density centrifugation mostly swing-out rotors are used, enabling a continuous separation in radial direction. Still there are some protocols where density centrifugation is performed in fixed-angle rotors (124).

4.2. Quantitative analysis of native protein complexes

For the analysis of protein complexes, quantification has become an indispensable tool. For example, during affinity purification, specific and non-specific interaction partners can be discriminated by quantitative methods. Furthermore, two different states of an interactome of a specific protein (e.g. wild type and mutated protein) can be compared in one experiment. These methods are based on mass spectrometry, nowadays a widely-used technique in protein sciences that almost completely replaced methods like 2D-gel electrophoresis.

4.2.1. Mass spectrometry and quantitative protein complex analysis

During recent decades mass spectrometry (MS) has become increasingly powerful tool to analyse protein complexes and their interactions (125). The development in computing power, software and databases offers new possibilities and challenges. The increase in sensitivity of mass spectrometers not only provides advantages but increases the background and the detection of non-specific binding partners as well (126). Therefore, the field of MS shifted more and more from qualitative to quantitative approaches. In contrast to identifying as many proteins as possible to generate a long list, the quantitative information is getting more and more important. The abundance and stoichiometry of the identified proteins now play a greater role which is of great help to illuminate biological mechanisms based on MS-based studies (127).

For general understanding the principle of mass spectrometry will shortly be introduced here. In mass spectrometric approaches there is a wide variety of different methods, but in general the main steps are the same and can be explained as depicted in Figure 12 (128).

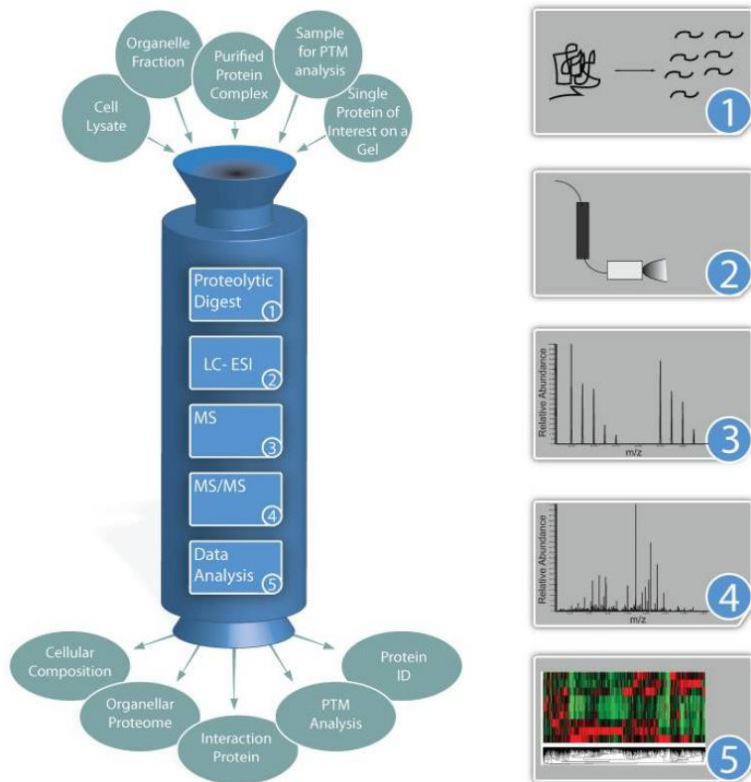


Figure 12: Typical workflow of a mass spectrometry approach.

Samples that are applied to mass spectrometry are prepared from various tissues and methods and enter the workflow. 1) Proteins are cleaved by the enzyme of choice into small peptides. 2) The peptides are enriched and separated by liquid chromatography (LC). In case of an electrospray ionisation (ESI) the LC system is directly connected to the MS and the peptides are introduced to the mass spectrometer. Other types of ionization require different treatment before being introduced to the MS and the eluting peptides can be fractionated at the elution step. 3) A precursor scan (full scan, MS) is performed to choose the most intense peptides. 4) The chosen peptides from the previous scan are fragmented and sequenced (MS/MS). 5) The generated data can afterwards be analysed by different software and databases according to the corresponding method or approach. Abbreviations: LC-MS/MS: liquid chromatography coupled online to mass spectrometry, MS: mass spectrometry, MS/MS: tandem mass spectrometry, PTM: post-translational protein modification, Protein ID: protein identification, m/z : mass-to-charge ratio. This figure is reprinted from Walther et al. (128) with friendly permission of Rockefeller University Press.

Firstly, the protein samples, deriving from different methods and sources enter the workflow before being cleaved by an enzyme into small peptides. The peptide mixture is then separated by a liquid chromatography (LC) system. The LC system can be directly coupled to the MS if an electrospray source is used. Otherwise, the fractions are collected and suitably prepared for being analysed by the MS. After ionization, the peptides entering the MS are detected by an initial so-called full scan where the most intense peptides can be chosen for further fragmentation. The

selected peptides are then fragmented in a collision cell and the fragments analysed to read out the peptides amino acid sequence. By the analysis of the generated spectra by different software tools and databases the derived data are assigned to the corresponding proteins and can be evaluated.

The combination of quantification with mass spectrometric analysis proved to be of great benefit. In this study several different quantitative mass spectrometric approaches were applied, therefore the most commonly used methods will be presented here.

4.2.2. Stable isotope labelling by amino acids in cell culture (SILAC)

Stable isotope labelling by amino acids in cell culture (SILAC) is the most commonly used approach for quantitative mass spectrometry (129). Isotopically labelled, essential amino acids are added to amino acid deficient cell culture media and therefore incorporated into all proteins as they are synthesized. Protein populations from experimental and control samples are mixed in equal amounts directly after harvesting and the samples are applied to the already mentioned workflow for mass spectrometry. As every peptide contains either normal or labelled amino acids, protein samples differ in mass, they appear as doublets in the acquired MS-spectra. SILAC is a relative quantitative technique and is considered to be the most accurate method since all peptides are labelled and samples can be combined at early stages of the experiment (130).

The analysis of mass spectrometric data from quantitative proteomics approaches is a big challenge for computational biology. The development of a powerful tool for their analysis was a milestone within this field. The software MaxQuant was developed by Cox and co-workers in 2008 and is a freely available tool for the analysis of raw-data from LTQ-Orbitrap mass spectrometers (131).

Quantitative mass spectrometric data, like those from SILAC experiments, are analysed by comparing the signals from differently labelled peptides of the same species. The signal of a peptide is represented by a curve, indicating its mass-to-charge ratio over the time in the mass spectrum (Figure 13). One peptide elutes in a peak over several seconds/minutes and is therefore detected several times by the MS. This results in the acquisition of several 2D peaks per peptide. Additionally, even more peaks for this peptide occur due to the natural isotope pattern of the atoms

within the peptide. Calculating the area beyond the peaks and summarizing the area of all of them for one peptide results in an accumulation of 3D (volume) peaks, which are then assembled to one single 3D peak. This volume peak represents the total abundance of the peptide within the sample by a 'number'. A protein consists of several peptides, occurring at different time points of the measurement. Adding up the volume peaks of all peptides gives information about the amount of protein within the sample. This value of a heavy-isotope labelled protein can now be compared to the value of a light-labelled protein to calculate its relative quantity within the sample.

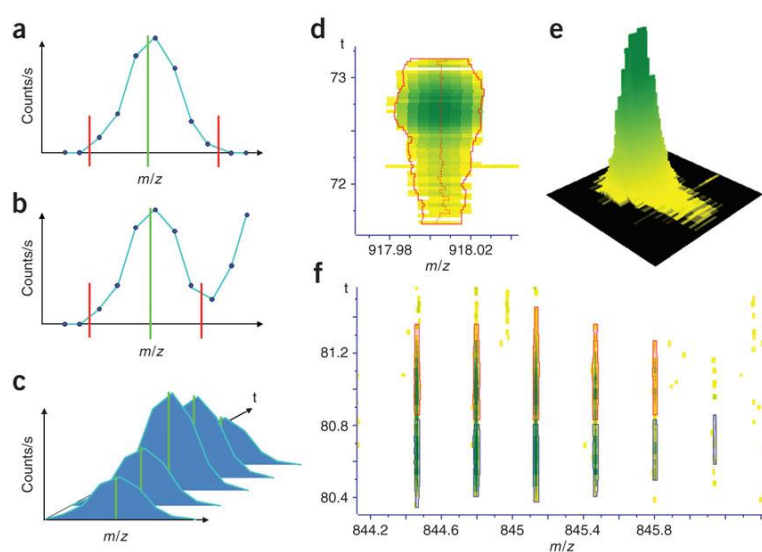


Figure 13: Three dimensional peak detection by the MaxQuant software.

a 2D peak with both edges dropping intensity to zero whose area is calculated by application of a Gaussian shape to the three central data points. **b** 2D peaks where not both sides reach zero are broken at the local minima. **c** 2D peaks that occur in near retention time are assembled to a 3D peak when the mass-charge ratio is close enough. **d + e** 3D peak over a retention time of 1.5 minutes with color-coded intensities. **f** Eleven 3D peaks that form in total two isotopic patterns. While the masses of the two isotopic patterns are the same, they have different retention times. The last peak on the right is only detected in the lower isotopic pattern, whereas it was not detected in the upper pattern. This figure is reprinted from Cox et al. (131) with friendly permission of Nature Publishing Group.

In a SILAC experiment the differences of one protein complex under different conditions (e. g. wild type bait protein versus mutated bait protein) can be analysed. The output normally shows a lot of non-specific proteins that have a ratio of 1:1 (ratio abundance condition 1 to abundance condition 2) and a few proteins that are altered. This can for example indicate the loss of interaction to a mutated bait protein in comparison to the wild type protein (50).

4.2.1. Further stable isotope labelled quantification methods

There is a wide variety of different labelling methods that are applied in proteomics and have been reviewed in detail elsewhere (132, 133). One has to distinguish between the different possibilities of introducing labels: metabolic labelling, chemical labelling and enzymatic labelling (134). The chemical labelling can be applied at different time points during the experiment, either whole proteins or peptides are labelled (Figure 14) and various mechanisms to introduce stable isotopes to the samples can be used (135). One possibility for MS-based quantification is the isotope coded protein label (ICPL), which is based on the isotopic labelling of all free amino groups in proteins (136). This method provides highly accurate and reproducible quantitation, high protein sequence information, including post-translational modifications (PTMs) and isoform information (137). Isobaric tags for relative and absolute quantification (iTRAQ) are a further technique (138). The iTRAQ technique is based on the reaction of isobaric labels with primary and secondary amines of peptides. iTRAQ labelling kits contain up to eight different labels that have an identical mass but fractionate differently in the mass spectrometric analysis by the generation of a reporter ion (139).

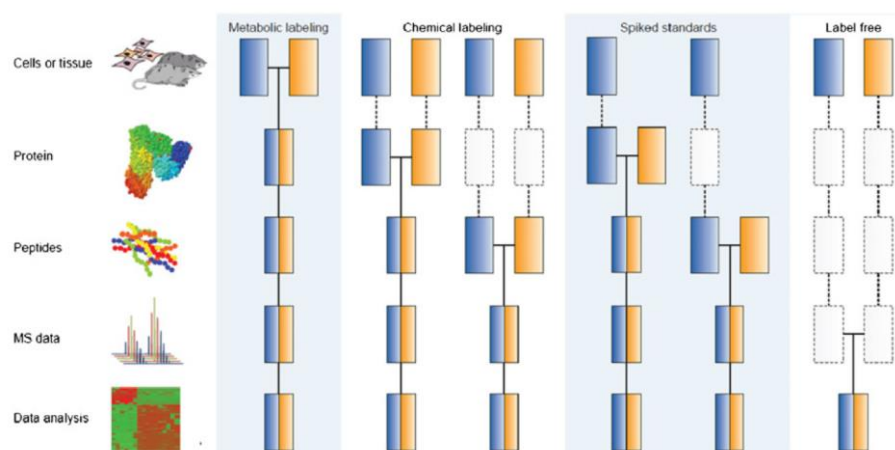


Figure 14: Workflows of commonly used proteomic labelling techniques.

The yellow and blue boxes represent the differently labelled samples. The horizontal lines indicate where the samples are combined and the dashed lines indicate points at which experimental errors can occur. This figure is reprinted from Bantscheff et al. (132) with friendly permission of Springer.

All of the techniques described here represent methods of relative quantification. For the modelling of interaction networks it is of great advantage to carry out absolute quantification as well. One method using absolute quantification is AQUA (140). In an AQUA experiment synthetic, stable isotope-labelled internal standard peptides are

introduced to a protein sample in known amounts (141, 142). Analysis of the proteolyzed sample by a selected reaction monitoring (SRM) experiment in a triple quadrupole tandem mass spectrometer results in the direct detection and quantification of both, the native peptide and isotope-labelled AQUA internal standard peptide. This enables the determination of the stoichiometry within a protein complex and allows to gain deeper understanding of its function (143). However, the complexity and costs of these approaches are not suitable for large-scale studies with protein complexes consisting of many members.

4.2.2. Label-free quantification

The label-free approach is a technique where unlabelled proteins from different MS runs can be quantified against each other. The efficiency of the ionization process of an electrospray source has a large variability between different MS runs due to various technical and chemical reasons for example ion suppression (144). Furthermore, even modest differences in handling of samples during the preparation process, as well as cross-talk between co-eluting compounds from the LC system, can affect the outcome of the mass spectrometric analysis. This presents a potential source of error and therefore these experiments have to be planned and executed very accurately. Still, this technique becomes more and more popular in the last years (145).

There are two different methods of label-free quantification which are based on different information from the MS data. For the first method the area under the chromatographic peak of a precursor ion of a specific peptide is calculated, indicating the relative intensity of the particular peptide (similar to the SILAC method already mentioned in section 4.2.2, (146)). The second method takes the number of the corresponding MS/MS spectra of a particular peptide into account and is therefore called spectral counting (147). Due to the higher variability of the data a relatively high number of replicates is needed to achieve reliable results. Yet, the improvement of reproducibility by the newly invented ultra-high pressure liquid chromatography systems (UHPLC) and high resolution mass spectrometers makes this technique more attractive in cases where metabolic or chemical labelling techniques are not available.

II. Aim of the study

The research field of cilia biology and ciliopathies has dramatically grown over the last few years. The understanding of the genetic basis of ciliopathies, has advanced particularly rapidly since the advent of next generation sequencing of large patient cohorts. With this rapid discovery of many new ciliopathy proteins many remain poorly characterized and little is known about their exact function within the cilium. A focus on determining their function in normal human development and human developmental disease and their function within the cilium in general, as well as their role within molecular machines is therefore of great importance.

Protein analysis is a research area which has changed a lot within the last few years. New standardized protocols for affinity purification of protein complexes in combination with high-resolution mass spectrometers represent the state of the art for high-throughput analysis of large protein networks, determining molecular machines and signalling pathways. Various labelling techniques, as SILAC, ICPL or iTRAQ, allow quantitative approaches and gain more sensitivity in purifying the analysed interactomes. The knowledge about the wiring, composition and dynamics of large protein networks, derived from proteomic approaches gain deeper understanding into molecular processes and pathways of those networks.

The main aim of this project was to gain further insights into the intraflagellar transport system. Various studies showed its importance to the function of the cilium and the extent of its dysfunction in human disease. Still, the detailed function of the transport mechanism as well as the exact composition of the IFT particle remains elusive. Therefore, the development, optimization and application of new proteomic methods to improve and expand understanding about the IFT were the focus of the present study.

Objective 1:

The first aim of this study was to develop and optimize a method to gain more insight into the sub-structure of large protein complexes. This is the basis for the elucidation of networks of those protein complexes, which is needed to understand the function of sub-modules within molecular machines and signalling pathways. Reproducibility and robustness as well as investment of time and cost should be optimized within this

method. Furthermore, this technique should be applicable to small amounts of protein sample, derived from cultured mammalian cells and be suitable for quantitative mass spectrometry to maximize the sensitivity of the assay. The protein complex of Lebercilin was used for validation of this method as it was characterized in detail in a previous study (50).

Objective 2:

Our previous work (50) showed the importance of the IFT complex for the function of the cilium. Therefore, it was of great interest for the deeper understanding of the IFT, to characterize the components of the IFT further. The detailed characterization of the IFT-B was selected as target for this study. The exact composition of the IFT-B was still not entirely known, several components were associated to the complex but their function remained elusive. This task was approached by the analysis of the interactomes of selected components of the IFT-B, using SF-TAP purification and sucrose density centrifugation coupled to mass spectrometry. Furthermore, the knockdown of several central components of the complex by siRNA was undertaken to gain more insight into their function within the IFT-B. The results of this study allow generation of a predicted network for the IFT-B to understand its sub-structure.

Objective 3:

Additional to the characterization of the IFT-B, the characterization of one of the IFT-B-associated proteins in more detail was of interest. The use of the technique developed in Objective 1 revealed the centrosomal protein 170 (CEP170) as a new candidate, associated to the IFT-B. The localization of this protein was analysed by immunofluorescence and siRNA knockdown, and its function was investigated using different purification strategies.

III. Material and Methods

5. Material

5.1. Chemicals

All chemicals were purchased from Sigma-Aldrich (Taufkirchen, Germany) or from VWR International (Darmstadt, Germany).

All cell culture reagents were purchased from Invitrogen (Karlsruhe, Germany). In this study, dH₂O refers to deionized water, ddH₂O ultra-pure water (Barnstead Nanopure, Thermo-Fisher Scientific, Bonn, Germany).

5.2. General equipment

Analytical balance ABJ120-4M	Kern&Sohn GmbH, Balingen, Germany
Autoclave Systec DX-150	Systec, Wettenberg, Germany
Cell culture plates 6-well/10cm/14cm	Nunc, Wiesbaden, Germany
Centrifuge HERAEUS Pico21	Thermo-Fisher Scientific, Bonn, Germany
Centrifuge HERAEUS Fresco17	Thermo-Fisher Scientific, Bonn, Germany
Falcon conical tubes 15/50 mL	BD Bioscience, Heidelberg, Germany
Magnetic stirrer Ikamag RCT	IKA Labortechnik, Staufen, Germany
Microspin columns	GE Healthcare, Freiburg, Germany
MILLEX GP; syringe filter unit, 0.22 µm	Millipore, Bedford, USA
Barnstead Nanopure	Thermo-Fisher Scientific, Bonn, Germany
Precision scales 572	Kern&Sohn GmbH, Balingen, Germany
Safe lock reaction tubes 0.5/1.5/2.0 mL	Eppendorf, Hamburg, Germany
Shaker Duomax 1030	Heidolph Instruments, Schwabach, Germany
SpeedVac concentrator SPD111V	Thermo-Fisher Scientific, Bonn, Germany
Refrigerated Vapor-Trap RVT400	Thermo-Fisher Scientific, Bonn, Germany
Vacuum pump Laboport	KNF Neuberger GmbH, Freiburg, Germany

Steritop-GP filter unit, 0.22 µm	Millipore, Bedford, USA
Ultra-low temperature freezer Forma 900 Series	Thermo-Fisher Scientific, Bonn, Germany
Sonorex Digitech DT103H	Bandelin, electronic, Germany
UV/VIS spectrometer T70	PG instruments, Wibtoft, England
Disposable cuvettes	Sarstedt, Nümbrecht, Germany
Quartz cuvette	Carl Roth, Karlsruhe, Germany
Vortex Genie 2	Scientific Industries, VWR, Darmstadt, Germany
Water bath WNB14	Memmert, Schwabach, Germany
Water bath shaking unit SV1422	Memmert, Schwabach, Germany
Water bath 2333	Thermo Fisher Scientific, Bonn, Germany
Microscope Primo Vert	Zeiss, Jena, Germany
Thermomixer Univortemp	Universal Labortechnik, Leipzig, Germany
Heraeus oven T20	Thermo-Fisher Scientific, Bonn, Germany
Vacuum pump 2522Z-02	Welch IImvac, Ilmenau, Germany
Metal block thermostat MBT250-2	EGT, Ilmenau, Germany
Rotating mixer RM5	Karl Hecht, Sondheim, Germany
Heraeus Multifuge X3R	Thermo-Fisher Scientific, Bonn, Germany
Ice machine AF200	Scotsman, Milan, Italy
Dishwasher Mielabor G7783	Miele, Gütersloh, Germany
pH meter PB11	Sartorius, Göttingen, Germany
Titramax 100 shaker	Heidolph, Schwabach, Germany
Intelli-mixer RM-2M	LTF Labortechnik, Wasserburg, Germany
Rotator 2-1175	Neolab, Heidelberg, Germany
Heraeus Megafuge 16	Thermo Fisher Scientific, Bonn, Germany
Diamond Tips DL10/D200/D1000	Gilson, Middleton, WI, USA

Disposable serological pipettes 5 mL/10 mL/25 mL	Greiner bio-one, Kremsmünster, Austria
Omnifix- luer lock syringes 5/50 mL	B. Braun Melsungen AG, Melsungen, Germany
2 mL centrifugation tubes 347356	Beckman Coulter, Krefeld, Germany
Optima TLX UZ ultra centrifuge	Beckman Coulter, Krefeld, Germany

5.3. Molecular biology

5.3.1. Special equipment

Incubator UE400	Memmert, Schwabach, Germany
Shaker Ecotron	Infors, Bottmingen, Switzerland
Primus PCR cyclers	MWG Biotech, Ebersberg, Germany
SubCell GT chambers	BioRad, Munich, Germany
UV transilluminator UVT-40M	Herolab, Wiesloch, Germany
BD Falcon 14 mL polypropylene round-bottom tubes	BD Bioscience, Heidelberg, Germany
7500 Real Time PCR system	Applied Biosystems, Forster City, USA

5.3.2. Kits and special reagents

Gateway BP Clonase II enzyme mix	Invitrogen, Carlsbad, USA
Gateway LR Clonase II enzyme mix	Invitrogen, Carlsbad, USA
Phusion High-fidelity PCR Kit	New England Biolabs, Ipswich,
GeneJET Plasmid Miniprep Kit	Thermo Fisher Scientific, Bonn, Germany
GeneJET Gel Extraction Kit	Thermo Fisher Scientific, Bonn, Germany
GeneJET PCR Purification Kit	Thermo Fisher Scientific, Bonn, Germany
EndoFree Plasmid Maxi Kit	Qiagen, Hilden, Germany
TRizol reagent	Invitrogen, Carlsbad, USA
Moloney murine leukemia virus reverse transcriptase (M-MLV RT)	Invitrogen, Carlsbad, USA

random primer	Invitrogen, Carlsbad, USA
5x M-MLV RT buffer	Invitrogen, Carlsbad, USA
RNAsin	Promega. Madison, USA
Power SYBR Green PCR Master Mix (5x)	Life Technologies, Darmstadt, Germany

5.3.1. Enzymes

All restriction enzymes and DNA ladders were purchased from New England Biolabs (Ipswich, USA). T4 DNA ligase and Taq DNA polymerase were purchased from MBI Fermentas (St.Leon-Rot, Germany).

5.3.2. *Escherichia coli* strains

DH5 α Invitrogen, Carlsbad, USA

5.3.3. Oligonucleotides

All oligonucleotides were purchased from Metabion (Martinsried, Germany).

Table 3: Oligonucleotides.

The following oligonucleotides were used for sequencing or cloning reactions. The sequences are displayed in 5' to 3' orientation.

primer name	sequence
pcDNA3_fw	GCGGTAGGCGTGTACGGTGGG-3'
pcDNA3_rv	GGGCAAACAACAGATGGCTGGC-3'
T3	AATTAACCCTCACTAAAGGG-3'
T7	TAATACGACTCACTATAGGG-3'
CEP170_NGW_f	AAAAGCAGGCTTCATGAGCTTAACATCCTGGTT
CEP170_NGW_r	AAGAAAGCTGGGTGTCATTCTTGTACTGTAACATC
CEP170_CGW_f	AAAAGCAGGCTTCGAAGGAGATAGAACCATGAGCTTAACATCCTGGTT
CEP170_CGW_r	AAGAAAGCTGGGTGTTCTTGTACTGTAACATCTTCC

Table 4: qPCR primer.

The oligonucleotides indicated in this table were used as primers for the quantitative PCR reactions. The sequences are displayed in 5' to 3' orientation.

primer name	sequence
For-Arl13b_ex5	AACAGCGAGCTCTTGAGGAA
Rev-Arl13b_ex6	ACCACTGGTCCCATCAAGTT
For-Cep170_ex14	GACTGCCCATCGAGAAGAGA
Rev-Cep170_ex15	GTGCCTGAGGAAGTCACTGA
For-lft52_ex12	CCCTGGAGCTGTTTGACCTA
Rev-lft52_ex13	TCGCCACACTTCCTGACATA
For-lft88_ex21	TGAAGTGGCAGCTGATGGTA
Rev-lft88_ex23	TGTGCAGAGACGAACCAAGA
For-Ttc30a1_ex1	TCCAGACTGTTGAAAGCTTTGA
Rev-Ttc30a1_ex1	TCAAAGCTTAGAGTTGAAACACA
For-Ttc30b_ex1	GGAATGTGTAATTACCGCTGACA
Rev-Ttc30b_ex1	GTGTACAAAGTCTCACAAGTAGCA
For-bActin_ex5	GCTGACAGGATGCAGAAGGA
Rev-bActin_ex5	CCACCGATCCACACAGAGTA
For-Gapdh_ex4	CTGCACCACCAACTGCTTAG
Rev-Gapdh_ex5	GTCTTCTGGGTGGCAGTGAT
For-Hprt1_ex2	GCGATGATGAACCAGGTTATGA
Rev-Hprt1_ex3	GCCTCCCATCTCCTTCATGA
For-Sdha_ex8	TGGAGAGATACGCACCTGTT
Rev-Sdha_ex9	TTGCTCAGGAGGCAGATGAT

5.3.4. Plasmids and constructs

5.3.4.1. DNA constructs

Table 5: DNA constructs.

This table shows the DNA constructs that were used for gateway cloning reactions. The providers are as follows, Invitrogen, Carlsbad, USA; JG: Johannes Gloeckner, Munich, Germany. Abbreviations: Amp ampicillin, Kan: kanamycin.

Plasmid name	Description	Resistance	Provider
pcDNA3	Mammalian expression vector	Amp	Invitrogen
pcDNA3-SF-TAP	SF-TAP expression vector	Amp	JG
pDEST-N-SF-TAP	GATEWAY SF-TAP vector	Amp	Invitrogen/JG
pDEST-C-SF-TAP	GATEWAY SF-TAP vector	Amp	Invitrogen/JG
pDONR201	GATEWAY donor vector	Kan	Invitrogen

5.3.4.2. DNA plasmids

Table 6: DNA plasmids.

This table shows the used DNA plasmids as well as their provider RR: Ronald Roepman, Nijmegen, The Netherlands; EN: Erich Nigg, Basel, Switzerland. Abbreviations: Amp: ampicillin, Kan: kanamycin.

Plasmid name	Description	Resistance	Provider
IFT20-N-SF-TAP	Mammalian expression vector	Amp	RR
IFT27-N-SF-TAP	Mammalian expression vector	Amp	RR
IFT52-N-SF-TAP	Mammalian expression vector	Amp	RR
IFT57-N-SF-TAP	Mammalian expression vector	Amp	RR
IFT88-N-SF-TAP	Mammalian expression vector	Amp	RR
IFT27-N-SF-TAP	Mammalian expression vector	Amp	RR
LCA5-N-SF-TAP	Mammalian expression vector	Amp	RR
TULP3-N-SF-TAP	Mammalian expression vector	Amp	RR
CEP170-eGFP	Mammalian expression vector	Kan	EN
CEP170-N-SF-TAP	Mammalian expression vector	Amp	-
CEP170-C-SF-TAP	Mammalian expression vector	Amp	-
RANBP9-N-SF-TAP	Mammalian expression vector	Amp	RR

5.3.5. siRNA sequences

Table 7: siRNA sequences.

This table shows the sequences of the siRNA pools used. One pool contains 4 siRNA duplexes targeting one gene. All siRNAs were ON-TARGETplus siRNAs provided by Dharmacon, a subsidiary of Thermo Scientific.

Gene name	gene-ID	name	sequence
<i>Arl13b</i>	68146	Arl13b_1	AGGACCAGUUCUUGCGAAU
		Arl13b_2	GGGCUGAACGAGUCCGGAA
		Arl13b_3	AGAGCAUCCUGAAGACGUA
		Arl13b_4	UGGAGAAGCUGGUCAACGA
<i>Cep170</i>	545389	Cep170_1	GAAAGAAAGUCCACGCAA
		Cep170_2	GAGAAGAGUGAGACGGAAA
		Cep170_3	GCAAGUAGACUCCGAGAAA
		Cep170_4	GAGGAUUCCAAGAGCAUUA
<i>lft52</i>	245866	lft52_1	GCAGAAAAGACUUCGGAGU
		lft52_2	ACCCAGAGAUUUCCGACUA
		lft52_3	GAUGAUGAUCCUUCGAGAA
		lft52_4	GAGAAGGAGCUGCGGAGUA
<i>lft88</i>	21821	lft88_1	GUAGCUAGCUGCUUUAGAA
		lft88_2	CGUCAGCUCUCACUAAUAA
		lft88_3	GCUUGGAGCUUAUUACAUU
		lft88_4	CGGAGAAUGUUGAAUGUUU
<i>Ttc30a1</i>	78802	Ttc30a1_1	AGAUGUAGGUUUUAGACGA
		Ttc30a1_2	GGAAGUACCAUCCGAUAAA
		Ttc30a1_3	CUAAAGUUCCCGACGGUGA
		Ttc30a1_4	UGUCAAAAGCACAUGAUAGU
<i>Ttc30b</i>	72421	Ttc30b_1	CAAAAGCACUAUUCGAUUAU
		Ttc30b_2	UGAGAUAAUUGGAUGGAAU
		Ttc30b_3	GUCAAGUGAGAUUGUGUAA
		Ttc30b_4	ACAAUUAUGCUAAGGGACA

5.4. Mammalian cell culture

5.4.1. Special equipment

CO ₂ incubator Hera cell 150i	Thermo Fisher Scientific, Bonn, Germany
Laminar flow Hera safe HS12	Thermo Fisher Scientific, Bonn, Germany
Suction Device for Cell Culture	Neolab, Heidelberg, Germany
Cryo tank MVE Tech 3000	GermanCryo, Jüchen, Germany

Pasteur pipette 230/120 mm	Witeg Labortechnik GmbH, Wertheim, Germany
Cryotubes, 1.8 mL	Nunc, Wiesbaden, Germany
Cell scraper 25 cm	Sarstedt, Nümbrecht, Germany

5.4.2. Special reagents

¹³ C6 L-Arginine-HCl	Thermo Fisher Scientific, Bonn, Germany
¹³ C6-L-Lysine	Silantes, Munich, Germany
¹³ C6 ¹⁵ N2-L-Lysine	Silantes, Munich, Germany
¹³ C6-L-Arginine	Silantes, Munich, Germany
¹³ C6 ¹⁵ N4-L-Arginine	Silantes, Munich, Germany
D4-L-Lysine	Silantes, Munich, Germany
FBS dialyzed	PAA, Pasching, Austria
L-Glutamine	PAA, Pasching, Austria
L-Proline	Silantes, Munich, Germany
L-Arginine	Silantes, Munich, Germany
L-Lysine	Silantes, Munich, Germany
SILAC DMEM	PAA, Pasching, Austria
Polyethylenimine (PEI)	PolySciences, Warrington, USA
RNAiMAX	Invitrogen, Carlsbad, USA
Dulbeccos's Modified Eagle Medium	Invitrogen, Carlsbad, USA
Dulbeccos's Modified Eagle Medium	Invitrogen, Carlsbad, USA
Opti-MEM and Ham's F12 medium	Invitrogen, Carlsbad, USA
Fetal bovine serum	PAA, Pasching, Austria
Dulbecco's PBS	PAA, Pasching, Austria
Trypsin/EDTA	PAA, Pasching, Austria
G418	Biochrom, Berlin, Germany

5.4.3. Mammalian cell lines

Table 8: Mammalian cell lines.

This table shows the used mammalian cell lines within this study.

Cell line name	Description	Provider
HEK293	Human embryonic kidney cells	DSMZ, Braunschweig, Germany
HEK293-T	Human embryonic kidney cells	Walter Kolch, Glasgow, UK
hTERT RPE1	Human telomerase reverse transcriptase retinal pigmentary epithelial cells	Ronald Roepman, Nijmegen, The Netherlands
IMCD3	Mouse inner medullary collecting duct	ATCC, Manassas Virginia

5.5. Protein chemistry

5.5.1. Special equipment

Agfa Curix 60 Developer	Agfa, Cologne, Germany
Scanmaker i800	Microtech, Hsinchu, Taiwan
Hybond PVDF membranes	GE-Helthcare, Freiburg, Germany
Immobilion-P Transfer membrane	Millipore, Bedford, USA
Mini Protean 3 for SDS-PAGE	BioRad, Munich, Germany
Mini Trans-Blot cell	BioRad, Munich, Germany
NuPAGE NOVEX Bis-Tris gels	Invitrogen, Carlsbad, USA
Power Supply Power Pac 3000	BioRad, Munich, Germany
Trans-Blot SD semi-dry transfer blot	BioRad, Munich, Germany
XCell SureLock Mini-Cell	Invitrogen, Carlsbad, USA
Multiscreen apparatus Mini-Protean II	BioRad, Munich, Germany
Amersham Hyperfilm ECL	GE-Helthcare, Freiburg, Germany
Hypercassette 18 x 24 cm	GE-Helthcare, Freiburg, Germany
Whatman chromatography papers	Th. Geyer, Renningen, Germany
Illustra MicroSpin columns	GE-Helthcare, Freiburg, Germany
Vivaspin 500 centrifugal concentrator	GE-Helthcare, Freiburg, Germany

5.5.2. Special reagents

Blotting Grade Blocker non-fat dry milk	BioRad, Munich, Germany
Bovine serum albumin (BSA)	PAA, Pasching, Austria
Enhanced chemiluminescence kit	GE-Healthcare, Freiburg, Germany
NuPAGE MES SDS running buffer	Invitrogen, Carlsbad, USA
PageRuler Prestained Protein Ladder	Thermo Fisher Scientific, Bonn, Germany
Bio-Rad Protein Assay Kit	BioRad, Munich, Germany
10x buffer E (Desthiobiotin)	IBA, Göttingen, Germany
Anti-FLAG M2 Affinity Gel	Sigma-Aldrich, Taufkirchen, Germany
Strep-Tactin Superflow	IBA, Göttingen, Germany
Protease Inhibitor Cocktail	Roche, Freiburg, Germany
Phosphatase Inhibitor Cocktail 3	Sigma-Aldrich, Steinheim, Germany
Phosphatase Inhibitor Cocktail 2	Sigma-Aldrich, Steinheim, Germany

5.6. Immunocytochemistry

5.6.1. Special equipment

Axio Imager Z1 ApoTome with an AxioCam camera	Zeiss, Oberkochen, Germany
Eclipse A1R confocal laser microscope	Nikon, Tokio, Japan
Operetta high-content wide-field fluorescence imaging system	PerkinElmer, Waltham, USA
Optical-bottomed 96-well View Plates	PerkinElmer, Waltham, USA
Superfrost glass slides	Thermo Fisher Scientific, Bonn, Germany
Coverslips round, 12 mm	VWR International, Darmstadt, Germany
Coverslips square 20 mm	VWR International, Darmstadt, Germany

5.6.2. Special reagents

Mowiol 4-88 mounting medium	Merck, Darmstadt, Germany
Vectashield Mounting Medium	Linaris, Dossenheim, Germany
Immersol TM 518F	Zeiss, Oberkochen, Germany
4',6-diamidino-2-phenylindole (DAPI)	Sigma-Aldrich, Steinheim, Germany
TOTO-3	Invitrogen, Carlsbad, USA

5.6.2.1. Primary antibodies

Table 9: Primary antibodies.

Santa Cruz: Santa Cruz, USA; Cell Signaling: Danvers, USA; Sigma-Aldrich: Taufkirchen, Germany; Millipore: Bedford, USA; Greg Pazour: University of Massachusetts Medical School; GeneTex, Irvine, USA; Abnova: Taipei City, Taiwan. Antibodies that were not tested in immuno-fluorescence are marked with n.i. (not identified).

Anti-	Species, type	Dilution western blot	Dilution immuno-fluorescence	Provider
FLAG-M2	Mouse, monoclonal IgG	1:1000	n.i.	Sigma-Aldrich
FLAG-M2- HRP	Mouse, monoclonal IgG	1:1000	n.i.	Sigma-Aldrich
GAPDH	Mouse, monoclonal IgG	1:5000	n.i.	Millipore
IFT52	Rabbit, polyclonal IgG	1:1000	1:200	Greg Pazour
TRAF3IP1	Mouse, polyclonal IgG	1:1000	1:300	Abnova
IFT57	Rabbit, polyclonal IgG	1:1000	1:200	Greg Pazour
IFT88	Goat, polyclonal IgG	1:1000	1:150	Abnova
IFT88	Rabbit, polyclonal IgG	1:500	n.i.	Abnova
WDR19	Mouse, polyclonal IgG	1:250	n.i.	Abnova
14-3-3-ε	Rabbit, polyclonal IgG	1:1000	n.i.	Santa Cruz
C20orf11	Rabbit, polyclonal IgG	1:1000	n.i.	Gene Tex
Acetylated alpha tubulin	Mouse, monoclonal IgG	1:2500	1:1000	Sigma-Aldrich
α/β-tubulin	Rabbit, polyclonal IgG	1:1000	1:50	Cell Signalling

5.6.2.2. Secondary antibodies

Table 10: Secondary antibodies.

The indicated antibodies were used for western blot analysis (HRP-conjugated) and immunofluorescence (Alexa-Fluor-/Cy3-conjugated). Dianova: Hamburg, Germany; Millipore, Bedford, USA; Invitrogen, Carlsbad, USA

Anti-	Species, type	Conjugate	Dilution	Provider
Goat-IgG	Donkey, polyclonal IgG	HRP	1:15000	Dianova
Mouse-IgG	Goat, polyclonal IgG	HRP	1:15000	Dianova
Rabbit-IgG	Goat, polyclonal IgG	HRP	1:15000	Dianova
Mouse-IgG	Goat, polyclonal IgG	Alexa-Fluor-488	1:300	Dianova
Mouse-IgG	Goat, polyclonal IgG fab-fragment	Cy3	1:100	Dianova
Mouse-IgG	Goat, polyclonal IgG	Alexa-Fluor-568	1:700	Millipore
Rabbit-IgG	Goat, polyclonal IgG	Alexa-Fluor-568	1:700	Millipore
Rabbit-IgG	Goat, polyclonal IgG	Alexa-Fluor-488	1:1000	Invitrogen
Mouse-IgG	Goat, polyclonal IgG	Alexa-Fluor-568	1:1000	Invitrogen
Goat-IgG	Donkey, polyclonal IgG	Alexa-Fluor-488	1:1000	Invitrogen
Mouse-IgG	Chicken, polyclonal IgG	Alexa-Fluor-594	1:1000	Invitrogen
Rabbit-IgG	Goat, polyclonal IgG	Alexa-Fluor-568	1:1000	Invitrogen
Mouse-IgG	Goat, polyclonal IgG	Alexa-Fluor-488	1:1000	Invitrogen

5.7. Mass spectrometry

5.7.1. Special equipment

LTQ Orbitrap XL	Thermo Fisher Scientific, Bonn, Germany
LTQ Orbitrap Velos	Thermo Fisher Scientific, Bonn, Germany
Inserts for 2 mL vials	CS Chromatographie Service, Langerwehe, Germany
2 mL autosampler vials	CS Chromatographie Service, Langerwehe, Germany
Caps for autosampler vials	CS Chromatographie Service, Langerwehe, Germany
Ultimate 3000 Nano-RSLC	Dionex, Idstein, Germany
Nano trap column 75 µm i.d. × 2 cm, packed with Acclaim PepMap100 C18, 3 µm, 100 Å	Dionex, Idstein, Germany
Analytical column 75 µm i.d. × 25 cm, Acclaim PepMap RSLC C18, 2µm, 100 Å	Dionex, Idstein, Germany

Stage Tips C-18 Thermo Fisher Scientific, Bonn, Germany

Polypropylen Insert with Bottom Spring Sigma-Aldrich, Taufkirchen, Germany

5.7.2. Kits and special reagents

RapiGestTMSF Waters, Eschborn, Germany

Trypsin from porcine pancreas (proteomics grade) Sigma-Aldrich, Taufkirchen, Germany

5.8. Software and databases

5.8.1. Software

Adobe Illustrator CS4 Adobe Systems, Seattle, USA

Adobe Photoshop CS4 Adobe Systems, Seattle, USA

Mascot 2.2 Matrix Science, Boston, USA

Mascot Daemon 2.2.2 Matrix Science, Boston, USA

MaxQuant J. Cox, M. Mann, Martinsried, Germany (<http://www.maxquant.org/>)

R The R project (<http://www.r-project.org>)

Xcalibur 2.07 Thermo Fisher Scientific, Bonn, Germany

Endnote X4 Thomson Reuters, Carlsbad, USA

Scaffold 3 Proteome Software, Portland, USA

Office 2010 Microsoft, Redmond, USA

AxioVision Zeiss, Jena, Germany

ImageJ NIH, Bethesda, USA

NIS Elements Microscope Imaging Software Nikon, Tokyo, Japan

Vector NTI Suite 9.0, Invitrogen, Carlsbad, USA

5.8.2. Databases and online tools

Ciliary Proteome Database <http://www.ciliaproteome.org/>

NCBI <http://www.ncbi.nlm.nih.gov/>

NCBI Blast <http://blast.ncbi.nlm.nih.gov/Blast.cgi>

NCBI Nucleotide <http://www.ncbi.nlm.nih.gov/entrez/query.fcgi?db=nucleotide>

NCBI Protein <http://www.ncbi.nlm.nih.gov/entrez/query.fcgi?db=protein>

NCBI Pubmed <http://www.ncbi.nlm.nih.gov/entrez/query.fcgi>

Swiss-Prot <http://www.expasy.ch/sprot/>

Uniprot <http://www.uniprot.org/>

Uniref <http://www.ebi.ac.uk/uniref/>

Human first search database <http://maxquant.org/>

Contaminant database <http://maxquant.org/>

6. Methods

6.1. Molecular biology

6.1.1. *Escherichia coli* cultures

Escherichia coli (*E. coli*) bacteria were grown differently depending on the application.

6.1.1.1. Liquid cultures

For the amplification of plasmid DNA liquid cultures of *E. coli* were used. 200 µL of LB-medium (Luria-Bertani; 1% (w/v) tryptone, 0.5% (w/v) yeast extract, 1% (w/v) sodium chloride) supplemented with the corresponding antibiotic were inoculated with single clones containing the target plasmid. After 8 hours of incubation at 37°C the suspension was transferred to 5 mL LB-medium for small scale plasmid purification and respectively to 200 mL for large scale plasmid purification and incubated at 37°C overnight at constant agitation.

6.1.1.2. Plating cultures

For clonogenic selection plating cultures were used. The bacterial suspension was streaked onto LB-plates (LB-medium, containing 1.5% agar, supplemented with the appropriate antibiotic) and incubated overnight at 37°C. Single clones were picked from the plates to inoculate liquid cultures.

6.1.1.3. Generation of cryo stocks

For long-term storage of bacterial cultures 500 μ L of overnight liquid cultures were mixed with 500 μ L 50% (v/v) sterile glycerol. The aliquots were then stored at -80°C .

6.1.1.4. Chemical transformation of *E. coli*

For chemical transformation of *E. coli* the competent bacterial strain DH5 α (Invitrogen) was used. The bacteria were thawed on ice and 50 μ L of the suspension was mixed subsequently with 10-30 ng of plasmid DNA or 5 μ L of a ligation reaction. The mixture was kept on ice for 30 minutes before being incubated at 42°C for 42 seconds to initialize the influx of DNA into the bacteria. Afterwards the suspension was cooled down on ice for one minute and 350 μ L of SOC medium (2% (w/v) tryptone, 0.5% (w/v) yeast extract, 0.05% (w/v) sodium chloride, 20 mM glucose) was added. The suspension was incubated at 37°C at constant agitation for one hour before being plated-out.

6.1.2. Plasmid DNA preparation

For small-scale plasmid DNA preparation 10 mL of liquid, overnight cultured bacteria, transformed with the plasmid of interest were pelleted and the DNA was prepared according to the manufacturer's protocol using the GeneJET Plasmid Miniprep Kit. The concentration of the extracted DNA was determined by photometric measurement of the absorbance at 260 and 280 nm. Therefore the DNA was diluted 1 in 100 in HPLC grade water. The concentration was calculated by the photometers software.

6.1.1. Agarose gel electrophoresis

DNA fragments were separated and isolated using agarose gel electrophoresis. 1% (w/v) agarose was dissolved in TAE buffer (40 mM tris-acetate, 1 mM ethylenediaminetetraacetate (EDTA), pH 8) by heating in a microwave. After boiling the solution was supplemented with 0.5 $\mu\text{g}/\mu\text{L}$ of ethidium bromide and applied to a gel tray with sample comb. Subsequent to solidification, the gel was transferred to an electrophoresis chamber and overlaid with TAE buffer. The DNA samples were diluted in loading buffer (6x: 0.25% (w/v) bromophenol blue, 40% (w/v) sucrose) and loaded onto the gel. For identification of the molecular weight a DNA ladder (GeneRuler 1 kb Plus DNA Ladder, Fermentas) was loaded in the first lane. The

separation was performed at 50V until the bromophenol blue front reached the end of the gel. The bands were visualized by UV light and a digital image was captured.

6.1.2. DNA sequencing

For DNA Sanger sequencing the DNA samples were diluted and adjusted to required volume as specified by the sequencing service Eurofins MWG operon. Standard primers are available at the company and do not have to be provided by the customer. The samples were shipped to the sequencing service and the results were transmitted electronically. The analysis of the sequencing was done using Vector NTI Suite 9.0 software package.

6.1.1. Purification of DNA

6.1.1.1. From agarose gels

After separation of DNA fragments on an agarose gel target bands were visualized under UV light and cut out using a clean scalpel. The DNA was extracted according to the manufacturer's protocol of the GeneJET Gel Extraction Kit

6.1.1.2. From enzymatic reactions

Subsequent to enzymatic reactions the DNA fragments were purified using the GeneJET PCR Purification Kit according to the manufacturer's instructions.

6.1.2. Polymerase chain reaction (PCR)

For the amplification of specific DNA sequences polymerase chain reaction (PCR) was performed according to a standard procedure (148). Two sequence-specific primers that hybridize to the sense and antisense strand of the target DNA and thus define the region of the DNA that is replicated by a DNA polymerase. A cyclic repetition of denaturation (separation of DNA strands), annealing (hybridization of the primers to their complementary sequence) and elongation (synthesis of the complementary strand by the DNA polymerase) results in an exponential replication of the DNA template. PCR reaction was performed on a thermal cycler with the following amplification program:

Step 1: 95°C 2 min denaturation of the dsDNA template

Step 2: 95°C 30 sec denaturation of the dsDNA template

Step 3: 55°C 30 sec	annealing of the primers
Step 4: 72°C 4 min	elongation of the primers
Step 5: 72°C 10 min	final elongation

The amplification stage comprised 30 cycles of step 2 to 4. Conditions of the PCR reaction were optimized according to the size of the PCR product and primers properties. Therefore, the annealing temperature (step 3) was set as the mean value of the melting temperature (T_m) of sense and antisense primer.

6.1.3. Enzymatic treatment of DNA

For restriction digest, 2 μ g of the construct were mixed with 30U of two appropriate restriction enzymes. The optimal buffer and temperature conditions were adapted for each enzyme combination according the manufacturer's instructions. The reaction mix was incubated for two hours before being separated and visualized on an agarose gel.

6.1.4. Gateway cloning

The GATEWAY cloning system is based on the recombination of the bacteriophage λ integrase, which is highly specific to defined recombination sites. The attachment of those recombination sites to a DNA fragment enables the integration of the latter by *in vitro* incubation with bacteriophage λ integrase into a new vector, also bearing the recombination sites (149). In the first step of the cloning procedure, the recombination sites were attached to the DNA fragment by PCR reaction. This was performed by a two-step PCR reaction, that attached the attB1 (attachmentB1) and respectively the attB2 (attachmentB2) sites to the ends of the DNA fragment and afterwards amplified the generated constructs to enhance the efficiency of the following reaction. In this study the primers for the attachment reaction were designed according to Gloeckner et al. 2009 (150). The primers differ, depending on the position of the fused tag to the protein (N- or C-terminal). The primers consist of a gene specific primer (gsp) for the annealing of the target sequence followed by the attB site. For C-terminal tagging, the primer containing the attB1 site additionally had a Kozak sequence in between the gsp and the attB1 site. The detailed structures of the primers are shown in Figure 15. The resulting primer sequences containing the gsp-sequences are listed in Table 3.

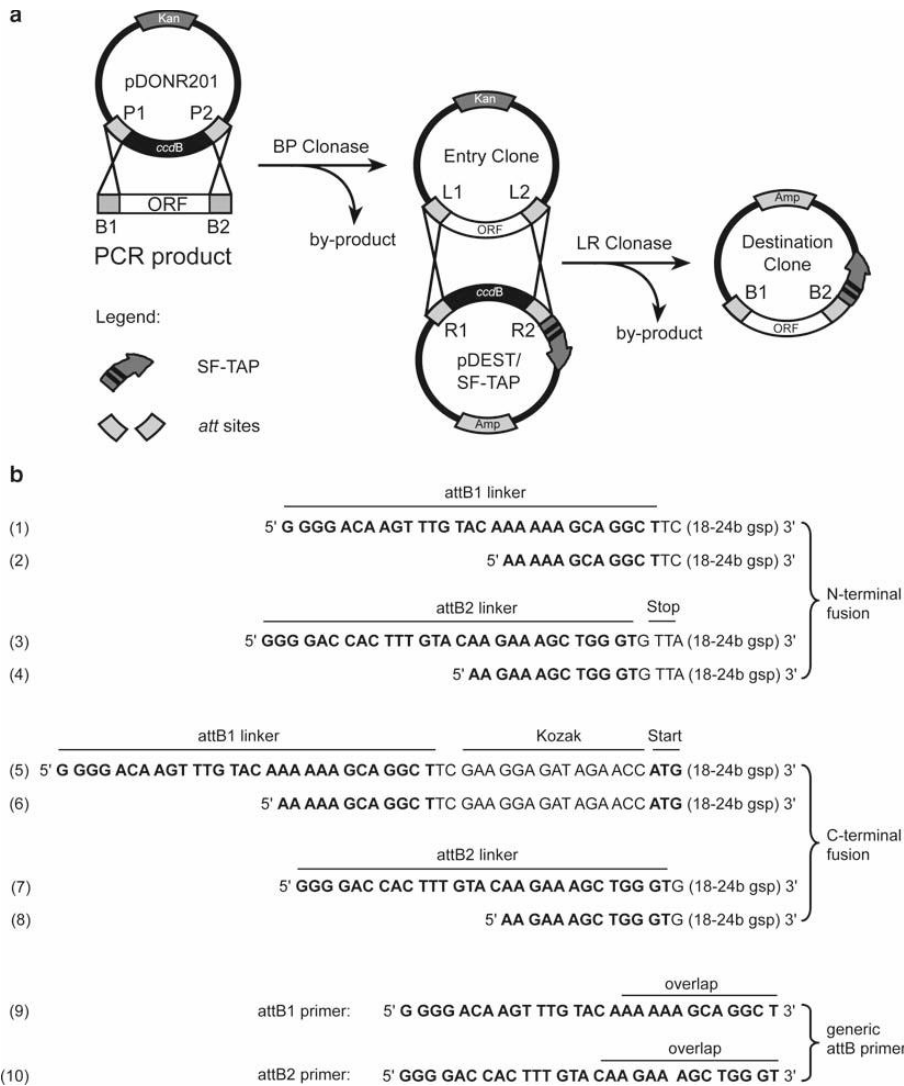


Figure 15: Overview of the GATEWAY cloning strategy.

In this figure the workflow and the primer design for the GATEWAY cloning strategy is shown. **a** Workflow of the GATEWAY cloning strategy. The att-sites are attached to a DNA fragment and the fragment is subsequently integrated to the pDONR201 vector by recombination (BP reaction) forming the Entry vector. Secondly, the target gene is cloned from the Entry vector to the pDEST/SF-TAP vector (LR reaction), which is the final destination clone. **b** Primer design for the initial PCR reaction attaching the attB1 and attB2 sites to the gene of interest. The primer design depends on the position where the SF-TAP tag is fused to the gene of interest (N-terminal or C-terminal). For N-terminal fusion a gene specific primer (gsp) is followed by the attB1 and respectively the attB2 site. In contrast, for C-terminal fusion a Kozak sequence has to be introduced in between the gsp and the attB1 site, whereas the attB2 site is again directly fused to the gsp. A two-step PCR is required for efficient amplification of the fragments; therefore a second PCR reaction is performed using the generic attB primers for the final amplification. This figure is reprinted from Gloeckner et al. (150) with friendly permission of Springer.

In the first step, primers attaching the attB sites to the DNA fragment were used. 10 ng of the DNA were mixed with 5 µL HF-Reaction buffer, 1.3 µL of forward and

reverse primers (10 μ M), 0.5 μ L dNTP mix (10 μ M) and 0.5 μ L of the Phusion Tag Polymerase. De-ionized water was added to a final volume of 25 μ L. The reaction was performed using the following program:

Step 1: 98°C 2 min

Step 2: 96°C 30 s

Step 3: 55°C 40 s

Step 4: 72°C 1 min / 1000 base pairs sequence length

The steps 2 to 4 were repeated for 16 cycles.

In the second step generic primers were used to amplify the generated PCR products. 5 μ L of the product of the first PCR was used as a template and combined with 10 μ L HF-Reaction buffer, 1.5 μ L of forward and reverse generic primers (10 μ M), 1 μ L dNTP mix (10 μ M) and 1 μ L of the Phusion Tag Polymerase. De-ionized water was added to a final volume of 50 μ L. The PCR reaction was performed using the same program as for the first PCR but performing 25 cycles (from step 2 to step 4) instead of 16 cycles. The product of this reaction was purified on a 1% agarose gel by excising and extracting the corresponding band with a GeneJET GelExtraction Kit.

Subsequent to the generation of the DNA fragments with the fused attB sites, the modified fragments were recombined into the pDONR201 vector (BP reaction). For the BP reaction, 90 ng of the donor vector DONR201 were mixed with 3 μ L of the purified PCR product and 1 μ L of BP Clonase II. De-ionized water was added to a final volume of 5 μ L and the reaction was performed at 25°C for 2 hours. Afterwards, 0.5 μ L Proteinase K were added and incubated for 10 minutes at 37°C. The reaction mixture subsequently was transformed into DH5 α and amplified in liquid cultures before the plasmid DNA was purified using the GeneJET Plasmid Miniprep Kit. The sequence of the insert was verified by sequencing.

The verified constructs were cloned into the destination vector (pDEST/SF-TAP) by LR-reaction. 90 ng of destination vector and 90 ng of entry clone were mixed with 2 μ L EB buffer and 1 μ L LR clonase. The volume was adjusted to 5 μ L with de-ionized water and the reaction mix was incubated for two hours at 25°C. Afterwards, 0.5 μ L Proteinase K were added and the mixture was incubated for 10 minutes at 37°C. The destination clones were transformed to DH5 α and amplified using liquid cultures. The

DNA was isolated using the GeneJET Plasmid Miniprep Kit and the sequence was verified by sequencing.

6.1.5. Gene silencing

Gene silencing by RNA interference (RNAi) is a commonly used method to functionally validate protein interactions within a network (7, 12). Short interfering RNAs (siRNA) can be used to analyse the phenotypes by down-regulating selected genes within a protein network and give a hint about its importance within a specific protein complex.

6.1.5.1. Target selection

For the knockdowns Dharmacon ON-TARGETplus siRNA SMARTpools were used. These pools contain four different siRNAs for each target gene. The targeted genes are shown in Table 7.

6.1.5.2. siRNA knockdowns

For forward transfection experiments on cover slips the siRNA duplexes were transfected using Lipofectamine RNAiMAX transfection reagent according to the manufacturer's instructions. 1×10^5 IMCD3 cells were seeded on sterile cover slips in 6-well plates in a volume of 2 mL one day before transfection. The cells were rinsed once with medium without serum (Opti-MEM), and transfected after 20 minutes with a final concentration of 50nM total siRNA duplex and 2 μ L Lipofectamine RNAiMAX per mL. The transfection solution was prepared in Opti-MEM and 2 mL of transfection solution was added per well of a 6-well plate. The cells were transferred to an incubator at 37°C, 5% CO₂ for 72 hours, transfection solution remained on the cells until fixation/lysis.

For screens in 96-well plates a reverse transfection approach was used. 2.5 μ L siRNA (100 μ M) were added to each well of an optical-bottom-96-well plate. To each well, 0.2 μ L Lipofectamine RNAiMAX transfection reagent, resuspended in 17.5 μ L Opti-MEM, was added. Afterwards, 80 μ L IMCD3 cell suspension with a density of 10^5 cells per mL in Opti-MEM were added to the wells. For minimization of edge effects, the plates with the transfection complexes and cells were kept at room temperature under the laminar air flow for one hour before being placed in the incubator at 37°C, 5% CO₂ for 72 hours.

6.1.5.3. Evaluation of knockdown efficiency

The evaluation of the RNAi knockdown experiments was performed using quantitative PCR. This method is based on the already introduced technique PCR (section 6.1.2), but monitors the amplification of the DNA fragment in real-time. The detection of the amplified DNA fragments was performed by a fluorescent dye, in this study SYBR green. The dye reacts specifically with the amplified dsDNA fragments, which accumulate during the PCR, and produces a fluorescent signal. The cycle number, at which the fluorescence exceeds the baseline fluorescence signal, is measured. This parameter is referred to as cycle threshold (C_T -value). During the PCR, the amount of amplified DNA and the PCR-cycles correlate in a linear fashion. This allows calculating inversely the starting amount of nucleic acid in the sample, relative to a reference fragment. To apply this method the total RNA had to be reverse transcribed to cDNA before the real-time PCR could be performed.

6.1.5.3.1. Isolation of total RNA

Total RNA was extracted from the cells using TRIzol reagent according to the manufacturer's instructions under RNase-free conditions. Cells were washed once with phosphate buffered saline (PBS) and then lysed in TRIzol reagent (1 mL per 10 cm²). After incubation for 5 minutes at room temperature the lysate was transferred to a microfuge reaction tube and 200 μ L chloroform were added per mL TRIzol. The samples were mixed by inverting several times, incubated for 3 minutes at room temperature and subsequently centrifuged for 15 minutes at 12,000 x g at 4°C. The upper, aqueous phase, containing the RNA was transferred to a new reaction tube. Afterwards, 500 μ L isopropanol per mL TRIzol were added, the solution was mixed by inverting several times and incubated for 10 minutes at room temperature. The RNA was then precipitated by centrifugation for 10 minutes at 12,000 x g at 4°C. The pellet was washed once with 1 mL 75% ethanol and centrifuged again for 5 minutes at 12,000 x g, 4°C. The pellet was dried and subsequently re-dissolved in RNase-free water.

6.1.5.3.2. Reverse transcription

Complementary DNA was produced from total RNA using Moloney murine leukemia virus reverse transcriptase (M-MLV RT). 3 μ g random primers were mixed with 1 μ g RNA and 10 μ L RNase-free water and incubated 70°C for 10 minutes. After being cooled down on ice, 4 μ L 5x M-MLV RT buffer, 2 μ L 0.1M DTT, 2 μ L dNTPs and 10

units of RNasin were added and incubated at 37°C for 2 minutes before adding 200 units of M-MLV RT. The reverse transcription was then performed for one hour at 37°C and the enzyme subsequently denatured by heating to 95°C for 5 minutes.

6.1.5.3.3. Determination of the amplification efficiency

Initially, the amplification efficiency of the primers was tested. This is a crucial step since the amplification rate during the quantification should be linear. This process had to be done separately for every primer pair. Therefore, six different concentrations of the cDNA were tested (1:5, 1:10, 1:20, 1:50, 1:100, 1:200). For each primer pair the cycle number was determined by which the fluorescence passes the threshold (C_T -value). The C_T -value is plotted on the y-axis against the cDNA amount on the x-axis and a linear regression is calculated. The efficiency (E) of the primer pair is calculated by the formula $E = 10^{(-1/\text{regression})} - 1$ and should optimally be at 100%. Primers with an efficiency of less than 92% were withdrawn and substituted by new candidates.

6.1.5.3.4. Quantitative analysis of RNA

The quantitative PCR was performed using Power SYBR Green PCR Master Mix according to the manufacturer's instructions. Therefore, the reactions were pipetted in triplicate as follows: 10 μL SYBR Green Mastermix, 2 μL forward and reverse primer (5 pmol/ μL), 1 μL de-ionized water and 5 μL cDNA (~12.5 ng, diluted 1:20 in water). The reaction was performed using the following program:

Step 1: 95 °C 10 min

Step 2: 95 °C 15 sec

Step 3: 60°C 1 min

The steps 2 to 3 were repeated 40 times on a real-time thermocycler.

Subsequent to the PCR, the software 'Best Keeper' (151) was used to evaluate the stability of the housekeeping genes (reference genes: bActin, Gapdh, Hprt1 and Sdha). At least two of the reference genes should be stable for a reliable relative quantification of the target genes. The quantification, considering the amplification efficiency was performed, using the software 'REST' (152).

6.2. Mammalian cell culture

6.2.1. Growth and maintenance of mammalian cells

HEK293, HEK293-T and hTERT-RPE1 cells were cultured in growth medium (DMEM, Dulbecco's modified eagle medium, containing 10% (v/v) fetal bovine serum (FBS), 50 units/mL Penicillin and 0.05 mg/mL Streptomycin) in 10 cm cell culture dishes at 37°C and 5% CO₂ in a cell culture incubator. hTERT-RPE1 cells were cultured in DMEM without antibiotics and without FBS during serum starvation to induce cilia formation. IMCD3 cells were cultured in a 1:1 mix of DMEM and Ham's F12, supplemented with 10% (v/v) FBS. Before use of FBS, it was heat inactivated by incubation at 55°C for one hour. The cells were split twice a week with a ratio of 1:10. The medium was removed, the cells washed once with 5 mL of DPBS (Dulbecco's Phosphate buffered saline) and then incubated with 2.5 mL trypsin/EDTA solution (0.5 mg/mL trypsin, 0.22 mg/mL EDTA in PBS) for 1-5 minutes. Then 7.5 mL of growth medium were added to the suspension and the cells were separated by pipetting, 1 mL of the suspension was added to 9 mL fresh medium in a new cell culture dish.

6.2.2. Generation of cryo stocks

Cells were trypsinized, separated and pelleted for 3 minutes at 500 x g. Afterwards, the pellet was re-suspended in 91% (v/v) FBS and 9% (v/v) DMSO. The suspension was applied to cryogenic tubes and cooled down stepwise, one hour at 4°C, one hour at -20°C, overnight at -80°C and then transferred to liquid nitrogen for long term storage.

6.2.3. Growth and maintenance of SILAC cultures

For SILAC cultures the cells were grown under the same conditions as the normal mammalian cells with the following modifications. L-lysine and L-arginine deficient DMEM medium was used instead of the normal DMEM. The medium was supplied with 4 mM L-glutamine, 0.23 mg/mL proline and the corresponding amino acids for the different conditions. For double labelling ¹³C⁶¹⁵N²-L-lysine and ¹³C⁶¹⁵N⁴-L-arginine were used for the heavy condition and normal amino acids for the light condition. The amino acids were added to a final concentration of 0.1 mg/mL. Proline was added to avoid arginine-proline conversion which would impair the quantification.

After sterile filtration 10% (v/v) dialyzed FBS, 50 units/mL Penicillin and 0.05 mg/mL Streptomycin were added. Heavy and light media were prepared the same way in parallel.

6.2.4. Growth on coverslips

Coverslips were sterilized by incubation in absolute ethanol for one day and dried afterwards under the laminar air flow. Alternatively the sterilization process was performed by dipping the coverslips into 100% acetone then in 100% ethanol and drying them under the laminar air flow afterwards. For cultivation the coverslips were placed on the bottom of a 24-well or 6-well plate and overlaid with 500 μ L of cell suspension. The cells were then grown to confluency on the coverslips.

6.2.5. Transient transfection of mammalian cells

Mammalian cells were transfected using the polyethylenimine (PEI, PolySciences) method. The PEI solution was prepared as followed: 0.1g of PEI were dissolved in 900 mL 150 mM sodium chloride (NaCl, pH 5.5), the pH was adjusted to 7.8 with hydrochloric acid (HCl) and 150 mM NaCl was added to a final volume of 1L. The solution was heated to 80°C for 4-8 hours. After cooling down, the pH was adjusted again, the solution sterile filtered, aliquoted and stored at 4°C.

The day before transfection, the cells were seeded at 50% confluency in fresh cell culture dishes. Depending on the size of the dish different volumes of PEI and different amounts of DNA were used for the transfection (Table 11). The transfection procedure was performed as followed: the PEI solution and the DNA were mixed by vortexing for 10 seconds and then incubated for 10 minutes at room temperature. The mixture was then added drop wise to the cell culture dishes and mixed with the medium by gently shaking the cell culture plate.

Table 11: PEI transfection.

The table shows the amount of DNA and the volume of PEI used for the transfection of mammalian cells for different assay formats.

Assay format	Volume PEI [μ L]	Amount DNA [μ g]
6-well plate	65	0.8
10 cm dish	500	3
14 cm dish	1000	8

6.2.6. Generation of stable cell lines

To generate cell lines stably expressing the protein of interest HEK293 cells were seeded and transfected as described above. 48 hours after transfection the cells were trypsinized and seeded at low density (1:100) and the normal growth medium was supplied with 750 µg/mL G418 selection antibiotic. The pcDNA3 vector contains the neomycin resistance gene that allows the transfected cells to survive the G418 while non-transfected cells die. The cells were cultivated for 3-4 weeks in the G418 medium, the medium was exchanged every second day. After the death of the non-resistant cells single colonies became visible, whereof 4-6 were transferred to a 24-well plate. Once the cells were confluent, each well was divided to two wells of a 6-well plate. One of the well was harvested at confluency for expression-tests by western blot while the second one was used for further culture and generation of cryo stocks.

6.2.7. Cell harvesting and generation of protein extracts

Before harvesting the cells, the growth medium was removed and the cells washed once with DPBS. Afterwards, lysis buffer (30 mM Tris-HCl, pH 7.4, 150 mM sodium chloride, 0.5% NP-40, protease inhibitor cocktail, phosphatase inhibitor cocktail II and III) was applied to the cell culture dish. The applied volume of lysis buffer depended on the size of the cell culture plate (6-well: 90µL, 10 cm dish: 500µL, 14 cm dish: 1 mL). The cells were scraped off the plates using a cell scraper, the cells were separated by pipetting, transferred to a reaction tube and incubated for 20 minutes at 4°C on an end-over-end shaker. The cell debris was then pelleted for 10 minutes at 10,000 x g and the supernatant used for further experiments.

6.3. Protein chemistry

6.3.1. Determination of protein concentration by Bradford assay

Protein concentration was determined using the Bradford (153) method.

The basis of the Bradford method is a complex formation of Coomassie brilliant blue with the proteins. The absorption of the unbound form of the dye shifts from 465 nm to 595 nm in the complexed form. The anionic form of the Coomassie mainly interacts with arginine, whereas reactions with other basic (histidine, lysine) or aromatic (tryptophan, tyrosine, phenylalanine) amino acids is relatively low. The

colour response during the assay is not linear over concentration (154, 155), still the usage of a calibration curve within each experiment enables high accuracy protein concentration determination (153). The method is not sensitive to reducing agents like DTT or β -mercaptoethanol, but the presence of detergents or chaotropic salts has to be limited. A calibration curve with the protein BSA (bovine serum albumin) from 0.2 mg/mL to 1 mg/mL was used. Lysis buffer was added to the calibration curve samples to ensure that the same amount of lysis buffer is present in the calibration as in the unknown protein sample. The Bradford reagent was diluted fivefold in water and subsequently 1 mL of the solution was added to each sample. The reactions were incubated for 5 minutes at room temperature before being measured in the photometer at 595 nm wavelength. The protein concentrations were calculated according to the calibration curve.

6.3.2. Protein concentration and purification

Prior to in-solution cleavage or gel electrophoresis the protein samples had to be concentrated and/or the interfering substances had to be removed. Therefore, protein concentrator units were used or protein precipitation was performed.

6.3.2.1. Protein concentration using centrifugal units

In order to concentrate proteins, vivaspin 500 centrifugal concentrator units with a molecular weight cut-off of 3 kDa or 10 kDa were used. The samples were transferred to the concentrator units and centrifuged at 13,000 x g at 4°C until the desired volume was reached. Then the insert of the concentrator unit was transferred bottom up to a new Eppendorf tube and the sample was recovered by centrifugation at 3,000 x g for 3 minutes.

6.3.2.2. Protein precipitation

Protein precipitation was performed by the methanol/chloroform method (156). The method is insensitive to contaminations by salts, lipids and detergents. It is therefore the method of choice for removing contaminants from samples designated for mass spectrometry.

For precipitation, the sample was diluted 4-fold by adding methanol, vortexed and centrifuged at 9,000 x g for 30 seconds. One sample volume of chloroform was added, mixed by vortexing and centrifuged at 9,000 x g for 30 seconds. Three

sample volumes of ddH₂O were added, mixed and centrifuged at 9,000 x g for one minute. After the centrifugation step the upper phase was removed, the three-fold volume of the sample of methanol was added, mixed and centrifuged at 16,000 x g for 2 minutes. The supernatant was discarded and the pellet air-dried for 15 minutes.

6.3.3. SDS-PAGE

Proteins were separated by their molecular weight using SDS-PAGE (sodium dodecyl sulfate-polyacrylamide gel electrophoresis) according to the method of Laemmli (157). To prepare the samples for electrophoresis 5-fold Laemmli buffer (100mM Tris-HCl, 5% SDS, 50% Glycerol, 500 mM 2-Mercaptoethanol, 0.05% Bromophenol blue) was added to the samples and the samples were boiled at 96°C for 5 minutes. The buffer contains β -mercaptoethanol which reduces the disulphide bonds within the proteins, which in combination with the heat results in their denaturation. Moreover, the buffer contains SDS, which binds to the protein and adds uniform negative charges, masking the intrinsic charges of the proteins. The result of this reaction is an almost constant mass-charge ratio for all proteins within the reaction mix that allows a migration speed which is relative to the mass of the protein. In this study, a discontinuous gel system consisting of a separating gel with a stacking gel on top was used. Proteins are concentrated on the interface of the stacking and the separating gel before being separated, due to the reduced acrylamide concentration and the more acidic conditions within the stacking gel. For mass spectrometric approaches pre-cast NuPAGE (Invitrogen) gels were used, for preparative gels and western blots the gels were cast using the Mini Protean 3 system from BioRad.

The volumes for ingredients for separating and stacking gels are listed in Table 12. The ingredients for the separating gel were mixed and poured in between a spacer plate of required thickness and a short plate. The gel was subsequently overlaid with isopropanol until it was polymerized. After removal of the isopropanol the ingredients for the stacking gel were mixed and applied on top of the separating gel. Immediately after pouring the stacking gel a comb of necessary thickness and required well number was inserted on top of the stacking gel. After polymerization the gels were placed in a Mini Protean 3 chamber and the chamber was filled with SDS-PAGE running buffer (200 mM glycine, 25 mM Tris, 1% SDS). For NuPAGE gels the corresponding running chamber with MES-buffer was used. For both systems, the

comb was removed and the wells were rinsed with electrophoresis buffer using a syringe to remove remaining gel particles or air bubbles. The boiled samples were cooled down and loaded onto the gel. The gel run was started with a constant voltage of 90V, the voltage was increased after 15 minutes to 120V. The run was stopped when the bromophenol blue running front was released into the running buffer from the end of the separating gel.

Table 12: Reagents and volumes for SDS-PAGE gels.

In this table the reagents and volumes to prepare SDS-PAGE separation gels of different percentages of acrylamide and for the stacking gel are shown.

Separating gel (10 mL)	8%	10%	12%
ddH ₂ O	4.7 mL	4 mL	3.3 mL
TRIS-HCl (pH 8.8)	2.5 mL	2.5 mL	2.5 mL
30% (w/v) Acrylamide: bisacrylamide (37.5:1)	2.6 mL	3.3 mL	4 mL
10% (w/v) SDS	100 µL	100 µL	100 µL
TEMED	10 µL	10 µL	10 µL
10% (w/v) APS	75 µL	75 µL	75 µL

stacking gel (5 mL)	4%
ddH ₂ O	2.95 mL
TRIS-HCl (pH 6.8)	1.25 mL
30% (w/v) Acrylamide: bisacrylamide (37.5:1)	0.7 mL
10% (w/v) SDS	50 µL
Temed	5 µL
10% (w/v) APS	37.5 µL

6.3.3.1. Staining of SDS-PAGE gels

After separation, SDS-PAGE gels were washed for five minutes in dH₂O to remove the remaining SDS and then fixed two times for 30 minutes in fixing solution (50% methanol, 12% acetic acid). Different methods of staining were used depending on the protein amount on the gel or on the following application. For subsequent use of the gel for mass spectrometry Coomassie staining was used due to its optimal compatibility with mass spectrometric analysis. Silver staining can also be used for mass spectrometry and has a higher sensitivity compared to Coomassie but is less optimal for following MS analysis. Colloidal Coomassie staining is not suitable to LC-MS due to the formed colloids that would block the pre-separation column of the LC-system.

6.3.3.1.1. Coomassie staining

Coomassie staining is a method with a detection limit of about 100 ng per protein band and is based on the binding of the Coomassie brilliant blue G250 dye to proteins (158). After fixation, the gels were stained with 0.4% Coomassie, dissolved in fixing solution until bands were visible. Afterwards, the background was removed by washing the gel in fixing solution. Therefore, the solution had to be exchanged several times and a final washing step in ddH₂O was added.

6.3.3.1.2. Colloidal Coomassie

To detect lower protein amounts, a more sensitive detection method, colloidal Coomassie staining, was used. Colloidal Coomassie is more sensitive than normal Coomassie staining, but less sensitive than silver staining. Coomassie brilliant blue G250 forms micro-precipitates in acidic media containing ammonium sulphate (159, 160). The background staining is decreased due to the low amount of free dye in the suspension. Still, the method is very sensitive as the micro-precipitates act as small reservoirs and provide enough dye to all free protein binding sites. Here, an adapted protocol of the method from Kang et al. (161) that was presented in the "Laborjournal" (<http://www.laborjournal.de>) was applied. The used staining solution (0.02% Coomassie brilliant blue G250, 5% aluminiumsulfat-18-hydrat, 10% ethanol, 2% ortho-Phosphoric acid) allows the staining in one step. The fixation step is not needed, making this procedure a one-step staining method. The gel can be stained from 3 hours up to overnight incubation. Afterwards, the gel is de-stained with water or if needed with de-staining solution (10% ethanol, 2% ortho-Phosphoric acid) to remove the background. As the background staining is very low the de-staining procedure is very rapid.

6.3.3.1.3. Silver staining

Silver staining is the most sensitive method to stain proteins in SDS-PAGE gels which was applied here. The sensitivity is 10-100 times higher than Coomassie staining and allows a detection around 1-10 ng per band. Under alkaline conditions silver ions are reduced to silver by formaldehyde (162, 163). The visualization of the proteins is achieved by the formation of complexes of silver with proteins.

After electrophoresis, the gel was fixed two times for 30 minutes in fixing solution (50% methanol, 12% acetic acid, 0.05% formaldehyde (37%). Afterwards, the gel was washed three times in 50% ethanol and then incubated for one minute in

sensitizer (0.2 g/L sodium thiosulfate) followed by two short washes in deionized water. Staining solution (2 g/L silver nitrate, 0.075% formaldehyde (37%)) was applied for 20 minutes and the gel was subsequently washed two times with deionized water. The time of incubation with developer (60 g/L sodium carbonate, 5 mg/L sodium thiosulfate, 0.05% formaldehyde (37%)) depended on the desired grade of staining and typically was reached after some seconds up to one minute. To stop the developing reaction, stop solution (50% methanol, 12% acetic acid) was applied.

6.3.4. Western blot analysis

The detection of proteins in complex mixtures was performed by Western Blot analysis. Proteins were separated on an SDS-PAGE gel by their molecular weight and then transferred to Hybond-P polyvinylidene difluoride (PVDF) membranes (164). This enabled the detection of specific proteins by their corresponding antibodies (Table 9). Two different transfer systems from the same manufacturer were used for the transfer. Both techniques will be described. Semi-dry blotting was used when the blot was incubated with the antibody directly after transfer, whereas the tank blotting system was used for overnight blotting at 4°C.

6.3.4.1. Semi-dry blotting

For semi-dry blotting, the gel was incubated for 5 minutes in anode II buffer (0.3 M Tris), the PVDF membrane was activated for 1 minute with methanol and subsequently washed and incubated shortly with anode II buffer. The semi-dry blotting apparatus was assembled from the bottom (anode) to the top (lid, cathode) as follows: three Whatman blotting papers, soaked with anode I buffer (0.025 M Tris), two Whatman blotting papers soaked with anode II buffer, PVDF membrane, SDS-PAGE gel, three Whatman blotting papers soaked in cathode buffer (40 mM ϵ -aminocaproic acid, 0.01% w/v SDS). A roller was used to remove air bubbles in between the single layers and afterwards the cathode plate was placed on top of the stack. The transfer was performed for 2 hours at 50 mA per gel (0.8-1 mA per cm²) and a maximum voltage of 20V.

6.3.4.2. Tank blotting

Tank or wet blot was performed using the corresponding transfer chamber from BioRad. The gel was incubated for 5 minutes in transfer buffer (192 mM glycine, 25

mM Tris, 20% (v/v) methanol). The PDVF membrane was activated in methanol for 1 minute, subsequently washed and also incubated in transfer buffer. The gel holder cassette was assembled as follows from the cathode (black side) to the anode (colourless side): sponge soaked with transfer buffer, 2 Whatman blotting papers soaked with transfer buffer, SDS-PAGE gel, PVDF membrane, 2 Whatman blotting papers soaked with transfer buffer, sponge soaked with transfer buffer. A roller was used to ensure that there were no air bubbles in between the single layers, the cassette was closed and placed into the electrode module. A pre-cooled ice pack was inserted into the transfer chamber and the chamber was filled up with transfer buffer. The chamber was placed in the cold room at 4°C, the transfer was performed for 90 minutes at 90V. Afterwards, the blotting chamber could be left at 4°C over night.

6.3.4.3. Ponceau staining

After the blotting process, Ponceau S staining was used to verify the success of the transfer process (165). Ponceau S solution (0.1% (w/v) Ponceau S in 5% (v/v) acetic acid) is a dye to reversibly stain proteins on PVDF membranes. The staining solution was applied for one minute to the membrane and the background staining was removed subsequently by washing with dH₂O. The staining allows the visualization of possible air bubbles that were present during the transfer process and shows the major protein bands on the membrane. The dye can be removed completely by washing with TBS-T (30 mM Tris-HCl, pH 7.4, 150 mM sodium chloride, 0.1% (v/v) Tween20).

6.3.4.4. Immunodetection

Subsequent to Ponceau staining the membranes were incubated with blocking buffer for one hour. The selection of the blocking solution depended on the use of the primary antibody and was either 5% (w/v) non-fat dry milk powder in TBS-T or 5% (w/v) BSA in TBS-T. After blocking, the membrane was incubated overnight at 4°C with the primary antibody, diluted in the corresponding blocking solution, in a 50 mL reaction tube on a roller-shaker. The antibodies with their corresponding dilutions are shown in Table 9. The membrane was washed three times for 15 minutes with TBS-T before being incubated for 1 hour at room temperature with horseradish peroxidase (HRP)-conjugated secondary antibodies, directed against IgG of the corresponding

species in which the primary antibody was raised, diluted in 5% (w/v) Milk/TBS-T. The dilutions and specifications of the secondary antibodies are shown in Table 10. Afterwards, the membranes were washed three times for 10 minutes with TBS-T and the HRP was detected by Hyperfilm enhanced chemiluminescence (ECL) films and ECL plus reagent. The incubation time of the films depended on the signal intensity and ranged from 5 seconds to 30 minutes.

6.3.4.5. Stripping of western blots

Stripping of western blot membranes describes the process of removing the bound primary and secondary antibodies from the PVDF membrane, while the transferred proteins will remain on the membrane (166). This allows the sequential detection with multiple different primary antibodies on the same western blot. This procedure was applied directly after immunodetection with ECL. Therefore, the membrane was overlaid with stripping buffer (2% (w/v) SDS, 62.5 mM Tris-HCl (pH 6.8), 100 mM β -Mercaptoethanol) and incubated at 58°C for 20 minutes under constant agitation. Afterwards, the membrane was washed three times with TBS-T before being blocked and subsequently incubated with the next primary antibody.

6.3.5. Digitalizing results from SDS-PAGE gels and western blot films

Images of stained SDS-PAGE gels and western blot films were digitalized using a Mikrotek scanmaker i800 flatbed scanner with transmitted light unit and the software Photoshop. Scans were performed at a resolution of at least 300 dpi.

6.4. Protein complex purification

For the analysis of protein complexes, the latter were purified or enriched using different techniques. The choice of the applied method depends on different parameters and varies for example in the degree of purity and the amount of co-purified interaction partners. For the analysis of protein complexes, the purity should be as high as possible. Still, the gain in purity correlates directly with the loss of weak or transient interaction partners as well as with the number of non-specific interactions. It is therefore very important to include controls to complex purification experiments to identify non-specifically bound proteins; however the lack of quantitative information lowers the reliability of their identification. For quantitative approaches, the degree of purity is not that important as the specific interactions can

be distinguished from the non-specific ones due to their significant enrichment compared to the control. Thus, it can even be an advantage of having a lot of background in those experiments to enhance the statistical significance of altered proteins. The methods described in the following are mainly based on the isolation of protein complexes bound to over-expressed fusion protein with an artificial peptide tag.

6.4.1. Strep-Tactin affinity purification

The Strep tag is a nine amino acid long fusion tag that can be fused to the C-terminus of a protein and has intrinsic streptavidin-binding activity (167, 168). The tag enables the purification of recombinant proteins by the use of streptavidin-sepharose beads. The first Strep tag was limited to fusion to the C-terminus of a protein. For that reason Schmidt and co-workers developed a newer version, the Strep-II-tag, that can also be fused to the N-terminus of proteins (169). The Strep-II-tag was further improved by mutation in its flexible loop, resulting in a higher affinity by one order of magnitude (170). The elution of the fusion proteins from the resin is achieved in mild buffer conditions by competition with D-desthiobiotin (171).

Cells were washed once with phosphate buffered saline (PBS) before 1 mL of lysis buffer (30 mM Tris-HCl pH 7.4, 150 mM NaCl, 0.5% (v/v) Nonidet-P40, Protease Inhibitor Complete, Phosphatase Inhibitor Cocktail II and III) for one 14 cm dish (5×10^7 cells) was added. The cells were scraped-off and the lysate was incubated for 20 minutes at 4°C on an end-over-end shaker. The cell debris was pelleted and the cleared lysate transferred to a new reaction tube. The purification of the SF-TAP-tagged proteins was performed by the use of Strep-tactin-superflow beads. 50 µL of beads were added to the lysate of one 14 cm dish and washed three times with lysis buffer before use. The beads were added to the lysate and incubated for one hour at 4°C on an end-over-end shaker. Afterwards, the beads with the bound proteins were centrifuged for one minute at 8000 x g, the supernatant was discarded and the beads were transferred to a microspin column. The beads were washed three times with wash buffer (30 mM Tris-HCl pH 7.4, 150 mM NaCl, 0.1% (v/v) Nonidet-P40, Phosphatase Inhibitor Cocktail 2 and 3) to remove unbound protein. Subsequent, the proteins were eluted by incubating the beads at 4°C for 10 minutes with the fourfold bead-volume of Strep-tactin elution buffer on an end-over-end shaker.

6.4.2. FLAG affinity purification

The affinity purification by FLAG-tag follows the same principle as the Strep-tag method. The efficiency and time effort for the purification is similar, still the binding capacity of the FLAG beads is clearly higher compared to Strep beads (172). The FLAG-tag and its corresponding antibody (anti-FLAG-M1) originally was developed by Hopp and co-workers and binding was a calcium-dependent process (108). The process was improved by the production of another monoclonal antibody (anti-FLAG-M2). Binding of this antibody to the tag is not calcium-dependent and therefore does not require EDTA as a chelating reagent for elution (173). With the anti-FLAG-M2 antibody the tag is captured specifically and after purification the fusion protein is released by competition with FLAG peptide. Alternatively, the elution can be performed under acidic conditions with glycine. The FLAG-purification is used instead of Strep purification, when the eluate is directly used for mass spectrometric experiments, since the desthiobiotin from the Strep elution would bind to the C18 material from the separation columns of the LC system. The interaction of desthiobiotin with the LC column would reduce the capacity of the chromatography matrix and therefore impair the resolution and detection.

Cell lysates were prepared as mentioned in the previous section. FLAG-M2-agarose beads were washed three times with lysis buffer and 25 μ L of beads per 14 cm dish were added to the cleared lysate. The amount of used dishes per bait depended on the abundance of the over-expressed protein and the application following the purification and ranged from one to three dishes. The mixture was incubated for one hour at 4°C on an end-over-end shaker. Afterwards, the beads were separated from the supernatant by centrifugation for one minute at 8000 x g and the supernatant was withdrawn. The beads were transferred to a microspin column, washed three times with wash buffer and subsequently eluted with 4-6 times the bead volume FLAG elution buffer (200 μ g/mL FLAG peptide in wash buffer) for 10 minutes at 4°C on an end-over-end shaker.

6.4.3. Tandem affinity purification by SF-TAP

The Strep-FLAG-Tandem-Affinity-Purification (SF-TAP) method is an improvement of the original tandem affinity purification (TAP) method (115). The fusion tag has been modified to a tandem Strep tag II / FLAG tag combination, separated by a linker

sequence. Additionally, the use of these medium affinity tags allowed the removal of the tobacco etch virus (TEV) cleavage site in between the two tags, reducing the size of the original TAP-tag (~25 kDa) to a fifth. The improvement of the SF-TAP tag allows reduction of the time for purification and simplifies the experimental process. Due to the two affinity purification steps and the stringent washing in between, the method results in a high purity combined with low background by non-specific binding proteins. This enables the purification of stably bound proteins to the bait protein that can be described as stable interactors (116).

The cells were harvested as described in section 6.4.1. Equal to Strep purification, 50 μ L of Strep-tactin superflow beads per 14 cm dish were washed three times with lysis buffer and applied to the cleared lysate. The mixture was incubated for one hour at 4°C on an end-over-end shaker. The beads were centrifuged for 1 minute at 8000 x g, the supernatant was discarded and the beads were transferred to a microspin column. Afterwards, the beads were washed three times with wash buffer and the proteins were eluted for 10 minutes at 4°C on an end-over-end shaker, with Strep-tactin elution buffer. The eluate was transferred to a sealed microspin column for the following purification step. FLAG-M2 agarose beads (25 μ L per 14 cm dish) were washed three times with lysis buffer and subsequently transferred to the eluate from the Strep purification. The mixture was incubated for one hour at 4°C on an end-over-end shaker. Afterwards, the seal of the microspin column was detached to remove the liquid and the beads were subsequently washed three times with wash buffer. The final elution was performed at 4°C by incubation with FLAG-elution buffer (200 μ g/mL FLAG peptide in wash buffer) on an end-over-end shaker.

6.5. Analysis of protein complexes

6.5.1. Sucrose density centrifugation

To analyse the differential sedimentation of the isolated protein complexes, sucrose density centrifugation was performed. A method described by Tanese and co-workers was adapted for this purpose (122). A discontinuous sucrose gradient (5/8/11/14/17/20%) was pipetted in a 2 mL centrifugation tube. The corresponding amount of sucrose was dissolved in sucrose gradient buffer (30 mM Tris-HCl pH 7.4, 150 mM NaCl, 1 mM EDTA, 0.1% (v/v) Nonidet-P40). After homogenization, the gradient was pipetted from the bottom to the top of the tube, from the highest to the

lowest concentration, by gently overlaying the different solutions. For each concentration a volume of 250µL was used. The eluates from two SF-TAP experiments were pooled (2 times 200 µL) and layered on top of the gradient immediately after pipetting the gradient. The tubes were placed in a swing-out rotor and centrifuged at 4°C for 4 hours at 166,000 x g. Subsequent to the centrifugation, the tubes were removed from the rotor and the gradients were fractionated by pipetting from the top of the gradient in 125 µL fractions.

6.5.2. Destabilization of protein complexes by treatment with SDS

Sodium dodecyl sulfate (SDS) is an anionic detergent commonly used to denature proteins prior to polyacrylamide gel electrophoresis (PAGE (174-176)). SDS destabilizes non-covalent interactions within the protein and thus induces the loss of the tertiary structure of the protein. This transformation of the proteins to a linear state is needed for the migration through the polyacrylamide gel and the separation by size. If SDS is used in very low concentrations it can cause partial destabilization within protein complexes and induce a controlled disassembly of the protein complex into its subunits (177). Affinity purification from the lysates of cultured HEK293 cells, over-expressing a fusion protein with an SF-TAP tag (115), were combined with the ability of SDS of destabilizing protein complexes. This method was named SDS-affinity purification (SDS-AP) and was used to analyse the structure of a well characterized protein complex in combination with high resolution mass spectrometry.

FLAG-M2 agarose beads were washed three times with lysis buffer, 30 µL of beads were used for one experiment (one 14 cm dish). The cleared lysates were transferred to the beads and incubated for 1 hour at 4°C on an end-over-end shaker. The beads were separated from the lysate by centrifugation for 1 minute at 8000 x g and the supernatant was discarded. The resin was washed 3 times with wash buffer. For the SDS-destabilization of the protein complexes, the resin was then incubated 3 minutes with each concentration of SDS (0.00025%, 0.0025%, 0.005%, 0.01%, 0.1%) in SDS-elution buffer (30 mM Tris-HCl pH 7.4, 150 mM NaCl, Phosphatase Inhibitor Cocktail 2 and 3), the flow through was collected after every step. The elution was performed at 4°C as long as the concentration was below 0.02% SDS, for the higher concentrations the incubation was performed at room temperature to avoid the precipitation of the SDS during the incubation. Subsequent to the SDS gradient, the

remaining protein complexes were eluted from the resin by incubation for 3 minutes with FLAG elution buffer (200 µg/mL FLAG peptide in wash buffer).

6.6. Immunohistochemistry

6.6.1. Fixation of cells

For fixation of cells, different methods can be used as for example paraformaldehyde, methanol or glutaraldehyde. Each method has its advantages and disadvantages and their application depends on different factors as for example the use of the antibody or the detection method. The use of these different methods can result in different staining patterns (178-180). For immunohistochemistry, cells were fixed using two different methods, depending on the used antibodies. The first method was fixation with paraformaldehyde (PFA). PFA fixation is a reversible fixation method and is usually used in a concentration range from 2-4%. The fixation is stable when the cells are kept at 1% PFA in PBS for several weeks. For fixation with PFA the cells were incubated with 2% PFA for 15 minutes at room temperature. Alternatively fixation by methanol was used. Methanol fixation is not reversible and the use of this fixation method permeabilizes the membranes due to its application at low temperature. For methanol fixation the methanol was pre-chilled at -20°C and applied to the cells, the cells were then incubated for 5 minutes at -20°C.

6.6.2. Staining on cover slips

For immunostaining on cover slips, the fixed cells were washed three times with PBS, permeabilized for 5 minutes by application of 0.3% (v/v) Triton-X-100 in PBS and subsequently blocked in 1% (w/v) BSA, 1% (w/v) Milk in PBS for half an hour. In case of too high background signal, 5-10% (v/v) normal serum from the species, in which the secondary antibody was raised, was added to the blocking solution. After blocking, the primary antibodies were incubated in blocking solution at 4°C overnight. After 4 times 5 minutes wash with PBS, the secondary antibodies were incubated in blocking solution for one hour at room temperature. Depending on the mounting medium, DAPI (final concentration 1 µg/mL) was added to the secondary antibody solution if needed. Afterwards, the coverslips were washed 4 times for 5 minutes with PBS and mounted upside-down on a glass slide.

For co-immunostaining with two unconjugated primary antibodies raised in the same species, a technique described by Brouns et al. (181) was applied. This method allows the subsequent staining with different primary antibodies raised in the same species, due to the blocking with monovalent fab fragments. Therefore, the cells were incubated with the first primary antibody as previously described. Afterwards, all free binding sites of the first primary antibodies were masked by incubation with fluorochrome-labelled fab fragments in a high concentration, raised in the same species as the primary antibody. This step blocks the access of the second primary antibodies to the first primary antibodies, as well as the access of the following secondary antibodies, used to detect the second primary antibodies. Subsequently, the second primary antibody was incubated as already described above. The second primary antibody could be detected normally by a corresponding Alexa-conjugated anti-IgG (H+L) secondary antibody.

6.6.3. Operetta screens

The medium was removed from the 96-well plates by inverting the plate and spotting it onto a clean paper towel to remove excess liquid. The cells were washed three times with PBS and subsequently fixed for 5 minutes at -20°C with ice-cold methanol. The cells were blocked with 1% (w/v) non-fat dry milk in PBS, previously clarified of particulates by centrifugation at $3000 \times g$ for 5 min. Acetylated tubulin antibody (Table 9) diluted in blocking solution was incubated for one hour at room temperature. The cells were subsequently washed four times with PBS and then incubated for one hour with the secondary antibody (goat-anti-mouse-Alexa-fluor488, Table 10) in a dilution of 1:2000, DAPI (1:5000) and TOTO-3 (1:5000) in blocking solution. The cells were then washed seven times with PBS and stored with 100 μL PBS per well at 4°C .

The optical 96-well-plates were processed using a PerkinElmer Operetta high-content wide-field fluorescence imaging system, coupled to Harmony software. The wells were imaged by an x20 objective lens, detecting three different colours in separate focal planes. The Operetta infra-red focussing laser detected the bottom of each well automatically and the focal planes for the detection of the different colours were calculated relative to this acquired value. The values for the single colours were set to the following: DAPI emission was detected for 60 ms 6 μm below the calculated bottom of the well, TOTO3 emission was detected for 500 ms 1 μm above the DAPI plane, and Alexa-Fluor 488 emission was detected for 700 ms 7 μm above

DAPI. Per well, 6 different fields of view were analysed, resulting in a total number of detected cells of around 4000 per well. The patterns for the different fields of view were identical for each well.

The used PerkinElmer algorithm for the image analysis was modified. Nuclei were detected by DAPI (blue) with fluorescent region greater than $30 \mu\text{m}^2$ and a contrast greater than 0.10. The cytoplasm was detected by TOTO-3 (far-red) as fluorescent regions around nuclei. Objects on the border of the field of vision were excluded to ensure that only whole cells were analysed. A 'find-spot' algorithm was used to detect cilia on the cells by identifying Alexa-Fluor-488 (green) fluorescent spots with radius smaller than 3.8 pixels, contrast greater than 0.1, spot-to-region intensity greater than 1.3 with a distance from all neighbouring spots greater than 5.6 pixels. Cells bearing more than one cilium were distinguished from cells with a single cilium. Output parameters of the screen were the number of whole cells as well as the number of whole cells with a single cilium. Furthermore, the number of cells with more than one cilium as well as the mean cilium intensity, indicating the length of the cilium, was acquired.

6.6.4. Microscopy

Immunostained cell cultures were analysed by fluorescence microscopy using an Axio Imager Z1 ApoTome with an AxioCam camera (Zeiss). Images of stained cells were captured using Zeiss (Axiovision 4.7) software. The contrast enhancement was performed using an image editing software (Photoshop CS5, Adobe Systems).

For co-localization studies in IMCD3 cells, confocal microscopy was applied. The imaging was done on a Nikon Eclipse A1R confocal laser microscope. The cells were first imaged by wide-field epifluorescence by eye and then captured using scanning confocal microscopy and Nikon NIS Elements Microscope Imaging Software. For all experiments three spots per slide were taken randomly and were acquired using a x100 objective lens. Afterwards, a representative spot was selected and imaged using a x100 objective lens + 3x scanner zoom. The contrast enhancement was performed using an image editing software (Photoshop CS5, Adobe Systems).

6.7. Mass spectrometry

6.7.1. Sample preparation

Sample preparation is one of the most challenging parts of modern mass spectrometry. The sensitivity of new high resolution mass spectrometers implicates enormous requirements to chemicals and solvents as well as to the samples themselves. Already tiny contaminations distort the measurements and data. It is therefore very important to use ultra-pure chemicals and to work very accurate during the whole process to generate reproducible data.

For the analysis of isolated protein complexes by mass spectrometry, the proteins have to be enzymatically processed to small peptides. This step is necessary since the analysis of intact proteins is still a difficult process and by far not as efficient as the analysis of the smaller peptides. The proteolytic cleavage of proteins is a critical step during the sample preparation and has to be performed very carefully.

6.7.1.1. Pre-fractionation by SDS-PAGE

The amount of compounds being analysed by a certain time by a mass spectrometer, is the most limiting factor in samples of high complexity. In order to extract all possible information from a sample, the complexity of the latter has to be reduced. This is can be done by the separation of the cleaved sample, due to the physicochemical properties of their peptides by online (ultra) high-performance liquid chromatography (HPLC), directly coupled to the mass spectrometer. Still, in case of higher complexity and dynamic range the separation by a HPLC system is by far not enough. The pre-fractionation by 1D- or 2D-gel electrophoresis prior to enzymatic cleavage can then be applied to analyse those samples in depth. The process of pre-fractionation is much more labour intensive than the direct cleavage of the samples. Furthermore, due to its additional working steps, there is a loss of sample as well. Therefore, a higher amount of starting material is required for this sort of sample preparation.

To this purpose, samples were concentrated to a final volume of 20 μ L by the use of protein concentrator units with 10 kDa cut-off (section 6.3.2.1) and 5 μ L of 5-fold Laemmli buffer was added to the concentrated samples. Alternatively the proteins were precipitated by methanol/chloroform (section 6.3.2.2) and subsequently re-

dissolved in Laemmli buffer. The samples were heated for 5 minutes to 96°C and after being cooled down, separated on a 1D-SDS-PAGE gel (10% pre-casted NuPAGE gel) by their molecular weight. The gel was run until the protein ladder started to separate (1-2 cm), depending on the complexity of the sample and was then stopped. The gel was stained with Coomassie as described before (section 6.3.3.1) and after the background was removed, the complete lane was excised with a clean scalpel. The lane was separated into 3-8 slices depending on the complexity of the sample.

6.7.1.2. In-gel cleavage

In-gel cleavage was first described by Rosenfeld and co-workers (182). Here, an adapted method was used, including reduction and alkylation of the samples before being cleaved by the required enzyme. In-gel cleavage can be used for the cleavage of samples, pre-fractionated on a 1D-SDS-PAGE gel, as well as for the cleavage of single spots or bands from a 1D or 2D gel. The procedure remains similar for those applications except for the gel run and the excision from the gel. The gel bands were cut into small pieces (~ 1mm³) and transferred to a well of a 96-well round bottom plate each. After washing for 30 minutes with 100 µL ddH₂O the gel pieces were destained, which is the only step that differs for Coomassie and silver stained gels during the in-gel cleavage process. Coomassie-stained spots were destained by incubating two times for 15 minutes in 100 µL 40% (v/v) acetonitrile (ACN), followed by incubation for 5 minutes in 50 µL 100% (v/v) ACN. If staining was still visible, this procedure was repeated until the staining was removed. Silver stained spots were destained via incubation for 5 minutes with 100 µL silver-destaining solution (1:1 solution of 30 mM potassium ferricyanide and 100 mM sodium thiosulfate), followed by 3 times wash with 100 µL dH₂O. After destaining, the gel pieces were incubated for 15 minutes at 60°C with 100 µL 5 mM dithiothreitol (DTT). The samples were cooled down to room temperature and the DTT solution was removed. 100 µL freshly prepared 25 mM 2-iodoacetamide solution was added and the samples were incubated for 45 minutes at room temperature in the dark. Subsequent, the solution was removed and the gel pieces were washed two times for 15 minutes with 100 µL 40% (v/v) ACN followed by 5 minutes wash with 50 µL 100% (v/v) ACN. The gel pieces were dried for 5 minutes and 50-70 µL trypsin solution was added (0.01 µg/µL trypsin in 50 mM ammoniumbicarbonate). The tryptic cleavage was performed at

37°C overnight. To stop the reaction, trifluor-acetic acid (TFA) was added to a final concentration of 0.5% and incubated for 15 minutes at room temperature. The supernatant (supernatant 1) was transferred to a new reaction tube, 100 µL 50% ACN, 0.5% TFA were added to the gel pieces and incubated for 15 minutes. The supernatant (supernatant 2) was again collected and combined with supernatant 1. The gel pieces were incubated for 5 minutes with 50 µL 99.5% ACN, 0.5% TFA and the supernatant afterwards combined with supernatant 1 and 2. The pooled supernatants were dried in a centrifugal evaporator (speed vac) and the samples were stored at -20°C until further use.

6.7.1.3. In-solution cleavage

The direct cleavage of samples in-solution is a method that can be used in case of lower complexity of samples, like for SF-TAP eluates. The amount of proteins within the sample allows their direct separation by the LC-system and their in-depth analysis by the mass spectrometer. For the in-solution cleavage, the samples were precipitated by methanol/chloroform as already described in section 6.3.2.2 and re-dissolved in 30 µL ammonium bicarbonate before proteolytic cleavage. 3 µL of RapiGest were added to a final concentration of 0.2%, the sample was vortexed and incubated 30 seconds at room temperature. 1 µL of 100 mM DTT was added and the samples were incubated at 60°C for 10 minutes. After the samples were cooled down to room temperature, 1 µL of 300 mM 2-iodoacetamide was added and the samples were incubated for 30 minutes in the dark. 1 µL of trypsin solution (0.5 µg/µL in 1 mM HCl) was added and the cleavage was performed overnight at 37°C. The reaction was stopped by acidifying the mixture by adding 2 µL of TFA (final concentration 5%). The samples were transferred to a polypropylene insert in a 1.5 mL reaction tube and incubated for 20 minutes. Subsequent, the samples were centrifuged for 15 minutes at room temperature at 16,000 x g. Afterwards, the sample interphase was collected and transferred to a new tube.

6.7.1.4. Purification with StageTips

To avoid contamination of the LC-system by insoluble contaminants or salts, the samples derived from an in-solution cleavage were purified using StageTip C18 columns. Therefore, the StageTip C18 matrix was activated by applying 20 µL 80% ACN and washed once with 20 µL wash solution (5% TFA). The acidified sample (5%

TFA) was applied to the matrix and washed once with 20 μL wash solution. Afterwards, the sample was eluted in two steps, first with 20 μL 50% ACN, 5% TFA, second with 20 μL 80% ACN, 5% TFA. Both fractions were collected in the same tube. Subsequently, the volume was reduced in the speed vac to remove the ACN and stored at -20°C until further use.

6.7.2. LC-MS/MS on the LTQ-Orbitrap XL and LTQ-Orbitrap Velos

The LTQ-Orbitrap is a high-resolution hybrid mass spectrometer that consists of an ion source (electro-spray or nanospray), a linear ion trap, a C-trap, a HCD collision cell and the Orbitrap mass analyser (Figure 16 (183)). The nanospray ion source is directly coupled to the liquid chromatography system and receives the sample with a constant flow. The sample is ionized by application of a high voltage potential between the capillary needle delivering the sample and the skimmer, where the sample enters the machine.

The sample is sprayed from the capillary in small droplets. Due to the differential potential between the solvent and the skimmer, the ions of opposite charge of the counter electrode (depending on the orientation of the potential) are moving to the surface of the droplets, whereas the solvent is driven to the antipole. This antagonizes the surface tension of the droplet, resulting in the so-called Taylor cone. Small charged droplets are separating from the bigger droplets, reducing their size due to evaporation. The reduction of the size of the droplets leads to a spatial concentration of the ions until the repulsion of the ions is higher than the surface tension (Rayleigh limit). The droplets explode into smallest droplets (Coulomb explosion), sometimes only consisting of one ion. The gas flow removes the remaining solvent resulting in a stream of single ions. The second hypothesis for the ionization process is that large molecules migrate from the surface to the gas phase before the Coulomb explosion takes place. Both hypotheses have been proved experimentally, so which hypothesis is correct remains controversial (184).

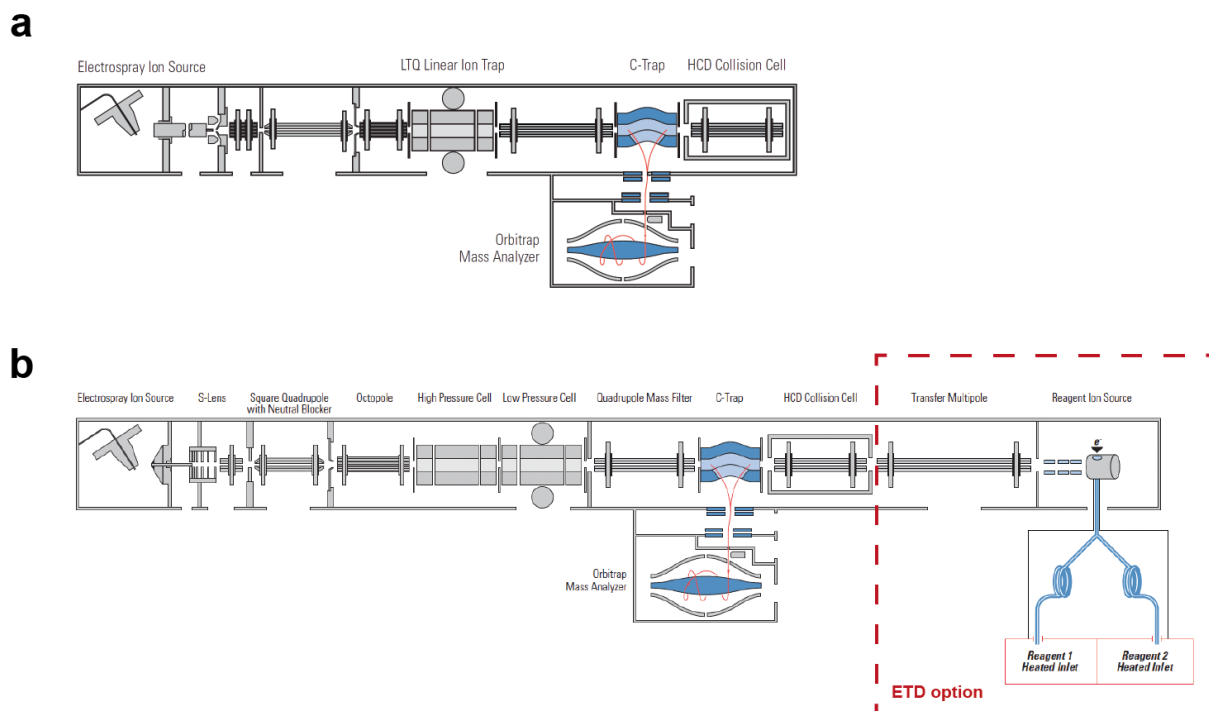


Figure 16: Scheme of the LTQ-Orbitrap XL and the LTQ-Orbitrap Velos mass spectrometer.

This figure shows the schematic overview of the LTQ-Orbitrap XL (**a**) and the LTQ-Orbitrap Velos (**b**) mass spectrometer. The composition of the LTQ-Orbitrap Velos is similar but varies in some details. Both machines consist of an electrospray ion source that can be coupled to an HPLC system, ion optics to focus the ions towards the linear ion trap. The C-Trap enables the injection of the ions into the Orbitrap mass analyser where the ions circle around the central pole. Alternatively to the fragmentation in the linear ion trap, the ions can be fragmented in the HCD collision cell. The ion optics of the XL and the Velos are different, the ion transfer tube is shorter in the Velos and in contrast to the XL a so-called S-Lens stack focusses the ions coming from the transfer tube before the ions are transferred to the linear ion trap. Furthermore, the linear ion trap was optimized in the Velos and was separated into a high-pressure and a low-pressure chamber. The ions are captured and fragmented at high-pressure, whereas the scan speed is enhanced at low-pressure. Moreover, the Orbitrap and the HCD cell were optimized in the Velos, resulting in an enhanced speed and sensitivity of the machine. The depicted ETD option was not present in the used setup. This figure was adapted with friendly permission of Thermo Scientific (www.planetorbitrap.com).

After ionization, the sample is transferred to the C-trap, a C-shaped storage trap that is used to cool down the ions by collision with helium atoms. Furthermore, the ions are focused at the center of the trap before being injected to the Orbitrap (185). In the Orbitrap, the so-called fullscan is performed by acquiring the m/z of all present precursor ions within the injected sample.

The Orbitrap is an orbital-shaped ion trap with a central electrode, which stores the ions by compensating the attraction of ions to the central electrode, by their

centrifugal force, resulting from the initial tangential velocity. The electrostatic field, which the ions experience within the trap lets them move in a complex spiral pattern, which resembles a planet in orbit. The axial component of this movement is independent of the initial energy and coordinates of the ions and can be read out as an image current. By application of Fourier transformation this image current is transformed into a m/z with a very high mass accuracy for the corresponding ions (186).

Subsequent to the full scan, the sample is transferred to a linear ion trap (LIT). A LIT is a circled electrode at which a radio frequency is applied to retain the ions from touching the electrode. Additionally, an electrostatic field at its beginning and its end can be activated to reflect the ions. Thus, the LIT forms a three dimensional field in which the ions can be captured. To capture the ions of interest the field at one end of the LIT is turned off and the trap is filled with the ions, coming from the ion source. The electrostatic field is then switched back on before the ions are returned from the second electrostatic field and the ions of interest are trapped within the LIT (187). During this process, the ions of a certain population are accumulated within the trap by their mass over charge ratio (m/z). The trapping process in the LIT is performed after the first screen of the sample (fullscan), when information about the composition of the existing precursor ions is present. In this study a so-called top10-method was used, isolating the 10 most intense precursor ions from the fullscan for further analysis.

After the isolation, the ions are fragmented within the LIT by application of a defined collision energy combined with the injection of a collision gas into the trap. This results in the controlled fragmentation of the ions into small pieces, a process that is called collision induced dissociation (CID). During this process, the resulting fragments can range from a single amino acid to the remaining ion wherefrom the single amino acid was removed, resulting in a peptide fragment spectrum containing all the possible fragments. These fragments are detected and represent the so-called MS/MS- or MS²-spectra, unravelling the exact amino acid sequence of the isolated precursor ions by calculating the mass difference between the occurring peaks.

Alternatively to the fragmentation in the LIT, the fragmentation can be performed in the higher-energy collision dissociation (HCD) cell. The collision energy for HCD is much higher than for CID, enabling a wider range of fragmentation pathways,

whereas the activation time is reduced. Due to the detection of the resulting HCD-fragments in the Orbitrap mass analyser, there is no low mass cut-off as there is in the LIT (188). The read-out in the Orbitrap mass analyser results in a high-high mass resolution (high resolution full scan and high resolution fragment spectrum) for the HCD-Orbitrap mode compared to the high-low mass resolution (high resolution full scan and low resolution fragment spectrum) output in CID-LIT mode, which in combination with the recently increased speed of the HCD-fragment transmission seems to be a very powerful tool for high resolution MS (189).

6.7.2.1. Liquid chromatography

Reverse phase liquid chromatography is commonly used in modern mass spectrometry to reduce the complexity of the analysed sample and to temporally separate the analytes before they are introduced to the mass spectrometer. The basis for this separation is the interaction of the analytes with a stationary phase, consisting of hydrocarbon chains covalently bound to silica particles (C18 matrix). The analytes are loaded onto this matrix under aqueous conditions and sequentially eluted according to their hydrophobicity to the matrix by applying an increasing percentage of organic solvent (e.g. acetonitrile) over a defined time (190).

For proteomic approaches with small sample volumes the use of standard HPLC systems with flow rates of several mL per minute are not suitable. Therefore, nano HPLC systems are applied, which operate at flow rates of 150 to 300 nL per minute. These nano HPLC systems are coupled to special electrospray ion sources with glass capillary emitters to allow the ionization of the sample at relatively low voltages (1-1.5 kV).

The liquid chromatography was performed on a Dionex NanoRSLC3000 HPLC system (Figure 17). The columns were heated to a temperature of 40°C. The tryptic peptides were automatically injected by an autosampler and loaded onto a nano-trap column at a flow rate of 6 µL per minute in 98% buffer C (0.1% trifluoroacetic acid in HPLC-grade water) and 2% buffer B (80% acetonitrile and 0.08% formic acid in HPLC-grade water) in forward flush orientation. This means that the elution of the sample was performed in the same orientation of the liquid flow as it was loaded onto the trap column before. After 5 minutes, the peptides were eluted from the trap column and separated on an analytical column by a linear gradient from 2% to 35%

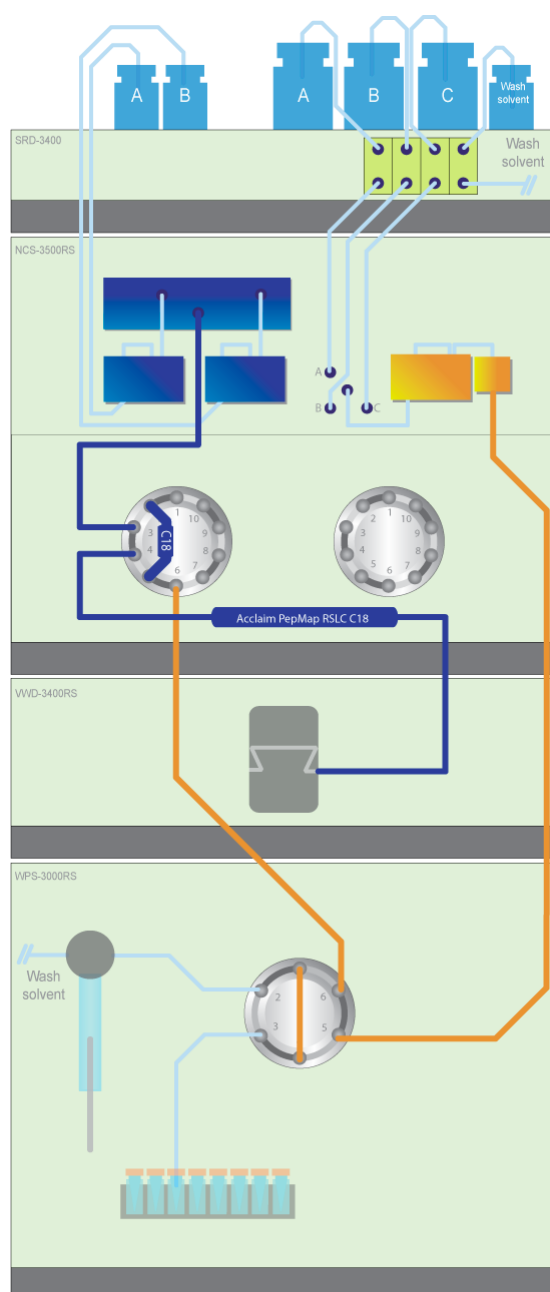


Figure 17: Schematic overview of the Dionex Ultimate 3000 Nano RSLC HPLC system.

This figure shows an schematic overview of the Dionex Ultimate 3000 Nano RSLC system. The samples are automatically injected by the autosampler unit that is shown in the lower part of the figure (green circuit) and loaded onto a C18 trap column (orange circuit). Afterwards, the 10-port valve is switched and the sample is eluted by a nano flow gradient from the trap column and separated on the separation column (Acclaim PepMap RSLC C18, blue circuit) before being transmitted to the mass spectrometer through the UV detector. This scheme shows a backflush configuration for the trap column, which means that the sample is eluted from the trap column by the opposite orientation of the liquid flow as it has been loaded before. In this study a forward flush configuration was used, where the orientation of the liquid flow is the same for loading and elution. The UV detector was not used within this study. This figure is reprinted with friendly permission of Thermo Scientific.

buffer B in buffer A (2% acetonitrile and 0.1% formic acid in HPLC-grade water) at a flow rate of 300 nL/min. The gradient time varied for the different applications (33-145 minutes) and depended on the sample complexity, as an example the gradient for a total LC runtime of 60 minutes is shown in Figure 18. After the gradient reached 35% B, a wash with 95% B for 5 minutes was performed to remove the remaining peptides bound to the column. The column was subsequently equilibrated at 2% B for 15 minutes before the next run. Before each sequence a 33 minute gradient run with a standard protein at a known concentration was performed as quality control. Additionally, two 5 minutes wash gradients were performed in between different samples, including the same standard protein.

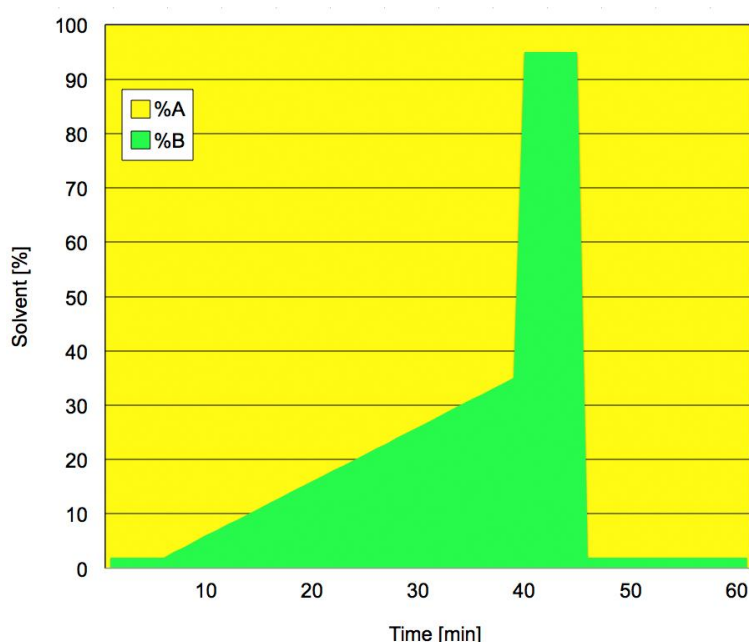


Figure 18: Gradient of an LC run.

This figure shows the gradients of the LC solvents of the nano pump over the time. The yellow area shows the concentration of the buffer A, the green area shows the concentration of the buffer B. The LC run here depicted has a total run time of 60 minutes, the gradient time is 33 minutes and starts from 2% B at 5 minutes and increases until 35% B in minute 38. Afterwards a wash peak at 95%B for 5 minutes follows before the column is again equilibrated at 2% B for 15 minutes.

6.7.2.2. Mass spectrometry methods

After elution from the LC column, the sample was transferred directly to the nanospray source of the LTQ-Orbitrap mass spectrometer by fused silica tubing and ionized instantly. From the fullscan in the Orbitrap mass analyser, the 10 most intense precursor ions were selected for fragment analysis in the LIT, if they

exceeded an ion count of at least 500 and were at least doubly charged. The detection in the LIT was performed at 'normal' resolution and the normalized collision energy for fragmentation was set to a value of 35. While the fragment analysis was performed in the LIT, a high resolution MS scan was acquired in the Orbitrap (30,000 FWHM) with a mass range from 300 to 1500 Da. To enable internal calibration, the lockmass option (191) was used with a background ion from the ionization with a mass of 445.120020. The dynamic exclusion option was used, excluding every ion for 20 seconds after it has been selected for fragmentation.

6.7.2.3. Database searching

For qualitative data analysis the acquired spectra were processed using the Mascot® search algorithm. The data were submitted using the Mascot daemon software to the in-house Mascot server (version 2.4). Monoisotopic masses and peptides with a maximum of 2 missed cleavages were selected. The peptide tolerance was set to 10 ppm and the fragment ion tolerance to 1 Da. As fixed modifications cysteine carbamidomethylation was chosen, as variable modifications asparagine and glutamine deamidation as well as methionine oxidation. The used database was Swiss-Prot, specific subsets of the database were chosen, depending on the species wherefrom the samples were prepared. The instrument type was set to ESI-TRAP, the molecular weight range was set from 300 to 5000 Da.

6.7.3. Data analysis using Scaffold

The search results from Mascot were analysed using the software Scaffold (version 3.6.5). The Scaffold software is based on an algorithm called PeptideProphet and calculates a single probability value for peptide identification from SEQUEST (search algorithm used by Thermo software) or Mascot scores (192). For Scaffold analysis, the search results from Mascot were directly imported to the software and analysed using the same database and modifications. The 'condense data' option was used and the data were analysed with high mass accuracy. After analysis of the data, the output parameters were set to the following: at least 80% probability for peptide identification, a minimum of two peptides identified and at least 95% protein probability.

6.7.4. SILAC quantification using MaxQuant

For the quantification of SILAC-labelled protein complexes from cultured cells, a one-step Strep purification (section 6.4.1) was performed. The samples were pre-fractionated on a 1D-SDS-PAGE, cleaved by trypsin in-gel and processed on the LC-Orbitrap mass spectrometer using a 80 minutes LC-gradients per gel slice. Afterwards, the software MaxQuant was used to analyse the data. The analysis of the spectra is performed using the algorithm 'Andromeda', which has been developed for this software.

Therefore, the raw-files were directly loaded into the application. If the labelling orientation was swapped for the biological replicates (reverse experiments) and if there was more than one experiment to be analysed, an experimental design template file had to be generated. Within this template, the affiliation to the corresponding experiments and their labelling orientation was specified. As fixed modification cysteine carbamidomethylation, as variable modifications methionine oxidation and N-terminal acetylation was selected. Multiplicity was set to two for two conditions, respectively to three for three conditions, the labels were chosen depending on the used labels of the experiment. The first search was set to 10 ppm and the main search to 6 ppm. A maximum of 3 labelled amino acids, a maximum of 5 modifications per peptide, a maximum missed cleavage of 2 and a maximum charge of 7 was set. For the MS/MS search the following settings were used for the ITMS: 0.5 Da MS/MS tolerance, 6 top peaks per 100 Da, de-isotoping off, higher charge on, water loss on, ammonia loss on, dependent ion on. For human cell lines, the human subset of the Swiss-Prot database was used as well as the human first search database. The first search database contains proteins that are commonly in samples and is used for the creation of calibration points for the main search, as well as for re-calibration in later steps of the analysis. The detection of contaminants as well as the reverse hits (calculation of the false discovery rate (131)) was enabled. The contaminant database is implemented in the software and contains common contaminants in mass spectrometric experiments like for example keratin proteins. The option to equal isoleucine with leucine was disabled. The false discovery rate (FDR) for peptides, proteins and sites was set to 1%, the site FDR was applied separately. Minimum number of peptides, razor and unique peptides as well as for unique peptides was set to 2. The maximum peptide posterior error probability (PEP)

was set to 1, minimum peptide length to 7. The unmodified counterpart peptides were not discarded. A minimum ratio count of 2 was set, the re-quantify option was enabled. MaxQuant calculates a ratio for the detected SILAC pairs which reflects the relative abundance of the corresponding protein within the sample.

After the MaxQuant analysis was finished, the statistical tool Perseus was used for further calculations. The ratios were normalized so that the median of logarithmized ratios was at zero. Furthermore, the significance B was calculated, which is based on the calculation of the significance of protein subsets (131). Hits with a significance of $p < 0.01$ were assigned as specific interactors. To graphically illustrate the outcome of the experiment a scatter plot was generated by plotting the intensity on the y-axis and the ratio on the x-axis. The values were shown in logarithmic (\log_2) scale; the minimum value for the y-axis was set to 10,000. The background proteins or proteins that are not altered within the experiment are distributed around a ratio of 1 and form a shape like a Gaussian distribution.

6.7.5. Label-free Quantification using MaxQuant and correlation profiling

For label-free quantification (LFQ) of the mass spectrometric data the software MaxQuant was used. Since no labelling was introduced to the proteins, the spectra of two different runs were quantified against each other. This results in a bigger variability between the samples due to technical reasons like for example spray stability. Still, this technique becomes a more and more popular method in cases that do not allow labelling methods. Here, the label-free approach was combined with a method called protein correlation profiling (PCP). This method originally was used to analyse the elution profiles of organelles, fractionated on a sucrose gradient (193, 194). In combination with LFQ, this technique can be used for the analysis of data from different approaches, as for example in this study for sucrose gradient centrifugation as well as for data from SDS-destabilization experiments.

First, the abundance of the proteins within the corresponding sample was determined using the software MaxQuant. The parameters for the MaxQuant software were selected similar as for the SILAC analysis in the previous section with some minor modifications. The multiplicity was set to one and no isotopic label was chosen. The label-free option was selected and the 'match between runs' option was enabled with a time window of 2 minutes. The fast label-free option was disabled and an

experimental design template was generated, defining each run as a single experiment. For every protein within one experiment, the parameter LFQ intensity is displayed, describing its abundance by the calculation of the volume beyond its intensity peaks for each isotope pattern of each peptide (analogue to the calculation of the volume peak for proteins in the SILAC approach, chapter I section 4.2.2 (195)). Analogue to the classical analysis, the ratio between two samples as well as their significance can be calculated, using the statistical software tool Perseus when two samples have to be compared. However, in this study the data were further analysed by PCP.

PCP was performed as described by Ishikawa et al. 2012 (196). To calculate the elution profile of a protein over several fractions, the relative abundance was calculated by dividing its LFQ intensity by the sum of all LFQ intensities from the fractions within the experiment series. The relative abundance was depicted in a diagram for every fraction and generated an elution profile. Additionally, a PCP-value was calculated, indicating the correlation of the elution profile of a protein to the elution profile of a consensus protein group. This consensus profile was calculated using the mean elution profile from known members of a sub-population. Therefore, the square of the difference between the relative abundance of for a protein in a certain fraction and the mean relative abundance for the consensus proteins in the same fraction was summarized for all fractions. The smaller this PCP-value is, the closer the elution profile matches to the consensus profile, indicating that the protein might belong to the same sub-population of a protein complex.

IV. Results

1. Establishment and optimization of the SDS-affinity purification (SDS-AP) using the interactome of Lebercilin

PCP was developed to define the components of organelle structures within cells (193). To this end, the organelles were partially purified and separated on sucrose density gradients. All proteins within the sample were quantified to generate distinct elution profiles for each protein. These elution profiles were then compared to those of already known components of the organelles of interest. The closer the profiles were to this template, the higher the probability of the protein being a component of the organelle under investigation.

In a recent study the ability of SDS to destabilize protein complexes was used to determine the sub-structure of protein complexes by blue native PAGE (BN-PAGE (177)). The authors analysed the sub-structure of mitochondrial complex I of *Arabidopsis thaliana* by de-stabilizing the complex using very low concentrations of SDS. Therefore, the complex was purified, treated with SDS for controlled disassembly and subsequently separated on a 2D-BN-PAGE. The resulting spots were then analysed by MS and the internal architecture of the complex was predicted.

Within this study, increasing concentrations of SDS were used to destabilize protein complexes purified with SF-TAP tagged Lebercilin by FLAG-affinity purification from HEK293-T cells. Proteins and sub-complexes were sequentially eluted, with decreased sensitivity of their binding to Lebercilin to SDS. By analysing each eluting fraction using mass spectrometry in combination with label-free quantification by MaxQuant, elution profiles for all components of the Lebercilin complex were generated. These elution profiles are very similar to elution profiles of the abovementioned sucrose density gradients. In contrast to this method, where only one organelle of interest was investigated, template profiles for several known or suspected sub-complexes were generated. This method, combining the destabilization of affinity purified protein complexes by SDS was termed SDS affinity purification (SDS-AP). The workflow, combining SDS-AP with liquid chromatography, coupled to quantitative tandem mass spectrometry (LC-MS/MS) and protein correlation profiling is shown in Figure 19.

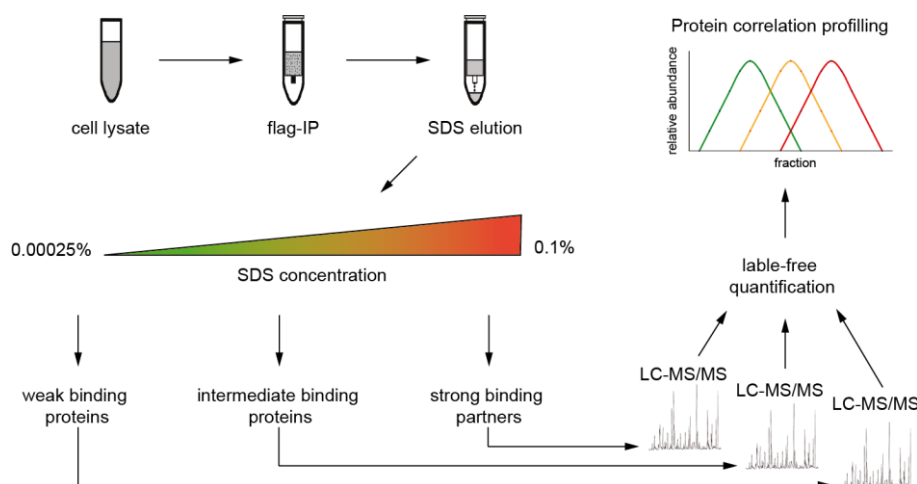


Figure 19: Workflow of the SDS-AP.

In this figure the workflow of the SDS-AP is shown. Protein complexes are purified by one-step affinity purification from crude cell lysates. The elution from the beads is performed sequentially by increasing the SDS concentration stepwise. The eluted fractions are analysed separately by LC-MS/MS and are subsequently quantified label-free by the software MaxQuant. Finally, the elution profiles of the proteins are calculated using protein correlation profiling.

1.1. Optimization of the concentrations for SDS destabilization

The optimal SDS concentrations for the destabilization of a protein complex depend on the composition of the involved proteins and need to be adapted for every protein complex. Therefore, a first series of experiments was performed analysing the dynamic range of the gradient for the protein complex. Three different gradients were used for the destabilization of the Lebercilin complex as shown in Figure 20. The first elution step was chosen at very low SDS concentration (0.00025%) to wash off the non-specific binding proteins. From the second to the sixth fraction a gradient was performed doubling the SDS concentration after each fraction. The last elution step is done by competition reaction with FLAG peptide, eluting all the remaining proteins. The first gradient was performed in a concentration range from 0.002% to 0.05%, the second gradient from 0.0025% to 0.075% and the third gradient from 0.003% to 0.1% SDS.

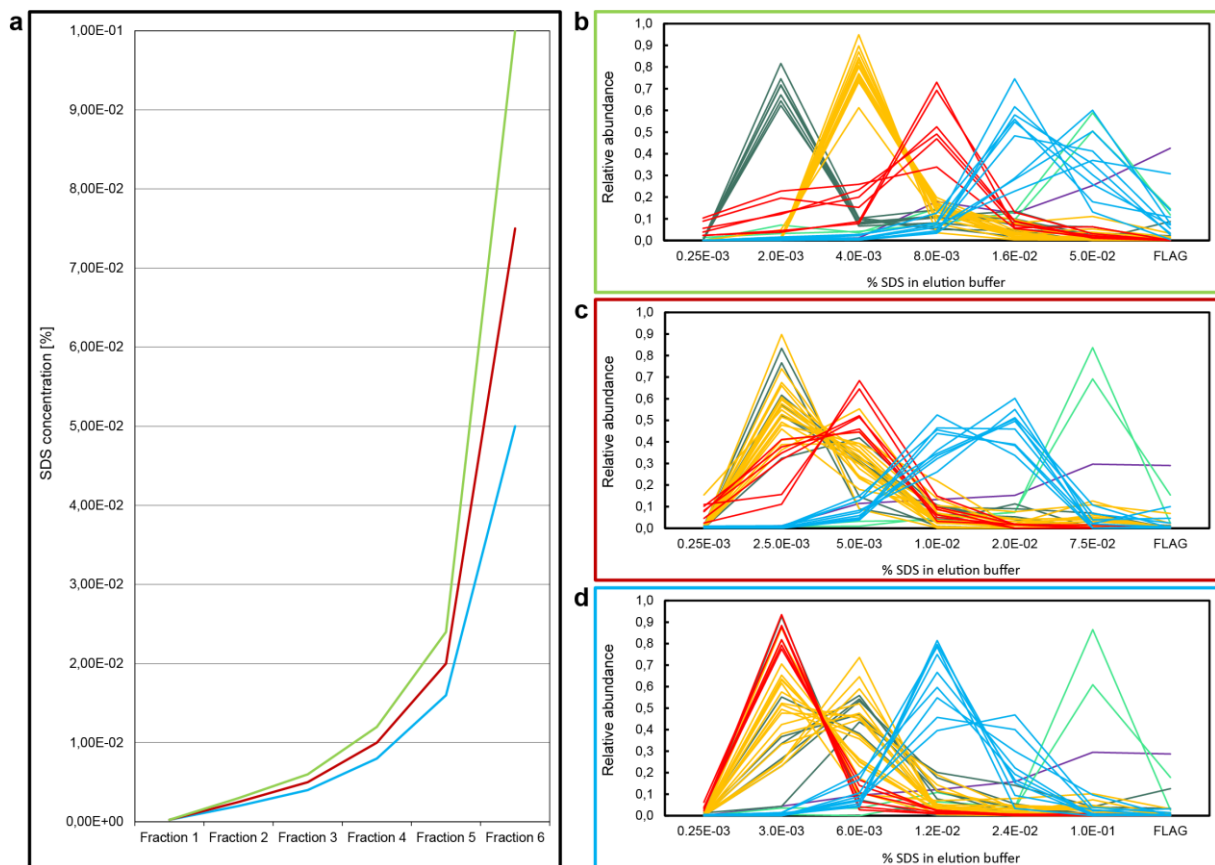


Figure 20: Optimization SDS-concentration.

This figure shows the destabilization of the Lebercilin complex with different SDS gradients. **a** In the left part the concentration curves for the different experiments are shown. In every experiment an initial washing step with a SDS concentration of 0.25E-03% was performed. Afterwards, the gradient followed by a final elution step with FLAG peptide was applied. **b-d** In the right part of the figure the results of the experiment are shown in form of the relative abundance of the known interaction partners of Lebercilin in fractions 1-7. The colour code of the curves is as follows: IFT-A proteins green, IFT-B proteins orange, 14-3-3-proteins red, LisH-CTLH-proteins light blue, dyneins light green and Lebercilin purple. The colour of the frame around the graphs corresponds to the concentration curve of the left part of the figure. The starting concentration of each gradient was doubled to the next fraction, five fractions per gradient. The concentrations for the gradients are as follows, green gradient (**b**) 2.0E-03% SDS, red gradient (**c**): 2.5E-03% SDS, blue gradient (**d**): 3.0E-03% SDS.

These first gradient series showed that the SDS-AP is able to separate single modules within the Lebercilin interactome. The concentrations were further optimized to show a clean separation of the modules. Therefore, different SDS-concentrations for every peak were tested and the PCP-values, reflecting the resemblance of the elution profiles of the proteins from a consensus profile, were taken into account for achieving the best possible resolution.

1.2. Destabilization of the Lebercilin complex by SDS-AP

A gradient with a starting concentration of 0.0025% SDS, doubling its concentration over three fractions and a final elution step at 10-fold SDS-concentration was chosen for the separation of the protein complex of Lebercilin (Figure 21). The IFT-A proteins eluted at a concentration of 0.0025% SDS and the calculation of their PCP-value, using several IFT-A proteins as a consensus (namely, IFT43, IFT122, WDR35, TTC21B, IFT140, WDR19 and TULP3) showed a clear separation from the other proteins within this experiment (PCP-IFT-A for IFT-A proteins is below 0.003).

The protein Tubby-like protein 3 (TULP3) elutes at the same concentration as the IFT-A proteins and its PCP-value indicates its resemblance to the IFT-A proteins (PCP IFT-A = 0.001). TULP3 was previously described to be associated with the IFT complex A and was found in the IFT complex A complex by tandem affinity purification based methods (197). To validate this, an expression vector for SF-TAP-tagged TULP3 was used to express the protein in HEK293-T cells. SF-TAP purification was performed and the eluted complexes were analysed by MS. This resulted in the detection of all IFT complex A proteins within the complex of TULP3 (Table 13), validating the SDS-AP results and showing that this method is also suitable for detecting novel components of the sub-modules of a protein complex.

The proteins of the IFT-B co-elute at an SDS concentration of 0.005%, their PCP-values (PCP-IFT-B for IFT-B proteins below 0.004) indicate that the elution profiles are very similar within this sub-module. For the calculation of the PCP-value for IFT-B the proteins IFT20, HSPB11, IFT46, IFT52, TRAF3IP1, IFT57, IFT74, IFT80, IFT81, IFT88, IFT172, IFT27, CLUAP1, RABL5, TTC26, TTC30A and TTC30B were used as a template. The protein CEP170 was chosen as an interesting candidate during the optimization process due to its high resemblance to the IFT-B elution profile. In this experiments, CEP170 varies from the IFT-B elution profile but is still mainly eluting at the same concentration as the IFT-B. The protein CEP170 and its association to the IFT-B was analysed in detail in section 3.

The 14-3-3 proteins elute at concentrations between 0.005% to 0.010%, the PCP-value using the 14-3-3 proteins eta and gamma as a template shows a high correlation of the elution profiles (PCP-14-3-3 for 14-3-3 proteins below 0.052). The only protein of the 14-3-3 module, which does not fit to the PCP-values is the 14-3-3 zeta/delta which is mainly eluting at 0.005% SDS (PCP-14-3-3 for 14-3-3 zeta/delta

0.135). Nevertheless, it is possible to clearly distinguish the elution profile of the 14-3-3 proteins from other eluting interaction partners, confirming published data that the 14-3-3 proteins form a stable complex (115, 198). A complete list of the determined PCP-values for the quantified proteins is available on the supplemental DVD, attached to the printed version of this study.

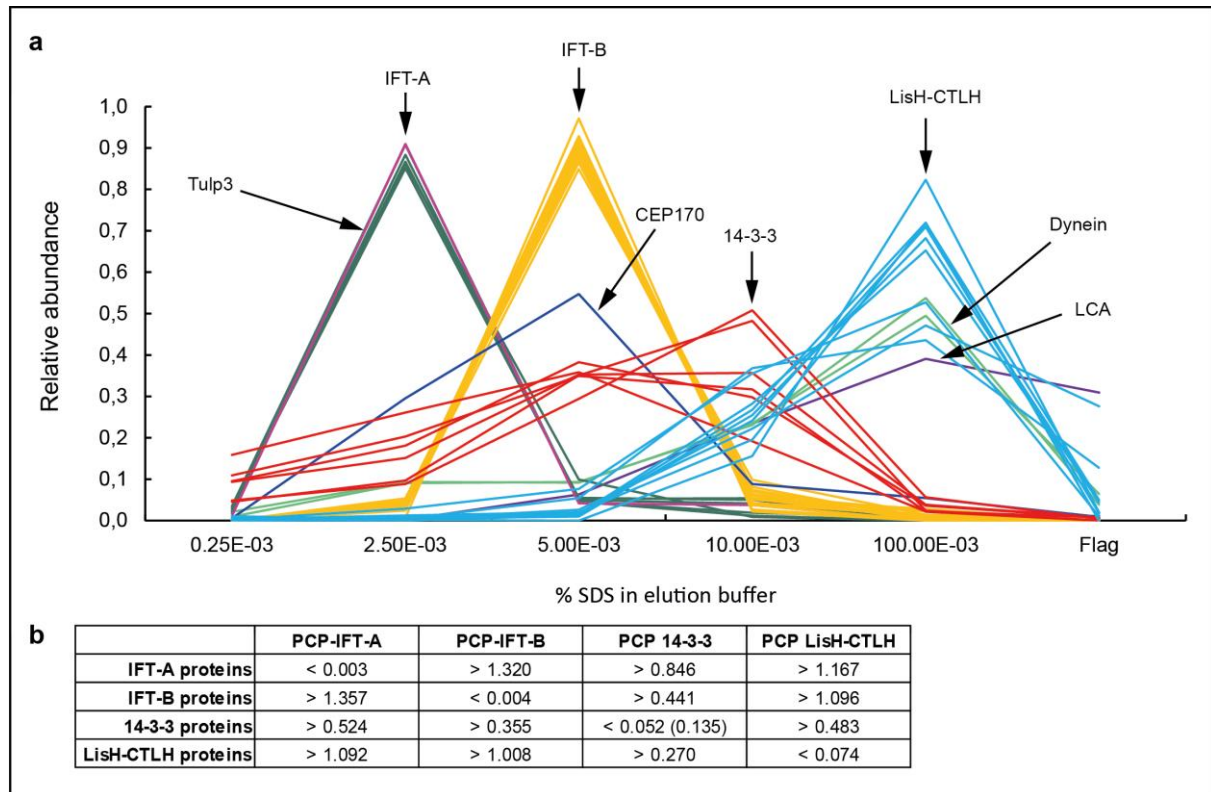


Figure 21: SDS destabilization of the Lebercilin protein complex.

This figure shows the destabilization of the Lebercilin protein complex. **a** Relative elution profiles of the components of the proteins interacting with Lebercilin. On the y-axis the relative abundance is plotted against the SDS concentration of the corresponding eluted fractions on the x-axis. Proteins of the IFT-A are shown in dark green and elute at a concentration of 2.5E-03% SDS, the protein TULP3 (pink) is perfectly co-eluting with the IFT-A. The proteins of the IFT-B are shown in orange and elute at a concentration of 5.0E-03% SDS, CEP170 (dark blue) is a potential IFT-B associated protein. The proteins of the 14-3-3 sub-module (red) mainly elute at concentrations of 5E-03 to 10E-03. The proteins of the LisH-CTLH complex (light blue) as well as the dyneins (light green) and the bait Lebercilin (purple) were mainly eluted by a final SDS concentration at 100E-03%. **b** In the lower part of the figure the corresponding PCP-values, calculated using different consensus groups for the corresponding sub-modules are depicted. The values for the proteins of a certain module are clearly below the values of the other proteins when using their own consensus pattern. Only in the case of the 14-3-3 zeta/delta one member of the 14-3-3 complex deviates significantly from the others (14-3-3: PCP₁₄₋₃₋₃ = 0.135). For this experiment a total number of 8 biological repetitions were performed.

The destabilization of the Lebercilin complex revealed a further sub-module, the LisH-CTLH complex. This complex consists of proteins that were described as miscellaneous in our recent study of the Lebercilin complex (50). However, some of these proteins were described to form a complex (199). Looking closer at the domain structure of the members of this module revealed that three out of these nine proteins contain a “Lissencephaly type-1-like homology” (LisH) and a “C-terminal to LisH” (CTLH) motif. The analysis of the whole human genome using the alignment tool SMART ((200) <http://smart.embl-heidelberg.de>) showed, that there are only 10 human proteins that contain both of these two motifs at once.

Table 13: SF-TAP-analysis of TULP3-N-SF-TAP.

This table shows the results of three SF-TAP experiments in HEK293-T cells with TULP3-N-SF-TAP as a bait. The indicated proteins were identified in three out of three experiments. Highlighted are the identified IFT-A proteins, the values indicate the number of unique peptides. The protein identification probability was set to 95%, the peptide identification probability to 80% as determined by Scaffold. The complete list of all interactors is available on the supplemental DVD, attached to the printed version of this study.

Identified Proteins	Gene name	Exp1	Exp2	Exp3
Tubby-related protein 3	TULP3	50	50	47
Intraflagellar transport protein 43 homolog	IFT43	6	9	8
Intraflagellar transport protein 122 homolog	IF122	46	42	42
WD repeat-containing protein 35	WDR35	57	38	48
Tetratricopeptide repeat protein 21B	TT21B	41	37	36
Intraflagellar transport protein 140 homolog	IF140	61	65	62
WD repeat-containing protein 19	WDR19	61	52	61

The LisH-CTLH module eluted at a 10-fold higher SDS concentration (0.1% SDS) than the 14-3-3 proteins, reflecting their stronger association with Lebercilin compared to the 14-3-3 proteins. The PCP-values for the LisH-CTLH module were calculated using the proteins C20orf11, MKLN1, RANBP9, RANBP10, RMND5A, YPEL5, MAEA, WDR26 and ARMC8 as a template (PCP-LisH-CTLH for LisH-CTLH proteins below 0.074) and are clearly separated from the members of the other modules. Although a part of the LisH-CTLH complex was already described by Kobayashi and co-workers (201), its function remain elusive and a comprehensive description is still necessary. Here, a SF-TAP experiment with RANBP9-SF-TAP was performed (Table 14) that showed that the LisH-CTLH module consists of at least 9 proteins and forms a stable sub-module within the Lebercilin interactome. The further

characterization of this module as well as its functional analysis is currently under investigation in collaboration with Ronald Roepman from Nijmegen.

Finally, two dynein light chain proteins (DYNLL1 and DYNLL2), co-elute with the LisH-CTLH module, indicating their strong interaction with the protein Lebercilin. DYNLL1 and DYNLL2 have been described to form a heterodimer (202) and in our previous study we described their association to Lebercilin (50).

Table 14: SF-TAP analysis of RANBP9.

SF-TAP experiment with over-expressed RANBP9-SF-TAP (Ran-binding protein 9). Highlighted are the identified proteins of the LisH-CTLH module that were identified in two experiments, the values indicate the number of unique peptides. The protein identification probability was set to 95%, the peptide identification probability to 80% as determined by Scaffold. The complete list of interactors is available on the supplemental DVD, attached to the printed version of this study.

Identified Proteins	Gene name	Exp1	Exp2
Macrophage erythroblast attacher	MAEA	18	20
Ran-binding protein 9	RANB9	33	38
WD repeat-containing protein 26	WDR26	37	38
Muskelin	MKLN1	44	44
Armadillo repeat-containing protein 8	ARMC8	19	17
Ran-binding protein 10	RBP10	13	13
Protein C20orf11	CT011	8	9
Protein RMD5 homolog A	RMD5A	8	13
Protein yippee-like 5	YPEL5	9	9

A fraction of the SDS eluates was used for western blot analysis (Figure 22). For the IFT-A no suitable antibody was available, whereas the other modules were detected by the following antibodies: IFT-B: anti-TRAF3IP1, 14-3-3: anti-14-3-3- ϵ , LisH-CTLH: anti-C20orf11 and Lebercilin with anti-FLAG-HRP. The IFT-B showed a signal in the third lane, which corresponds to a SDS concentration of 0.005%. The second panel shows the elution of the 14-3-3-module, represented by 14-3-3- ϵ , which elutes mainly in the fractions three and four (0.005% to 0.01% SDS), but also shows a faint band in fraction one. The LisH-CTLH module is represented by the protein C20orf11 that has its elution peak in fraction 5 (0.1% SDS) and an additional faint band in fraction 6 (FLAG-peptide elution). The bait protein LCA5-N-SF-TAP was faintly detected in fraction 3 and showed stronger bands at higher SDS concentrations. It was still detectable in the final elution step with FLAG peptide. These results confirm the MS data and show the sequential elution of the corresponding modules.

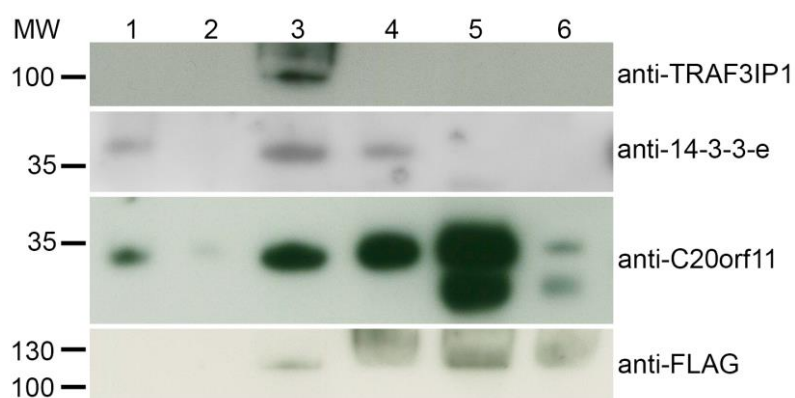


Figure 22: Western blot of the proteins eluted by SDS destabilization of the Lebercilin protein complex.

This figure shows the western blot analysis of the SDS-AP of the protein complex of Lebercilin. The eluates of three biological replicates were pooled, applied to an SDS-PAGE gel and subsequently transferred to PVDF membrane. The numbers correspond to the different elution steps with different SDS concentrations, 1: 0.00025% SDS, 2: 0.0025% SDS, 3: 0.005% SDS, 4: 0.01% SDS, 5: 0.1% SDS, 6: FLAG peptide. After incubation with each antibody the membrane was stripped to remove the bound antibodies. TRAF3IP1 is a member of the IFT-B and elutes in fraction three at a SDS-concentration of 5.0E-03%. The 14-3-3-module is represented by 14-3-3-ε and elutes mainly in the fractions 3 and 4 in a concentration range of 0.005% to 0.01%. Additionally, a band in the first fraction occurs for the the 14-3-3-module. The LisH-CTLH-module is detected by anti-C20orf11 and shows a strong band in fraction 5 (0.1% SDS). The bait protein Lebercilin was fused to a SF-TAP-tag and therefore was detected by an anti-FLAG antibody. The elution of Lebercilin starts in the fraction 3 (0.005% SDS) and is further detected with higher SDS concentrations until the last elution step with FLAG-peptide in fraction 6.

2. The intraflagellar transport complex B

2.1. Determination of the components of the IFT complex B

2.1.1. Detection of the IFT-B by transient overexpression of IFT88-SF-TAP in HEK293-T

Before determining the sub-structure of the IFT-B, it was essential to comprehensively describe the complex. To this end, SF-TAP experiments with IFT88-SF-TAP as bait were performed. Therefore, HEK293-T cells were transfected transiently with IFT88-SF-TAP and tandem affinity purification was performed. Subsequent, the eluates were cleaved tryptically and liquid chromatography coupled to tandem mass spectrometry was applied. The results of this experiment are shown in Table 15. Despite the stringent washing conditions of the two step affinity

purification, not only the central core of the IFT-B, but also proteins that were thought to be associated to the IFT-B (TTC26, TTC30A, TTC30B, RABL5 and HSPB11 (50)) were detected reproducibly by mass spectrometry. The detection of most of the components of the IFT-B indicates a central role for IFT88 within this complex.

Table 15: SF-TAP experiment of IFT88-SF-TAP in HEK293-T cells.

This table shows the result of an SF-TAP experiment in HEK293-T cells, transiently overexpressing IFT88-SF-TAP. Shown are the proteins belonging to the IFT-B or associated with the IFT-B, the complete list is available on the supplemental DVD, attached to the printed version of this study. The numbers show the unique peptides, identified per experiment. The protein identification probability was set to 95% the peptide identification probability to 80% as determined by Scaffold and at least 2 unique peptides had to be detected. Proteins that are indicated with n.i. (not identified), were not detected in the corresponding experiment

Protein	Uniprot	Gene Name	Exp1	Exp2	Exp3
Intraflagellar transport protein 20 homolog	Q8IY31	IFT20	n.i.	n.i.	n.i.
Rab-like protein 5 (IFT22)	Q9H7X7	RABL5	3	6	6
Intraflagellar transport protein 25 homolog	Q9Y547	HSPB11	n.i.	3	2
Intraflagellar transport protein 27 homolog	Q9BW83	IFT27	2	6	3
Intraflagellar transport protein 46 homolog	Q9NQC8	IFT46	5	7	6
Intraflagellar transport protein 52 homolog	Q9Y366	IFT52	6	12	9
Intraflagellar transport protein 54 homolog	Q8TDR0	TRAF3IP1	n.i.	n.i.	n.i.
Intraflagellar transport protein 57 homolog	Q9NWB7	IFT57	2	n.i.	n.i.
Intraflagellar transport protein 74 homolog	Q96LB3	IFT74	14	20	18
Intraflagellar transport protein 80 homolog	Q9P2H3	IFT80	2	2	n.i.
Intraflagellar transport protein 81 homolog	Q8WYA0	IFT81	8	22	17
Intraflagellar transport protein 88 homolog	Q13099	IFT88	38	36	36
Intraflagellar transport protein 172 homolog	Q9UG01	IFT172	7	n.i.	n.i.
Clusterin-associated protein 1	Q96AJ1	CLUAP1	n.i.	n.i.	n.i.
Tetratricopeptide repeat protein 26	A0AVF1	TTC26	3	14	12
Tetratricopeptide repeat protein 30A	Q86WT1	TTC30A	2	n.i.	n.i.
Tetratricopeptide repeat protein 30B	Q8N4P2	TTC30B	7	6	5

2.1.2. Detection of the IFT-B by stable expression of IFT88-SF-TAP in HEK293

To improve the purification of the IFT-B while reducing the negative effects of overexpression, like misfolding or disturbed stoichiometry, HEK293 cells stably expressing IFT88-SF-TAP were produced. The analysis of the IFT-B using these stable lines as source for SF-TAP experiments increased the number of detected IFT-B proteins within the experiments. All published proteins that were assigned to the IFT-B (50) were reproducibly detected using this cell line (Table 16). Therefore, this cell line was chosen as starting point for further experiments for characterizing the IFT-B.

Table 16: SF-TAP experiment with a stable IFT88-SF-TAP HEK293 cell line.

This table shows the results of an SF-TAP experiment with IFT88-SF-TAP that was stably expressed in HEK293 cells. Depicted are the proteins that belong to the IFT-B and were found with at least two or more unique peptides. Indicated are the numbers of unique peptides for every experiment. The protein identification probability was set to 95%, the peptide identification probability to 80% as determined by Scaffold. The listed proteins are the detected members of the IFT-B, the complete list of the interactors is available on the supplemental DVD, attached to the printed version of this study

Protein name	Uniprot	Gene name	Exp-1	Exp-2	Exp-3
Intraflagellar transport protein 20 homolog	Q8IY31	IFT20	6	8	8
Rab-like protein 5 (IFT22)	Q9H7X7	RABL5	9	10	11
Intraflagellar transport protein 25 homolog	Q9Y547	HSPB11	4	4	6
Intraflagellar transport protein 27 homolog	Q9BW83	IFT27	7	8	8
Intraflagellar transport protein 46 homolog	Q9NQC8	IFT46	6	11	11
Intraflagellar transport protein 52 homolog	Q9Y366	IFT52	15	19	22
Intraflagellar transport protein 54 homolog	Q8TDR0	TRAF3IP1	3	14	11
Intraflagellar transport protein 57 homolog	Q9NWB7	IFT57	8	14	20
Intraflagellar transport protein 74 homolog	Q96LB3	IFT74	26	34	41
Intraflagellar transport protein 80 homolog	Q9P2H3	IFT80	9	24	32
Intraflagellar transport protein 81 homolog	Q8WYA0	IFT81	29	42	44
Intraflagellar transport protein 88 homolog	Q13099	IFT88	53	49	45
Intraflagellar transport protein 172 homolog	Q9UG01	IFT172	30	69	80
Tetratricopeptide repeat protein 26	A0AVF1	TTC26	17	26	29
Tetratricopeptide repeat protein 30A	Q86WT1	TTC30A	5	8	8
Tetratricopeptide repeat protein 30B	Q8N4P2	TTC30B	13	26	29
Clusterin-associated protein 1	Q96AJ1	CLUAP1	8	11	20

2.2. Determination of the substructure of the IFT complex B

2.2.1. Transient overexpression of several IFT proteins in HEK293-T

To confirm the data generated by the SF-TAP experiments with IFT88-SF-TAP and possibly extend the information on the IFT-B, further IFT proteins were tagged by SF-TAP and SF-TAP purifications were performed. The analysis of the IFT-B by transient expression with different IFT-B members as bait showed a separation of the IFT-B into two different sub-modules (Table 17). Using IFT27 and IFT52 as bait resulted in the purification of a group of IFT-B proteins that are thought to form the IFT-B core complex (45). In contrast, the purification with IFT20 and IFT57 as baits isolated the

remaining components that were not co-purified with the other two baits. These two sub-modules show no overlap except for IFT52, which was found in both sub-modules. Nevertheless, the determination of a second module by purification with IFT20 and IFT57, that was termed sub-complex B1, is not in line with the results from literature. Until now the IFT-B was thought to consist of a core complex (the here described sub-complex B2) and other associated proteins that dissociate from the complex when ionic strength is applied to the latter. The results shown here however, led to the hypothesis that the IFT-B is divided into two discrete sub-modules.

Table 17: SF-TAP experiments with different baits.

This table shows the results of a SF-TAP experiments isolating the protein complexes of IFT20-SF-TAP, IFT27-SF-TAP, IFT52-SF-TAP and IFT57-SF-TAP, transiently overexpressed in HEK293-T. Proteins that were identified in at least in two out of three experiments are marked with a hook. The here listed proteins are all the members of the IFT-B, TTC30A and TTC30B were not identified (n.i.). The complete list of the interactors is available on the supplemental DVD, attached to the printed version of this study. The protein identification probability was set to 95%, the peptide identification probability to 80% as determined by Scaffold.

Protein	UniProt	Gene name	IFT20-SF-TAP	IFT27-SF-TAP	IFT52-SF-TAP	IFT57-SF-TAP	Sub-complex
Intraflagellar transport protein 88 homolog	Q13099	IFT88					n.i.
Intraflagellar transport protein 20 homolog	Q8IY31	IFT20	✓				1
Intraflagellar transport protein 54 homolog	Q8TDR0	TRAF3IP1	✓				1
Intraflagellar transport protein 57 homolog	Q9NWB7	IFT57	✓			✓	1
Intraflagellar transport protein 80 homolog	Q9P2H3	IFT80	✓				1
Intraflagellar transport protein 172 homolog	Q9UG01	IFT172	✓			✓	1
Clusterin-associated protein 1	Q96AJ1	CLUAP1	✓				1
Intraflagellar transport protein 25 homolog	Q9Y547	HSPB11		✓			2
Intraflagellar transport protein 27 homolog	Q9BW83	IFT27		✓	✓		2
Intraflagellar transport protein 46 homolog	Q9NQC8	IFT46		✓	✓		2
Intraflagellar transport protein 74 homolog	Q96LB3	IFT74		✓	✓		2
Intraflagellar transport protein 81 homolog	Q8WYA0	IFT81		✓	✓		2
Tetratricopeptide repeat protein 26	A0AVF1	TTC26		✓	✓		2
Rab-like protein 5	Q9H7X7	RABL5		✓	✓		2
Intraflagellar transport protein 52 homolog	Q9Y366	IFT52		✓	✓	✓	1+2
Tetratricopeptide repeat protein 30A	Q86WT1	TTC30A					n. i.
Tetratricopeptide repeat protein 30B	Q8N4P2	TTC30B					n. i.

2.2.2. Sucrose density centrifugation

To validate the hypothesis of the IFT-B existing as two discrete sub-complexes, the whole IFT-B was isolated by SF-TAP purification from a HEK293 cell line, stably

expressing SF-TAP-tagged IFT88 and separated by sucrose density centrifugation. The SF-TAP eluates from two experiments were pooled and applied to a discontinuous sucrose gradient from 5-20% sucrose. The protein complex was then separated by centrifugal force at 200,000 x g for four hours. Afterwards, the gradient was fractionated from top to the bottom, the proteins were precipitated, cleaved and applied to quantitative LC-MS/MS. The relative abundance for each complex member was plotted and protein correlation profiling was applied (Figure 23).

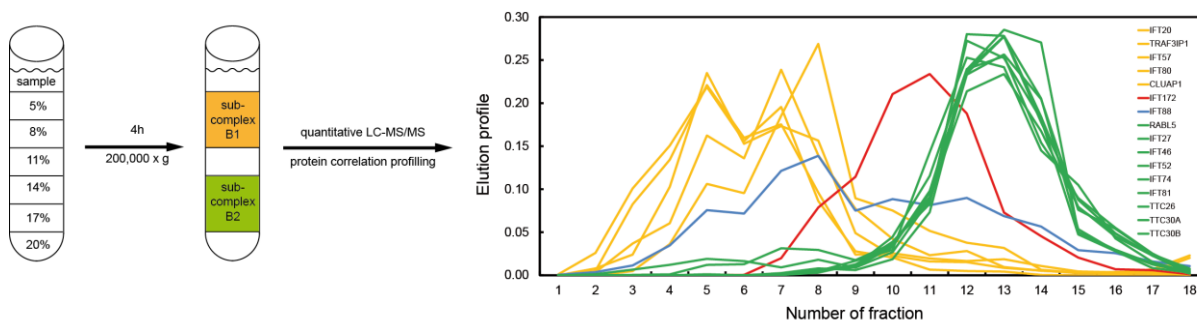


Figure 23: Isolation of IFT-B sub-complexes by sucrose density centrifugation.

This figure shows the isolation of the IFT-B sub-complexes by sucrose density centrifugation applied to SF-TAP-eluate from HEK293 cells stably expressing IFT88-SF-TAP. The SF-TAP eluate was applied to a 5-20% sucrose gradient. After centrifugation, the gradient was fractionated from top to bottom and the resulting fractions were subjected to LC-MS/MS analysis. After label-free quantification by MaxQuant, co-eluting proteins were detected by protein correlation profiling (PCP) using IFT-B1 and IFT-B2 mean values as templates. The elution profiles of the components of the sub-complex B1 are shown in orange, the components of the sub-complex B2 are shown in green. IFT88 is indicated in blue and IFT172 in red. The elution profiles of the different proteins over the fractions show a clear separation of the two sub-complexes except for IFT172 and the bait IFT88. The protein HSPB11 was only found in one of the three experiments and occurred in fraction 15.

The results showed a clear separation into two different populations, matching with the two postulated sub-complexes from previous SF-TAP experiments. The sub-complex B1 sedimented at lower sucrose concentrations than the sub-complex B2, indicating that B1 is lighter than B2. The protein IFT172 represents an outlier and sedimented at a sucrose concentration between both sub-complexes. The different behaviour of IFT172 already is described in the literature, Cole et al. observed a partial dissociation of IFT172 from the IFT-B when applying low ionic strength to the complex (35). The protein IFT88 was found in both sub-complexes. The protein HSPB11 only was found in one of the three experiments (fraction 15) and was therefore excluded from the plot.

2.3. Analysis of functional differences between the IFT-B sub-complexes B1 and B2

To determine the importance of the function of some selected components of the IFT and potentially of the two sub-complexes determined, siRNA knockdown experiments in IMCD3 cells were performed. Subsequent, the difference in cilia morphology and the localization of the IFT-B were analysed by immunostaining. The proteins *Ift52*, *Ift88*, *Ttc30a1* and *Ttc30b* from the IFT-B were chosen for these experiments. Bioinformatic analysis of the generated SF-TAP data by two of our collaboration partners (Grischa Toedt, EMBL Heidelberg and Konstantinos Kontroumpas CNRS Paris) predicted the mentioned proteins as possible central components of the IFT-B, linking the two sub-complexes. Additionally, the protein *Arl13b*, that plays an important role within the ciliary transport (203) was knocked down by siRNA. Additionally, a double knockdown, using the siRNAs for *Ift52* and *Ift88* was performed. Two different types of experiment were performed. First an approach, using the automated imaging system Operetta was executed. Cells were reverse transfected in 96-well plates with siRNAs and fixed with methanol and immunostained 72 hours later. Nuclei were stained with DAPI, cytoplasm with TOTO-3 and cilia with acetylated alpha tubulin and a secondary antibody conjugated to AlexaFluor 488. 6 fields of view were imaged per well using a 20x objective lens on the Operetta automated imaging system. Cells, nuclei and cilia were automatically detected using custom detection algorithms using Perkin Elmer Columbus software. The percentage of cells having a single cilium was compared to a negative control that was transfected with a non-targeting siRNA pool. This experiment showed a different effect for all of the chosen candidates (Figure 24). In the control experiment 33% of the cells had a single cilium, the knockdown of *Ttc30b* does not have a large effect, 28% of the present cells had a single cilium. Similar results were obtained for the knockdown of *Arl13b* (26%) and *Ttc30a1* (22%). In contrast, the knockdown of *Ift88* led to half of the amount of cells bearing a cilium compared to the control (16%) and the knockdown of *Ift52* even reduced the number of cilia to a third of the control (11%). The statistical significance for all knockdown experiments was determined by student t-test (p-value < 0.02).

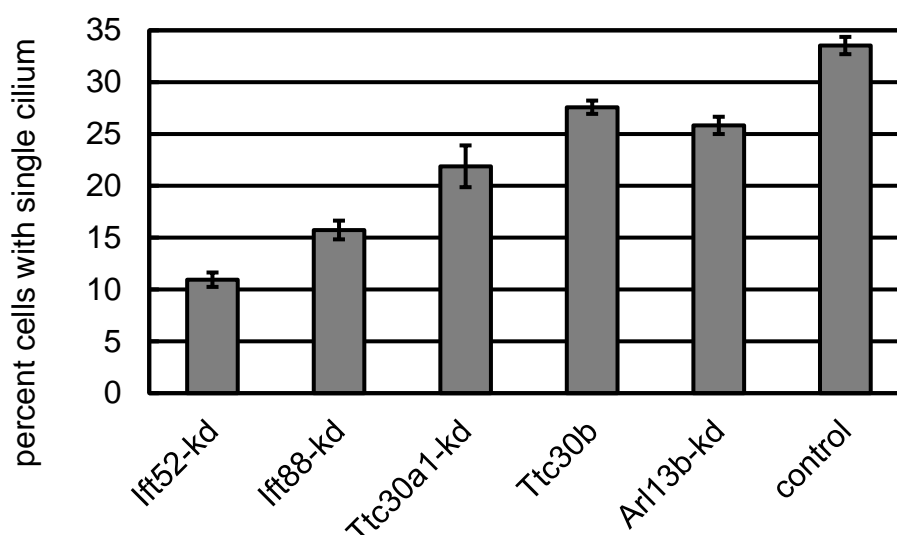


Figure 24: Knockdown of several IFT proteins in IMCD3 cells.

Effect of the knockdown of lft52, Ttc30a1, Ttc30b, Arl13b and lft88 by siRNA on cilia formation in IMCD3 cells. Depicted are the percentages of cells with a single cilium compared to the control experiment with non-targeting siRNA. The experiment was performed with three to four biological replicates the p-value for all knockdowns was below 0.02 (calculated by students t-test).

Additionally to the Operetta screen, the morphology of the cilia and the localization of the IFT-B during the same knockdowns were analysed by confocal microscopy. The cells were grown on glass coverslips, forward transfected after 24 hours and fixed and subsequently stained after a further 72 hours using different antibodies against components of the IFT-B. For the staining anti-IFT52, anti-TRAF3IP1 and anti-IFT88 were used in combination with an antibody against a ciliary marker protein (acetylated alpha tubulin or alpha/beta-tubulin), secondary antibodies conjugated to AlexaFluors 488, 568 and 594 and DAPI. The images of these experiments were acquired on a Nikon A1R scanning confocal microscope and are shown in Figure 25. The control experiment for these knockdowns is shown in Figure 26.

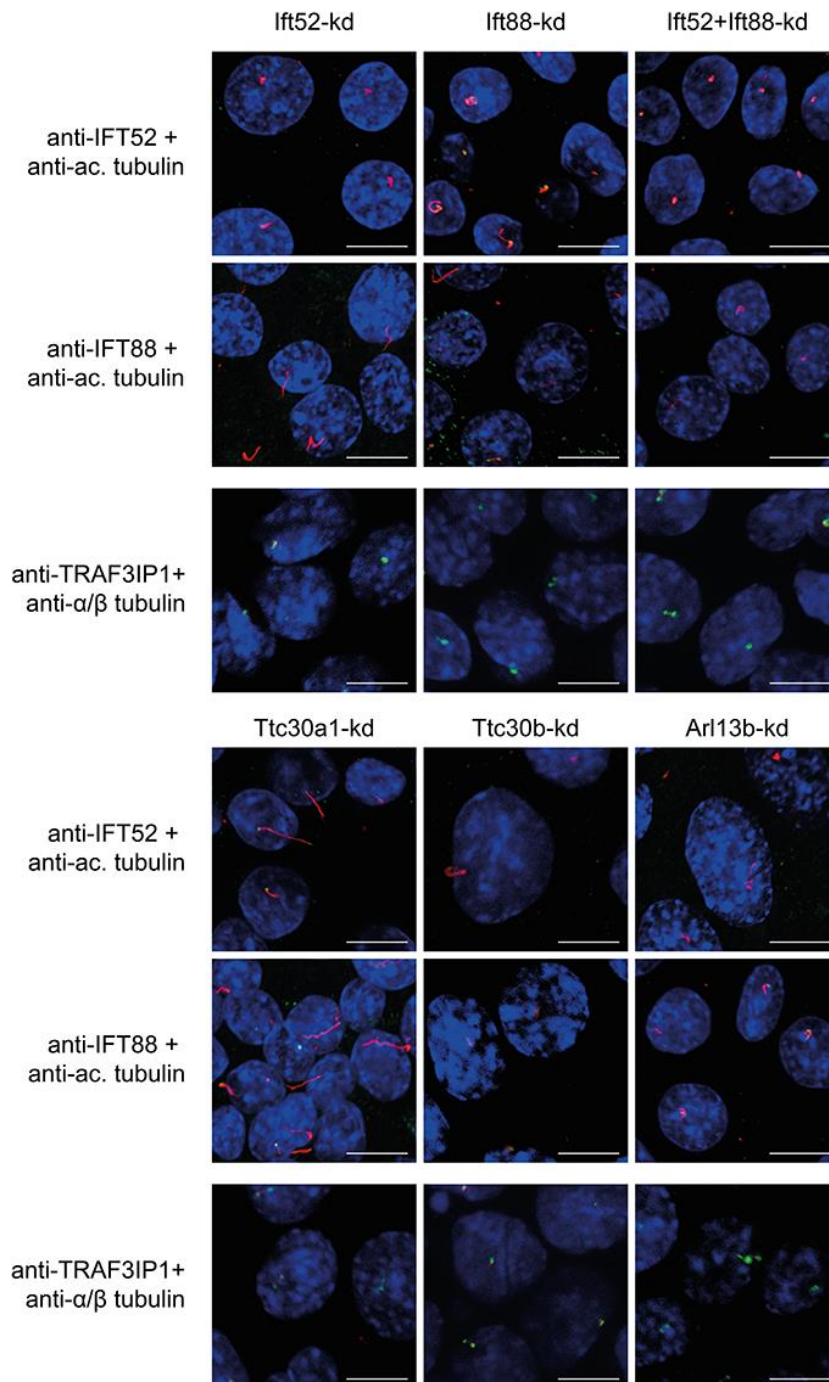


Figure 25: Localization of IFT particle during knockdown of different IFT proteins.

This figure shows the localization of the IFT particle, represented by IFT52, IFT88 and TRAF3IP1 at the cilium during knockdown of different IFT proteins in IMCD3 cells. The knockdowns were achieved by transfection with siRNAs in starved IMCD3 cells. As marker protein for the cilium (red) anti-acetylated alpha tubulin or anti-alpha/beta tubulin were used. For the localization of the IFT particle (green) anti-IFT52, anti-IFT88 and anti-TRAF3IP1 were used. The nuclei of the cells were visualized by DAPI (blue). Shown are the experiments for the knockdown of lft52, lft88, double knockdown lft52+lft88, Ttc30a1, Ttc30b and Arl13b stained with the above mentioned antibodies. The scale bars represent 10 μ m, the contrast of the pictures was enhanced using Photoshop image software.

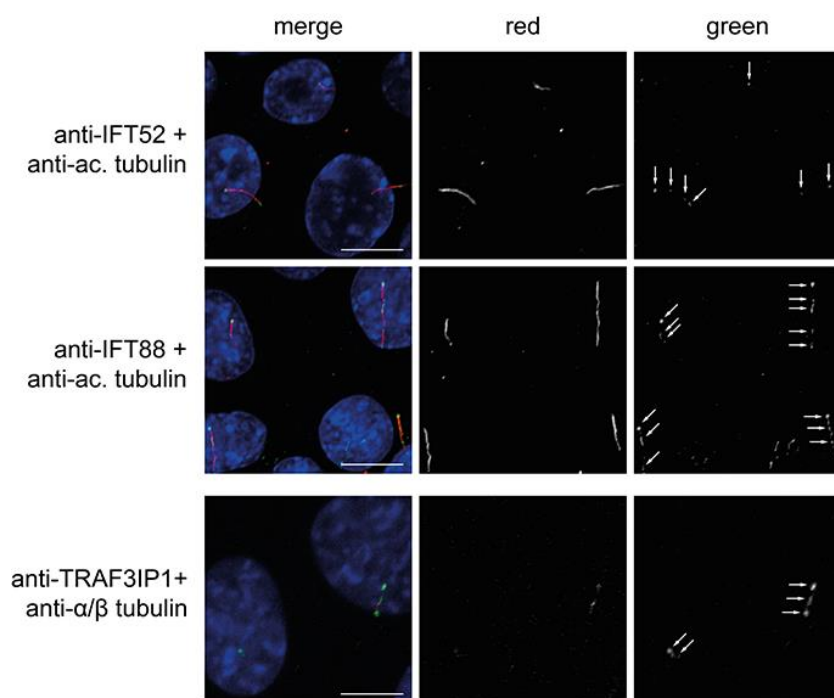


Figure 26: Control experiment for the knockdown of IFT proteins by siRNA in IMCD3 cells.

This figure shows the control experiment for the knockdown experiments of different IFT proteins in starved IMCD3 cells. The cells were starved and transfected with non-targeting siRNA. The localization of the IFT particle at the cilium was visualized by staining with IFT52, IFT88 and TRAF3IP1. As marker protein for the cilium (red) anti-acetylated alpha tubulin or anti-alpha/beta tubulin were used. For the localization of the IFT particle (green) anti-IFT52, anti-IFT88 and anti-TRAF3IP1 were used. The nuclei of the cells were visualized by DAPI (blue). Depicted are the overlays of the the signals generated by using the different antibodies as well as the single channel view for the red channel (ciliary marker) and the green channel (IFT antibodies). The scale bars represent 10 μ m, the arrow heads indicate staining position of the IFT antibodies in the control sample. The contrast of the pictures was enhanced using Photoshop image software.

The knockdown of *Ift52* (Figure 25) can be confirmed by the staining with anti-IFT52, there is no staining along the axoneme of the cilium and only a small accumulation at the base of the cilium. The cilia are shortened within this knockdown as visualized by the staining with ac. tubulin or malformed as visible in the co-staining with anti-IFT88. The staining with anti-IFT88 also shows a very weak signal at the base of the cilium. The same is true for the staining with anti-TRAF3IP1, only very short cilia can be observed, indicating that the IFT might be impaired by the knockdown of *Ift52*. When *Ift88* is knocked down, the cilia are also shortened or malformed. The staining of *Ift52* is still visible along the malformed cilia. In contrast, *Ift88* is only slightly visible at the base of the cilium, confirming its knockdown. The staining with TRAF3IP1 is restricted to a small spot, also indicating the shortening of the cilia since it stained the

whole cilium in the control sample. The double knockdown of *Ift52* and *Ift88* led to a clear shortening of the cilia compared to the control (Figure 26). The knockdown of both targets can be confirmed visually; still one can see that the knockdown efficiency is better for *Ift52* in comparison to *Ift88*, which corresponds to results of the knockdown validation by qPCR (Table 18). The knockdown of *Ttc30a1* (Figure 25) results in an elongation of the cilia, compared to the control (Figure 26). The staining pattern of the IFT proteins appears to be reduced along the axoneme and at the tip of the cilium, whereas the accumulation at the ciliary base resembles the staining pattern of the control experiment. Furthermore, the cilia are not straight and appear as wiggly lines in the tubulin staining. The knockdown of *Ttc30b* causes shorter cilia, the staining with *Ift52* is very weak. The same is true for the staining with *Ift88* and *TRAF3IP1*, where an accumulation at the ciliary tip and a very faint staining along the ciliary axoneme can be observed. Finally, the knockdown of *Arl13b* results in a malformation and shortening of the cilia. No staining for *Ift52* can be observed, the staining with *Ift88* is reduced and there is no accumulation of *Ift88* at the ciliary tip. The cilia have a circled shape and *TRAF3IP1* also only accumulate at the ciliary base.

The knockdown efficiency was monitored by quantitative real-time PCR. The RNA of IMCD3 cells, transfected with the corresponding siRNA, was isolated, reverse transcribed and quantified relative to a control experiment with non-targeting siRNA. The results show a reduction of the expression levels for all of the targeted genes within this screen (Table 18). The expression of *Ift52* was reduced to 39.3% in comparison to the control experiment. The expression of *Ift88* was slightly less reduced to a percentage of 40.3. In the double knockdown experiment of *Ift52* and *Ift88*, the expression level of *Ift52* was reduced less (55.2%) than the one of *Ift88* (47.3%). As the sequence homology and the gene locus of *Ttc30a1* and *Ttc30b* is very similar, the expression level for both genes was determined for both knockdown experiments to ensure that there are no off-target effects on the other gene. For the knockdown experiment of *Ttc30a1* the expression level of *Ttc30a1* is reduced to 36.9% whereas the expression of *Ttc30b* is still at 96.8%, indicating that the siRNA are specific. The same is true for the knockdown of *Ttc30b* where the expression of *Ttc30b* was determined with a percentage of 27.2, whereas *Ttc30a1* is still at 92.7%.

The efficiency for the knockdown of Arl13b was determined with an expression level of 38.6% compared to the control.

Table 18: Knockdown efficiency of IFT proteins in IMCD3 cells.

This table shows the knockdown efficiency of the genes *Ift52*, *Ift88*, *Ttc30a1*, *Ttc30b*, *Arl13b* and the double knockdown of *Ift52* and *Ift88* by transfection with siRNA in IMCD3 cells. In the first column the experiment name is shown, in the second column the targeted genes. In the third column the expression level of the targeted gene compared to a control experiment with non-targeting siRNA is shown. The last column indicated the p-value for the corresponding knockdown experiment. For each experiment three biological replicates were produced and three technical repetitions were performed for each condition.

Experiment	Knockdown	expression	p-value
Ift52-kd	Ift52	39.30%	0.000
Ift88-kd	Ift88	40.30%	0.000
Ift52+Ift88-kd	Ift52	55.20%	0.004
Ift52+Ift88-kd	Ift88	47.30%	0.003
Ttc30a1-kd	Ttc30a1	36.90%	0.000
Ttc30a1-kd	Ttc30b	96.80%	0.836
Ttc30b-kd	Ttc30b	27.20%	0.000
Ttc30b-kd	Ttc30a1	92.70%	0.294
Arl13b-kd	Arl13b	38.60%	0.000

2.4. Predicted network of the IFT complex B

The data from SF-TAP experiments and the sucrose density centrifugation experiments of the IFT-B allowed the generation of a predicted network for the IFT-B, using the software Cytoscape. Therefore, the interactions derived from these experiments, were visualized as edges between the proteins that are depicted as nodes within a network (Figure 27). The network shows a separation of the IFT-B into two distinct sub-modules, the sub-complex B1 (orange) and the sub-complex B2 (green) as well as the proteins IFT88 and IFT52 that are thought to play a central role as linker between these two modules. The role as central nodes is deduced from the SF-TAP data (2.2.1). In these experiments there was not a single interaction detected between proteins of the two sub-modules. IFT52 was found in both sub-complexes and IFT88 in none of them, which raised the hypothesis that they might function as linkers. Additionally, bioinformatic analysis of the data shown in this study by two of our collaboration partners (Konstantinos Kontroumpas, CNRS Paris and Grischa Toedt, EMBL Heidelberg) further supported this hypothesis. The blue line indicate an

interaction in SF-TAP experiments and the red, dashed line an interaction determined by sucrose density centrifugation. The proteins IFT88 and IFT172 showed a different elution profile within the sucrose density centrifugation experiment. Therefore, although their curves are intersecting with the curves of the members from the two sub-complexes, no interaction was added. Moreover, no stoichiometry data were taken into account for this figure, for this reason one or more of the IFT-B members could exist with multiple copies within the complex.

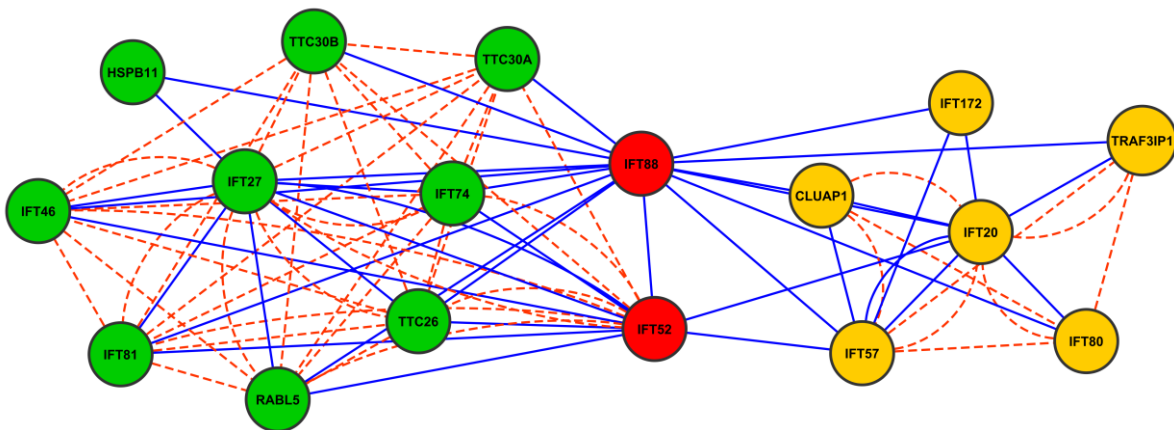


Figure 27: predicted network for the IFT-B.

This figure shows a predicted network for the IFT-B. The edges represent different experiment types, the blue edges derive from interactions determined by SF-TAP experiments while the red, dashed edges derive from sucrose density centrifugation data. The arrangement of the nodes was done arbitrarily and represents a possible arrangement of the complex. The stoichiometry was not considered for this figure and several copies of the proteins might exist within the complex. The proteins of the sub-complex B1 are shown in orange, the proteins of the sub-complex B2 in green and proteins that are considered to play a central role are depicted in red. The protein IFT172 and IFT88 have no interactions assigned within the sucrose density centrifugation experiment because they showed a different elution pattern. The network was created using the software Cytoscape.

3. The centrosomal protein 170 is associated with the IFT-B

The centrosomal protein 170 (CEP170) was previously described to localize to the mature centrioles of centrosomes and cilia (204). The destabilization of the Lebercilin complex showed the co-elution of CEP170 with the IFT-B, which could hint towards a specific function of this protein enabling the IFT along cilia. To validate the association of CEP170 to the IFT complex B as well as its co-localization, the protein CEP170 was characterized using different methods.

3.1. Analysis of the interactome of SF-TAP-tagged CEP170 in HEK293-T cells

To determine whether CEP170 interacts with the IFT-B, SF-TAP-tagged CEP170 was expressed in HEK293-T cells, its complex was purified by SF-TAP and analysed by mass spectrometry. The result of this experiment is shown in Table 19. By applying this method, it was not possible to detect an interaction of IFT-B proteins with CEP170. Among the interactors the 14-3-3 protein complex that was detected in the analysis of the Lebercilin complex was detected. Furthermore three serine/threonine phosphatases as well as three different casein kinases were found. As a possible link to the cilium, tubulin alpha 1B chain and kinesin-like protein KIF2A were detected. Additionally, the WD repeat-containing protein 62 (WDR62) was detected, a further indication to the interaction with IFT, since almost all IFT members have a WD-repeat domain.

To analyse the CEP170 protein complex by a more sensitive method, we combined quantitative mass spectrometry with SILAC-labelling and one-step purification. Therefore, CEP170-N-SF-TAP was overexpressed in SILAC-labelled HEK293-T cells and one-step affinity purification was performed. Using this method, the more transient interaction partners of CEP170 could be detected (Table 20, Figure 28). However, this experiment also did not show an interaction between CEP170 and the IFT-B. Interestingly the list of interactors varies from the interactors determined by SF-TAP. For the SILAC approach only the N-terminal tagged version of CEP170 was used, which seemed not to be the best choice as many of the interactors are not present anymore. Nevertheless, the protein WDR62 that was already observed by SF-TAP is highly enriched within this experiment, further validating it as a interactor of CEP170. Another protein that was enriched significantly more than 7-fold is the protein Procollagen-lysine,2-oxoglutarate 5-dioxygenase 3 (PLOD3) and the 60S ribosomal protein L11 (RPL11) that was enriched threefold.

Table 19: SF-TAP analysis of CEP170-SF-TAP.

This table shows the results of the mass spectrometric analysis of an SF-TAP experiment with C- and N-TAP-tagged CEP170-SF-TAP. Three experiments were performed for each construct, only proteins that were present in at least two out of three experiments with more than two unique peptides, a protein identification probability of 95%, a peptide identification probability of 80% as determined by Scaffold and that were not present in the empty vector control are listed here. Indicated are the numbers of unique peptides per protein, the bait protein is highlighted in grey.

Identified Proteins	Uniprot	Gene name	Exp1 C-SF-TAP	Exp2 C-SF-TAP	Exp3 C-SF-TAP	Exp1 N-SF-TAP	Exp2 N-SF-TAP	Exp3 N-SF-TAP
14-3-3 protein beta/alpha	P31946	1433B	8	9	9	14	10	10
14-3-3 protein epsilon	P62258	1433E	16	13	15	25	18	17
14-3-3 protein eta	Q04917	1433F	8	7	7	11	12	11
14-3-3 protein gamma	P61981	1433G	9	8	9	14	8	8
14-3-3 protein theta	P27348	1433T	8	8	10	11	8	8
14-3-3 protein zeta/delta	P63104	1433Z	9	7	10	13	9	10
40S ribosomal protein S12	P25398	RS12	4	6	5			2
Archaemetzincin-2	Q86W34	AMZ2				7	5	6
BAG family molecular chaperone regulator 2	O95816	BAG2	5	5	5			
Casein kinase II subunit alpha	P68400	CSK21	5	7	13	6	7	5
Casein kinase II subunit alpha'	P19784	CSK22		2	2		3	
Casein kinase II subunit beta	P67870	CSK2B	3	5	6	5	5	4
Centrosomal protein of 170 kDa	Q5SW79	CE170	101	90	96	110	98	98
Complement component 1 Q subcomponent-binding protein, mitochondrial	Q07021	C1QBP	2		2			
DBIRD complex subunit KIAA1967	Q8N163	K1967	3	3	8			
Heat shock 70 kDa protein 4	P34932	HSP74	6	6	8	14	15	14
Heat shock 70 kDa protein 4L	O95757	HS74L	2			4	6	3
Heat shock protein 105 kDa	Q92598	HS105		4	3	8	10	8
Kinesin-like protein KIF2A	O00139	KIF2A			2	8		2
Replication protein A 70 kDa DNA-binding subunit	P22336	RFA1	2	5	3	3	2	
SNARE-associated protein Snapin	O95295	SNAPN	4	5	4	2		
SWI/SNF-related matrix-associated actin-dependent regulator of chromatin subfamily E member 1	Q969G3	SMCE1	3	2	3			
Serine/threonine-protein phosphatase 2A 65 kDa regulatory subunit A alpha isoform	P30153	2AAA	7	6	6	2		
Serine/threonine-protein phosphatase 2A regulatory subunit B' subunit beta	Q9Y5P8	P2R3B	3		2			
Serine/threonine-protein phosphatase PGAM5, mitochondrial	Q96HS1	PGAM5	2	4	4			
Single-stranded DNA-binding protein, mitochondrial	Q04837	SSBP	5	2	3	2		3
Tubulin alpha-1B chain	P68363	TBA1B	2			2	2	3
WD repeat-containing protein 62	O43379	WDR62	3		2			

Table 20: STREP-SILAC analysis of the CEP170 interactome.

This table shows the results of the quantitative analysis of the CEP170 interactome using one-step affinity purification from SILAC-labelled HEK293-T cell lysates combined with quantitative tandem mass spectrometry (LC-MS/MS). Depicted are the proteins that are significantly enriched compared to the control with a p-value of less than 0.01, the complete list of interactors is available on the supplemental DVD, attached to the printed version of this study. The data of these experiments were analysed using the software MaxQuant.

Protein name	Gene name	Uniprot	ratio	p-value
Centrosomal protein of 170 kDa	CEP170	Q5SW79	15.85	2.06E-290
14-3-3 protein eta	YWHAH	Q04917	1.28	1.52E-03
14-3-3 protein gamma;14-3-3 protein gamma, N-terminally processed	YWHAG	P61981	1.33	2.40E-04
2-oxoisovalerate dehydrogenase subunit alpha, mitochondrial	BCKDHA	P12694	1.32	5.94E-03
60S ribosomal protein L11	RPL11	P62913	3.33	2.29E-22
Acid ceramidase;Acid ceramidase subunit alpha;Acid ceramidase subunit beta	ASAH1	Q13510	1.41	3.41E-03
Ataxin-2-like protein	ATXN2L	Q8WWM7	1.22	9.30E-03
BRISC and BRCA1-A complex member 1	BABAM1	Q9NWW8	1.47	1.10E-03
Casein kinase II subunit alpha	CSNK2A1	P68400	1.48	1.17E-04
DBIRD complex subunit KIAA1967	KIAA1967	Q8N163	1.36	6.46E-05
Dihydrolipoyllysine-residue succinyltransferase component of 2-oxoglutarate dehydrogenase complex, mitochondrial	DLST	P36957	1.24	5.91E-03
Eukaryotic translation initiation factor 4 gamma 2	EIF4G2	P78344	1.29	9.97E-03
Lipoamide acyltransferase component of branched-chain alpha-keto acid dehydrogenase complex, mitochondrial	DBT	P11182	1.36	5.57E-05
MMS19 nucleotide excision repair protein homolog	MMS19	Q96T76	1.46	2.03E-04
Nuclear fragile X mental retardation-interacting protein 2	NUFIP2	Q7Z417	1.25	4.30E-03
Probable ATP-dependent RNA helicase DDX6	DDX6	P26196	1.25	3.35E-03
Procollagen-lysine,2-oxoglutarate 5-dioxygenase 3	PLOD3	O60568	7.03	3.49E-77
Protein FAM195B	FAM195B	C9JLW8	1.27	2.25E-03
Protein LSM12 homolog	LSM12	Q3MHD2	1.23	7.84E-03
Syntaxin-12	STX12	Q86Y82	1.41	3.13E-03
UTP--glucose-1-phosphate uridylyltransferase	UGP2	Q16851	1.5	5.44E-04
WD repeat-containing protein 62	WDR62	O43379	7.34	1.62E-80
Wiskott-Aldrich syndrome protein family member 1	WASF1	Q92558	1.31	7.21E-03

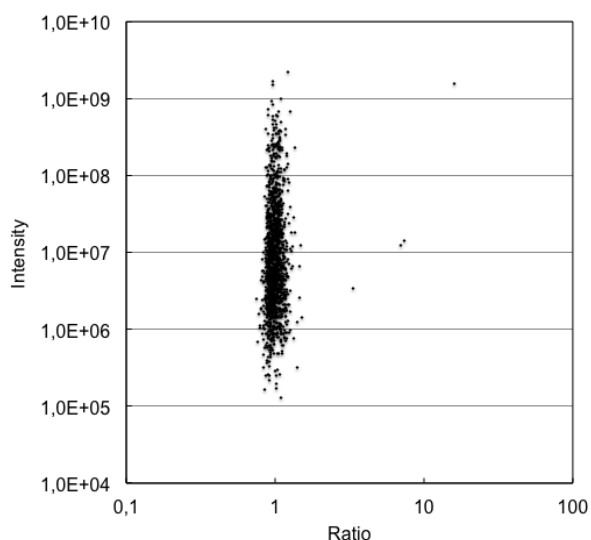


Figure 28: Scatter plot of the STREP-SILAC analysis of CEP170-N-SF-TAP.

This figure shows the scatter plot of the STREP-SILAC analysis of the CEP170 interactome. The intensity was plotted on the y-axis against the ratio on the x-axis. The non-specific interactors are distributed around a ratio of 1, the enriched proteins show a ratio greater than 1. The experiment was performed two times, the data were analysed by the software MaxQuant.

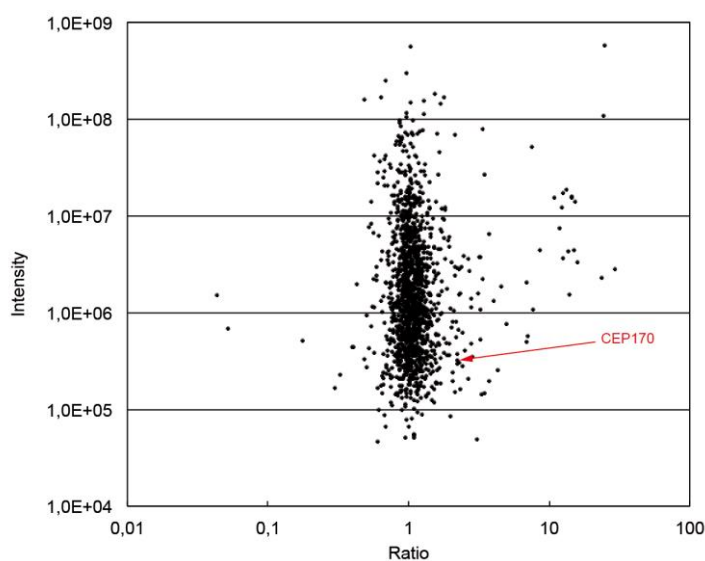


Figure 29: Scatter plot of the STREP-SILAC analysis of the interactome of IFT57.

This figure shows the result of a one-step affinity purification of SILAC labelled lysates from a HEK293 cell line stably expressing IFT57-SF-TAP. Plotted is the intensity over the ratio, showing the distribution of the non-specific binders at a ratio around 1 and the enrichment of specific binders to the right of this distribution, respectively the depletion on the left side. Among the enriched proteins CEP170 was found as a specific interactor of IFT57 (indicated by the arrow, ratio: 2.21, p-value: 2.64E-03). The experiment was performed three times, the data were analysed by the software MaxQuant.

To test the association of CEP170 to the IFT-B, the reciprocal experiment was also performed by using a HEK293 cell line stably expressing IFT57-N-SF-TAP. The one-step affinity purification of IFT57-SF-TAP from these SILAC-labelled cells allowed the detection of a significant enrichment of CEP170 within the interactome of IFT57 (Figure 29). The complete list of the resulting interactors of this experiment is not shown due to the large number of hits but is available on the supplemental DVD, attached to the printed version of this study. These results indicate that the binding of CEP170 to the IFT-B might be rather transient because it was only possible to detect it by this very sensitive approach.

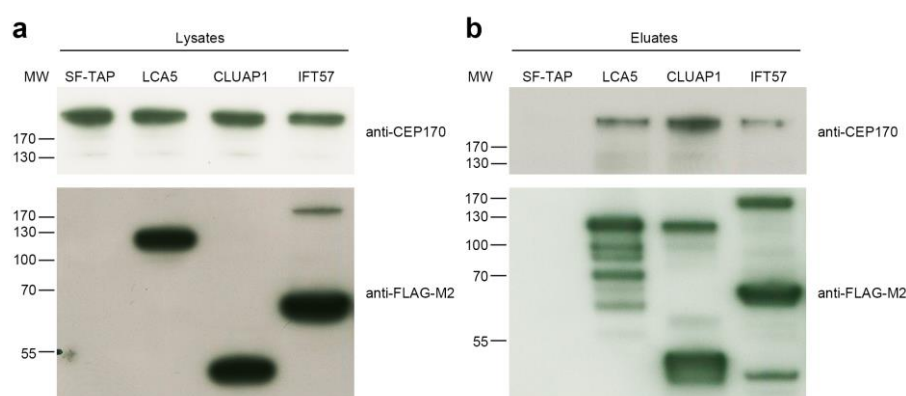


Figure 30: Western Blot experiments with anti-CEP170.

Western Blot analysis of lysates and eluates from a one-step FLAG-purification from HEK293-T cell lysates, transiently transfected with different SF-TAP-tagged IFT-B-proteins. **a** For the analysis of the lysates 20 μ g of protein were applied to each lane for incubation with anti-CEP170 and 5 μ g of protein for incubation with anti-FLAG-M2. **b** For the analysis of the eluates with CEP170 25% of each eluate was applied to the corresponding lane, for anti-FLAG-M2 2% of the eluates were loaded. As a control for the purification the empty vector N-SF-TAP was used.

Additionally, western blot experiments using eluates from a one-step purification were performed to further validate the association of CEP170 to the IFT-B. HEK293-T cells were transiently transfected with LCA5, CLUAP1, IFT57 and SF-TAP as a control. Subsequent, one-step purification using the FLAG-epitope of the SF-TAP-tag was performed. The western blot experiments (Figure 30) show a signal for each bait protein by an anti-FLAG-M2 antibody at the corresponding molecular weight of the bait proteins. The incubation with an anti-CEP170 antibody showed a signal in the lysate of the negative control (Figure 30 **a**) detecting the endogenous protein, which is not present anymore after the purification process in Figure 30 **b** showing its depletion. Furthermore, the anti-CEP170 antibody detects CEP170 in the eluates of

LCA5, CLUAP1 and IFT57, indicating a co-purification with these proteins. These results are further strengthening the hypothesis that the protein CEP170 is associated to the IFT complex.

3.2. CEP170 localizes to the basal body of the cilium in hTERT cells

The localization of CEP170 was determined within ciliated cells by immunofluorescence. hTERT RPE1 cells were starved of serum for 16 hours to induce cilia formation, subsequently fixed and stained with different antibodies. TRAF3IP1 (IFT54) was used as a representative of the IFT-B and a CEP170-specific antibody was used for localization of the target protein. Since both antibodies (anti-TRAF3IP1, mouse and anti-CEP170, mouse) were raised in the same species, secondary antibodies would cross react with both and therefore normal double staining was not possible. The ciliary marker alpha/beta tubulin (rabbit) was used as a reference to determine the localization of both proteins to the cilium (Figure 31 a+b).

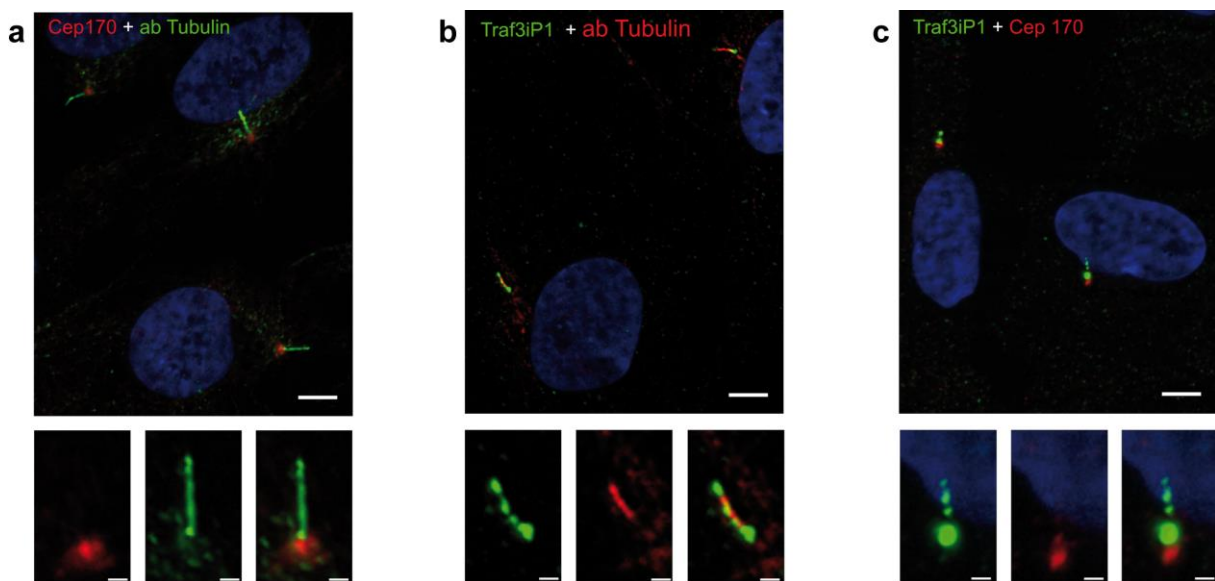


Figure 31: Immunofluorescence of CEP170 and TRAF3IP1 in hTERT RPE1 cells.

This figure shows the co-staining with different antibodies in serum-starved ciliated hTERT RPE1 cells. **a** Co-staining of anti-CEP170 (mouse, red) with anti-alpha/beta tubulin (rabbit, green). **b** Co-staining of anti-TRAF3IP1 (mouse, green) and anti-alpha/beta tubulin (rabbit, red). **c** Co-staining of anti-TRAF3IP1 (mouse, green) and anti-CEP170 (mouse, red) using a technique to detect two different antibodies of the same species in one assay. The nuclei were visualized using DAPI in all parts of the figure. The scale bar in the upper part of the figure indicates 5 μm , in the lower part to 2 μm .

TRAF3IP1 localizes to the axoneme of the cilium whereas CEP170 localizes at the base of the cilium. Additionally, a technique to mask the fab-fragments (Chapter III section 6.6.2) was applied to perform a subsequent co-staining of the two antibodies of the same species (Figure 31 c). CEP170 localizes to the cilium but shows no co-localization with TRAF3IP1 in this experimental setup.

3.3. CEP170 co-localizes with TRAF3IP1 during ciliogenesis

To characterize the localization of CEP170 and TRAF3IP1 further, a time course during different stages of ciliogenesis was performed (Figure 32).

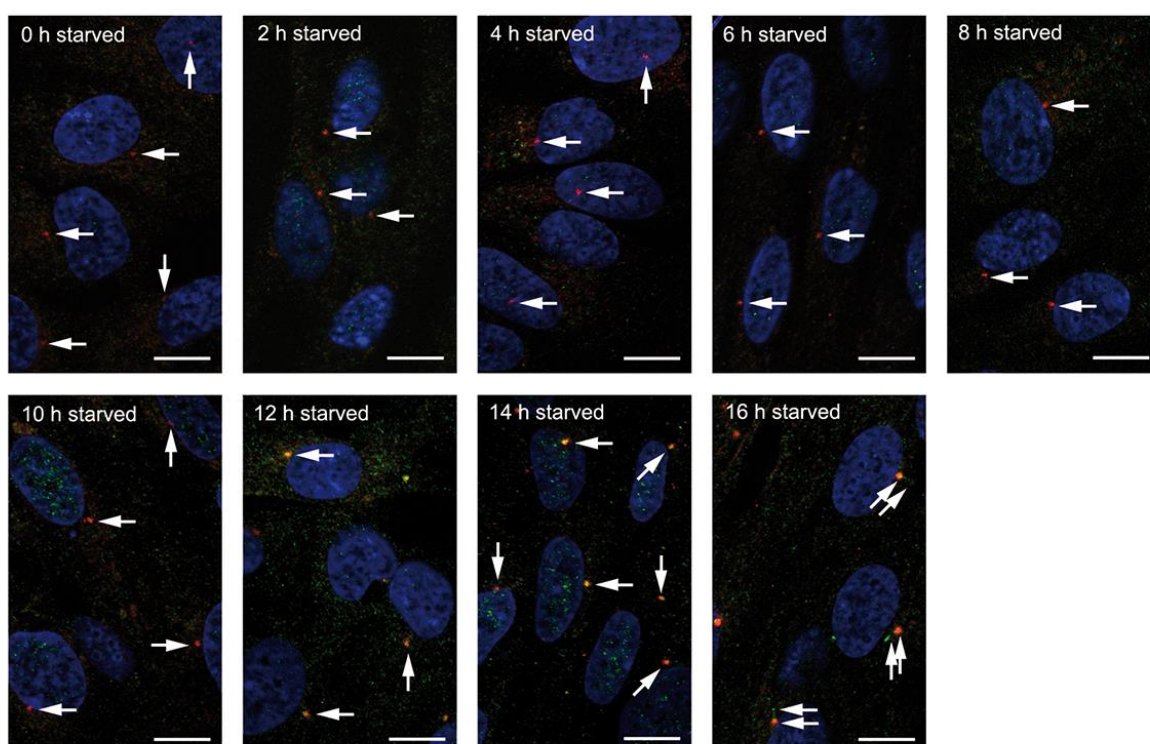


Figure 32: Immunofluorescence of TRAF3IP1 and CEP170 during ciliogenesis.

This figure shows the localization of TRAF3IP1 (green) and CEP170 (red) during ciliogenesis in hTERT RPE1 cells. The ciliogenesis was induced by serum starvation and the localization was observed in two hour steps from 0-16 hours. TRAF3IP1 is not detected at the beginning of the time course whereas CEP170 localizes at the basal body region. CEP170 and TRAF3IP1 co-localize between 12 to 14 hours of starvation. At later time points, TRAF3IP1 localizes to the axoneme of the cilium whereas CEP170 remains at the basal body. The arrows indicate the position of CEP170 at the time points 0-10 hours starved, of CEP170 and TRAF3IP1 at the time points 12 to 16 hours starved. The nuclei were stained with DAPI, the scale bars correspond to 10 μ m.

This experiment was performed in hTERT RPE1 cells and the ciliogenesis was induced by serum-starvation. Every two hours, cells were fixed with 16 hours of

starvation as an end-point of measurement. CEP170 localizes to the centrosome/basal body at all time points. In contrast, and as expected, TRAF3IP1 is not detected at the time point '0h starved' and appears as small dots in the region of the nucleus at two hours starvation. At the time points 12 and 14 hour of starvation the two proteins show a co-localization at the basal body. TRAF3IP1 then moves into the cilium and localizes to the axoneme of the cilium whereas CEP170 remains at the basal body.

3.4. Knockdown of *Cep170* in IMCD3 cells

To determine whether *Cep170* is essential for the IFT and/or the function of the cilium, the gene was knocked down by siRNA in IMCD3 cells. The impact of the knockdown on the localization of the IFT-B and the morphology of the cilium was analysed using confocal microscopy and the Operetta imaging system.

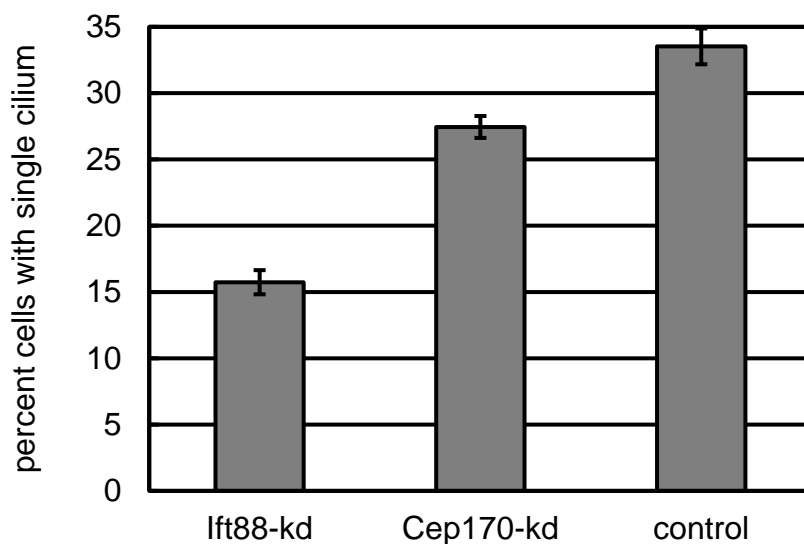


Figure 33: Knockdown of *Cep170* in IMCD3 cells.

This figure shows the effect of the knockdown of *Cep170* by siRNA and the knockdown of *lft88*, which was used as a positive control, on the percentage of cells with a single cilium, compared to a control experiment with non-targeting siRNA in IMCD3 cells. The experiment was performed with four biological replicates, the error bars represent the standard deviation.

In this screen, the percentage of cells with a single cilium is compared to a control, which was treated with non-targeting siRNA, thereby giving information about the potential effect of KD on ciliogenesis. The results are depicted in Figure 33 and show a slight but still significant effect of the knockdown of *Cep170* on the amount of cells bearing a single cilium. Compared to the control experiment with non-targeting

siRNA, where around 33 percent of the cells have a single cilium, the knockdown of *Cep170* led to a reduced number of cells with single cilium of about 27 percent. The effect of the knockdown of *Cep170* is not as large as for the knockdown of *Ift88* which shows a reduction to 16 percent of cells bearing a single cilium.

Furthermore, the effect of the knockdown of *Cep170* on the IFT-B was determined by the staining of different IFT-B components by confocal microscopy. Therefore, IMCD3 cells were grown on coverslips, fixed and subsequently stained with anti-IFT52, anti-TRAF3IP1 and anti-IFT88 antibodies in combination with a ciliary marker (depending on the species of the primary antibody either with anti-acetylated tubulin either anti-alpha/beta tubulin). The results (Figure 34) did not show a difference in ciliary length. However, the localization of the IFT proteins differed for the *Cep170* knockdown. While the IFT-B proteins IFT52, IFT88 and TRAF3IP1 are stained at the base and the tip of the cilium in the control experiment, the localization is restricted to the base of the cilium when *Cep170* is knocked down (Figure 34 a). Furthermore, the intensity of the IFTs signal is reduced along the axoneme and in some cases is even not detectable anymore, indicating a reduction in transport along the ciliary axoneme (Figure 34 b and c).

The efficiency of the knockdown was evaluated by quantitative real-time PCR. Therefore, the RNA from the transfected cells was isolated, reverse transcribed and analysed using gene-specific primers. The efficiency of the primers was verified before the quantification process and considered for the calculation of the knockdown efficiency. Four different housekeeping genes were used for the normalization of the cDNA concentration across the samples. The expression level was determined relative to a control sample, transfected with non-targeting siRNA. The experiment was performed using three biological replicates and three technical replicates per condition. The results of the qPCR showed a clear knockdown of *Cep170* to an expression level of 39.9% with a p-value of 0.000 (Table 21).

Table 21: Knockdown efficiency of *Cep170* in IMCD3 cells.

This table indicates efficiency of the knockdown of *Cep170* by transfection with siRNA in IMCD3 cells compared to a control experiment with non-targeting siRNA. The experiment was repeated three times and three technical replicates were performed.

Knockdown	expression	p-value
<i>Cep170</i>	39.90%	0.000

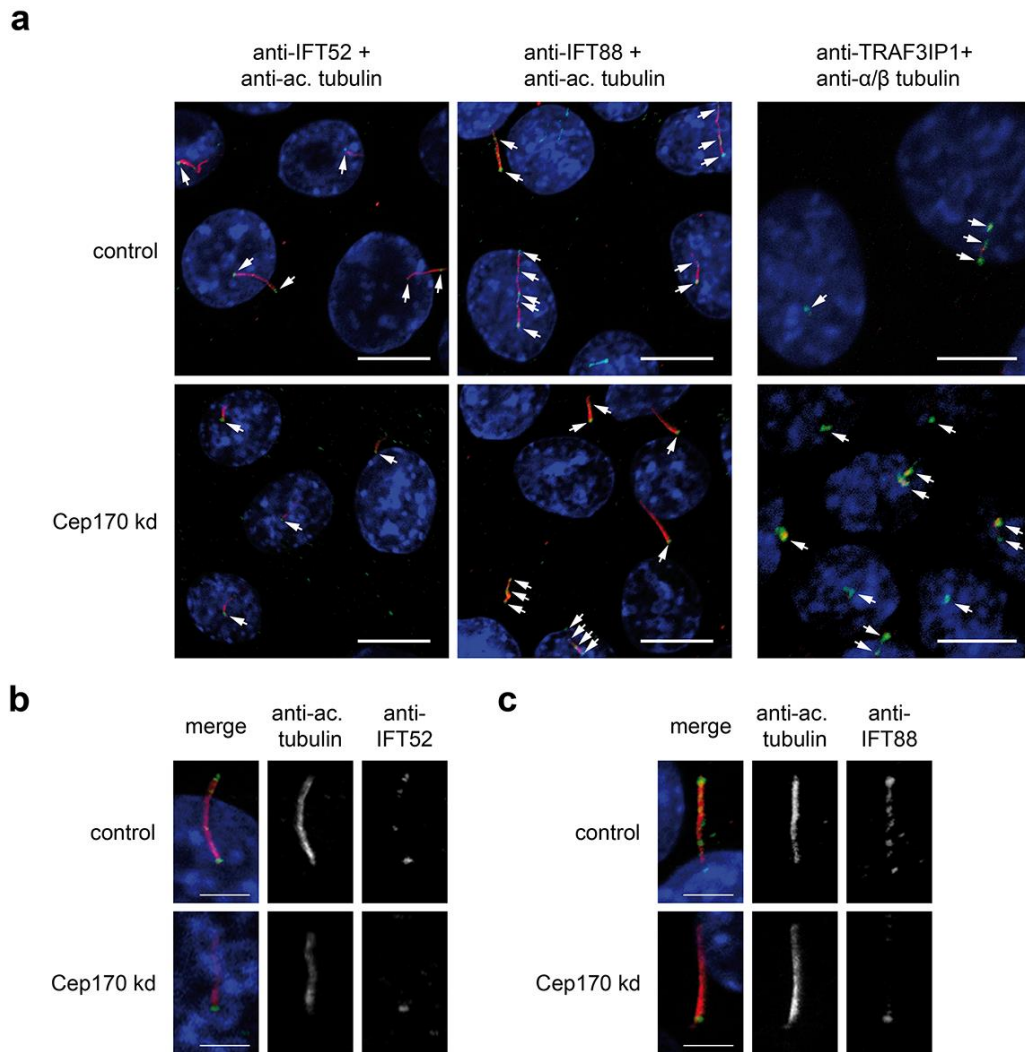


Figure 34: Localization of the IFT-B during *Cep170* knockdown in IMCD3 cells.

This figure visualizes the localization of different IFT-B proteins at the cilium after *Cep170* knockdown by confocal microscopy in IMCD3 cells. *Cep170* was knocked down by siRNA, the localization was compared to a negative control, transfected with a non-targeting siRNA. DAPI was used to visualize the nuclei (blue), antibodies against the ciliary marker proteins (red) acetylated alpha tubulin or alpha/beta-tubulin (for co-localization with TRAF3IP1) indicate the axonemal structure of the cilium. Antibodies against the IFT-B proteins IFT52, TRAF3IP1 and IFT88 were used to indicate the localization of the IFT complex B (green). All images were acquired using a x100 objective lens + 3x scanner zoom. **a** Overview of the different staining patterns in comparison to the negative control. The arrows indicate the localization of the IFT proteins along the cilium. In the control experiment the IFT-B seems to accumulate at the base and the tip of the cilium, whereas in the knockdown experiment of *Cep170* the IFT-B mainly localizes to the base of the cilium. **b+c** Zoom to one cilium for the staining with anti-IFT52 and anti-IFT88 from figure **a** of the negative control and the knockdown experiment in split and merged view. The IFT-B localizes along the whole cilium in the control experiment, whereas it localizes only to the ciliary base in the knockdown experiment. The scale bar indicates 10 μ m in figure **a** and 1 μ m in figure **b+c**. The contrast of the pictures was enhanced using the image software Photoshop.

V. Discussion

1. The SDS-AP - a fast and easy method to analyse protein complexes

In the first part of this study a new combination of methods to analyse native protein sub-complexes is presented. The analysis of protein complexes by affinity purification has become an extremely valuable tool for the determination of the biological function of whole protein complexes and/or their components. Affinity purification combined with quantitative tools can dramatically improve the sensitivity further and allow the determination of transient or weak interactions of proteins within complexes (50). A major drawback of the common protein complex purification methods, like TAP or similar methods, is that the outcome is only a list of proteins co-precipitating with the target protein. No information about the stoichiometry or the sub-structure of the complexes can be deduced from those approaches. Therefore, a technique to reproducibly increase the value of the generated data from protein complex analysis further is of great interest. Different methods for the separation of protein complexes, as for example sucrose density centrifugation (122), to analyse the protein complexes subsequent to purification were evaluated. A very promising technique was recently published by Klodmann et al. (177), where low SDS concentrations were used to destabilize a protein complex prior to 2D blue native gel electrophoresis to resolve the sub-module architecture of a protein complex. However, for the analysis of protein complexes on blue native gels, very high amounts of starting material are needed. Additionally, the procedure is very time consuming, labour intensive and rather artificial buffer conditions are necessary to achieve separation on blue-native gels. Furthermore, it is hard to achieve standardized and robust workflows using this approach. In view of these limitations, this approach was not followed up further. Still, the excellent potential of this approach to identify functional sub-modules within a complex was convincing. This led to the evaluation of the combination of the standardly used affinity-based purification with the destabilization by SDS, label-free quantitative analysis and protein correlation profiling in a single workflow, the SDS-AP.

The destabilization of the Lebercilin complex resulted in the elution of different sub-modules by increasing the SDS concentration. The PCP-values clearly show that the

members of the two sub-modules, losing their connectivity to the Lebercilin complex at the lowest concentrations are the IFT complex A and the IFT complex B. Within the IFT-A, the protein TULP3 was detected as a potential new member of the IFT complex A. Recently, TULP3 already was postulated to be associated to the IFT-A (197). The authors proposed that TULP3 promotes trafficking of GPCRs to the cilium by its phosphoinositide binding properties, indicating its important role for the ciliary function. The analysis of the interactome of TULP3 by SF-TAP clearly confirmed its interconnectivity to other IFT-A proteins and indicates it as a potential member of the IFT-A.

Within the IFT-B sub-module we detected CEP170, a protein which was not described to be associated with the complex yet. CEP170 was shown to localize to the mature centriole and is thought to be involved in microtubular organization and cell morphology (204). The SDS-AP data suggest that CEP170 might be associated with the IFT-B, as it shows a similar PCP-value as IFT-B members. Still, the deviation from the IFT-B PCP-profiles is higher than for other IFT-B components, indicating that CEP170 is most likely not an integral part of the complex but still linked to Lebercilin via IFT-B. Its detailed characterization was performed in the last part of this study and will be discussed in more detail in the later parts of this discussion. In contrast, the proteins that were described to be associated to the IFT-B did not show a significant deviation from the PCP-profiles of known IFT-B members. As a consequence, their interaction to the other components of the IFT-B seems to be very strong and they are therefore more likely integral members of the IFT-B.

The third module, co-eluting from the LCA complex by increasing the SDS concentration, consists of five 14-3-3 adapter proteins mainly eluting in the fourth fraction. The function of 14-3-3 proteins has extensively been characterized in many different studies and organisms (205, 206). 14-3-3 proteins are present in almost every eukaryotic cell and participate in fundamental biological processes like signal transduction, metabolism and transport (207). They behave like ordered hubs and bind to a wide variety of phosphorylated targets (208). The discovery that 14-3-3 proteins bind to specific phospho threonine / phospho tyrosine (pThr/pTyr)-containing motifs, not only suggested their importance within signal transduction but also indicated a possible role for Ser/Thr phosphorylation in protein-protein complex assembly (198), which might explain their occurrence within a large protein complex

like the interactome of Lebercilin. The 14-3-3 proteins do not co-elute as a perfect peak like the IFT-A and IFT-B proteins, still they all show a resemblance in their elution profile. Furthermore, the formation of a stable 14-3-3 protein complex already was shown in a previous study (150) and additionally validated by SF-TAP analysis.

Nine proteins eluting at a concentration of 0.1% SDS belong to the recently described LisH-CTLH module (201). The association of some of these proteins with the IFT-complex has already been shown in a recent study (50). Another recent study describes the association of the protein muskelin to microtubular transport, mediated by dynein or myosin motor units (209), but the exact function of the complex remains unknown. Using SF-TAP, we were able to show that the LisH-CTLH module is a stable complex. Interestingly, in the first experiments for the determination of the dynamic range within this study, this module seemed to dissociate further into two sub-modules. This could give more information about the sub-structure of this module. Further effort will be needed to determine the function and structure of this module within the IFT complex. This work is under current investigation in collaboration with Ronald Roepman (Nijmegen, The Netherlands).

The data of the initial screen in Figure 20 showed that shifting the starting concentration, but retaining the gradients shape, can disturb the resolution of one peak while enhancing the resolution of another one. For optimization to the needs of a specific complex, it is therefore crucial to not stick to identical curves or to follow a mathematical series for the gradient when maximizing the resolution. Individual concentrations for each module seem to be the best solution. A systematic approach for the determination of the exact concentrations, for the elution of each module, might be an analogue process to the fine-mapping that is used in genetics. This approach is based on the assumption that below a certain threshold distances between the data points result in reduction of resolution of data. Therefore, the data points are acquired at a relatively large distance and several experiments are combined to finemap the gaps in between. This can be exemplified by the graph shown in Figure 35 for the SDS-AP method. A linear gradient with equal distances between the fractions could be used and three experiments with a shifted starting concentration are performed at the same time. Thus it will be possible to analyse the three experiments as one single experiment, reducing the 'fuzziness' while enhancing the resolution and determining the exact concentration for the elution of every single

sub-module. After the concentrations are determined, a new gradient, containing the specific concentrations for each sub-module, can be performed to achieve the best possible resolution.

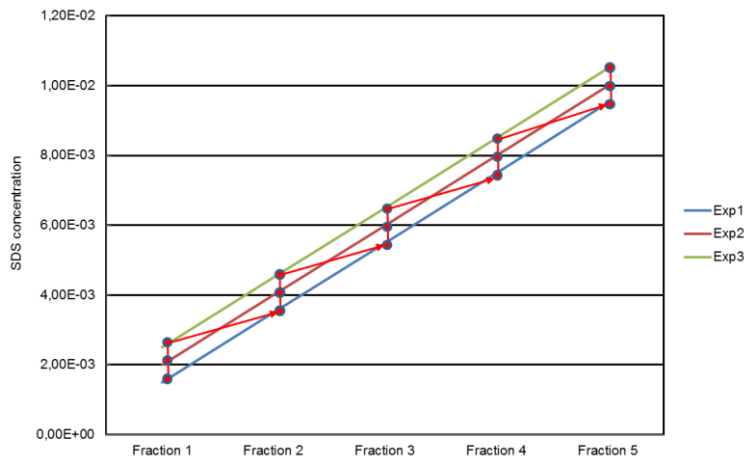


Figure 35: Concentration profile SDS-finemapping.

This figure shows a possible concentration profile for the optimization of the SDS concentrations by finemapping. Three experiments with equal distances between the fractions and shifted starting concentrations are depicted. The red arrows indicate the evaluation of the data through the different experiments, reducing the concentration steps while remaining to larger steps in the single experiments. This will lead to a reduction of the disturbance within the single experiments while enhancing the resolution over the complete data set.

The method presented here for the destabilization of protein complexes by SDS coupled to quantitative mass spectrometry and protein correlation profiling, is a very powerful tool for the analysis of the sub-structure of partially known protein complexes which, as a result can lead to the more detailed description of the complex architecture and function. It can highlight the rough structure of a complex in a highly time effective manner with very small amount of starting material. Furthermore, it can easily be adapted to different complexes by optimizing the concentrations of SDS or the profile of the gradient. Moreover, the calculation of the protein correlation profiling value (PCP-value) allows the identification of potential new members of sub-complexes or associated proteins to particular modules. The analysis of the Lebercilin complex by SDS-AP clearly shows its applicability to research topics of interest within the field of ciliopathy research and beyond.

2. Analysis of the IFT complex B

The research on the intraflagellar transport increasingly gained in interest since its first description by Cole et al. (35) in 1998. Its importance for the development and function of the cilium was pointed out by multiple studies concerning various diseases in the last years (40-43, 46, 210, 211). Nevertheless, the composition of the IFT-B and its detailed function remains elusive. Of course it is known that it is involved and essential for the transport mechanisms along cilia, but not how this is exactly achieved. This includes the mechanism of cargo selection and/or selectivity as well as the mechanism by which IFT proteins link cargo to the motor proteins. Different hypotheses of these processes have been proposed (53, 212-216) but little is known about the exact molecular mechanisms. Within this study, the complex was further characterized to gain more insight into the role of this molecular machine or its components for the function of the organelle cilium.

First, the comprehensive composition of the IFT-B was determined by SF-TAP. Using this approach, it was possible to identify the already published core components of the IFT-B (45, 50). Furthermore, proteins that were thought to be associated to the IFT-B (TTC26, TTC30A, TTC30B, TRAF3IP1, RABL5, HSPB11 and CLUAP1 (50)) were purified using this method. As SF-TAP is a method with very stringent washing conditions, purifying only stably bound interaction partners, these results indicate that these proteins are more likely to be a part of the complex than being associated by transient interactions. For the proteins TTC30A and CLUAP1 for example, this hypothesis has been confirmed in the meantime (217, 218). Additionally, the purification of all IFT-B components, using IFT88 as bait suggests that this protein might play a central role within this complex.

There are certain disadvantages resulting from the use of transient over-expression that might influence the outcome of an experiment. First to mention is that, due to standardly used strong promoters the amount of bait protein is much higher than under physiological conditions. This can result in an alteration of stoichiometry within the resulting protein complexes and therefore lead to the generation of artificial complexes. Furthermore, the massive amount of synthesized protein results in higher amounts of misfolded proteins, which in turn leads to the presence of a lot of chaperones interacting with the formed protein and increased retention of proteins in the ER. It is therefore of great interest to generate cell lines which express the bait

protein at an expression level that is near to the endogenous expression level. Thus, the generated data are more likely to reflect the physiological conditions. Still, for high throughput studies analysing great amounts of target proteins the effort to establish stable cell lines on a large scale is not time or cost effective. Within this study, the generation of a HEK293 cell line stably expressing IFT88-SF-TAP was performed to reduce the disadvantages of over-expression. Using this cell line as source for SF-TAP experiments, the whole IFT-complex B could be purified reproducibly together with all of its components.

Subsequent to the determination of the IFT-B components, its substructure was analysed using different methods. As a starting point, four different members of the complex were chosen for SF-TAP analysis. Interestingly, IFT20 and IFT57 purified another subset of the IFT-B than IFT27 and IFT52. However, these subsets matched for IFT20 and IFT57 respectively for IFT27 and IFT52, raising the hypothesis of the IFT-B existing as two distinct and rather stable sub-complexes. The fact that these two sub-complexes remain stable under the stringent conditions of SF-TAP indicates their stability, which is not in line with the knowledge from literature describing the second sub-complex as associated proteins, diffusing from the core unit (35). The protein IFT88 was not found within one of these two sub-complexes and IFT52 was found in both. These findings might indicate a central role for one or both of these proteins. As they are reproducibly described as members of the stable IFT-B and because all IFT-B proteins can be purified when using IFT88, it might be possible that they play a role as linker between the two sub-complexes. The proteins TTC30A and TTC30B could also not be detected within these experiments. TTC30A and TTC30B are highly homologous, suggesting similar, overlapping behaviours for both proteins and even functional redundancy. However, since TTC30A only is associated with IFT46 in the literature and was not assigned as a member of the IFT-B yet, it is more likely that both proteins may play an important role in stabilizing the complex by transient interactions than being central components like IFT52 and/or IFT88.

Analysis of the protein complexes of SF-TAP-tagged IFT20, IFT27, IFT52 and IFT57, stably expressed in HEK293 lines by SF-TAP resulted in the purification of the whole IFT-B. These results raised the question of whether the previous SF-TAP data from over-expressed cells, showing the formation of the two sub-complexes, were artefacts derived from over-expression. Therefore, a method to validate the

hypothesis of the two sub-complexes was needed. The isolated IFT-B complexes from a stable IFT88 cell line were separated by sucrose density centrifugation to analyse if they dissociate into the two postulated sub-complexes. The data from these experiments (Figure 23) clearly showed a separation into the already determined subsets confirming this hypothesis. The reason for the shift of IFT172 from the smaller sub-complex B1 to the larger sub-complex B2 can only be speculated. It is described that IFT172 dissociates from the core complex (35), still it remains attached to the sub-complex B1 during SF-TAP experiments. Supposing that IFT172 could occur as a multi-mer, this multimer could attain a bigger size than the rest of the sub-complex B1 that is assembled by smaller proteins and therefore sediments at a sucrose concentration between the two sub-complexes. The protein HSPB11 (IFT25) was only found in one experiment and therefore was not added to the plot in Figure 23. Nevertheless, in this single experiment it was found at similar sucrose concentration than the sub-complex B2 which is in line with the data from SF-TAP. HSPB11 seems to be a weakly bound interaction partner of the IFT-B as it was not observed in every repetition of the SF-TAP experiments. Furthermore, it was not described as an IFT-B member in the work of Lucker et al. 2005 (45). Still, a recent publication showed convincingly its complex formation with IFT27 (48), further validating its association to the postulated sub-complex B2.

The above mentioned method of SDS-AP was applied to the IFT-B complexes, purified from the different stable cell lines to show their dissociation into the two sub-complexes as performed by sucrose density centrifugation. But in contrast to the sucrose density centrifugation method it was not possible to clearly separate the two sub-complexes. Sodium dodecyl sulfate (SDS) is an anionic detergent commonly used to denature proteins prior to polyacrylamide gel electrophoresis (SDS-PAGE (174-176)). SDS destabilizes non-covalent interactions within the protein and thus induces the loss of the tertiary structure of the protein. This transformation of the proteins to a linear state is needed for the migration through the polyacrylamide gel and the separation by size. If SDS is used in very low concentrations it can cause partial destabilization within protein complexes and induce a controlled disassembly of the protein complex into its subunits (177). The interaction within the sub-modules of the IFT-B might be mediated by the same type or stability of interactions as the interactions between the two sub-complexes. It is therefore possible that the loss of

interaction to the Lebercilin complex, that was described before is more sensitive to the destabilization by SDS and therefore the IFT-B-module dissociates from the other sub-modules, whereas the IFT-B itself will be destabilized totally when the SDS concentration is increased further. Nevertheless, this hypothesis has to be further validated by different approaches. This hypothesis would at least explain why the sub-complexes can be observed under the stringent washing conditions of SF-TAP purification and are not visible when the conditions become harsher due to the use of the detergent SDS. The introduction of a perturbation like the overexpression of a component or the conditions far from physiological in sucrose density centrifugation experiments might be necessary to separate the two complexes.

To analyse the importance of different IFT proteins to the function of the cilium and the localization of the IFT-B, knockdown experiments in IMCD3 cells were performed. These knockdown studies were analysed using two different approaches. First, the automatic imaging system Operetta was used to determine the effect of the knockdowns on the amount of cells bearing a single cilium. The results showed only 33% of cells with a single cilium within the control experiment, which normally should be at a rate of 48-63%. This might be explained by the fact that the machine was serviced just before the experiment and that the cells were not in perfect focus. Still, as the aim of this experiment only was to determine if the knockdown of the corresponding gene has a significant impact on the amount of cilia compared to the negative control experiment, the absolute numbers are not important and do not affect the significance of the resulting data. The knockdown of *Ttc30b* and *Arl13b* did not have a large effect on the amount of cells with a single cilium compared to the control with non-targeting siRNA. The knockdown of *Ttc30a1* reduced the amount of cells with a single cilium by a third. The knockdown of *Ift88* reduced the amount to less than a half compared to the control and the knockdown of *Ift52* even lowered the number of cells with a single cilium to a third of the control experiment. The results of these experiments cannot indicate the importance of a certain gene to the cilium's function, but allow a prediction on the severity of the phenotype that will be observed by confocal microscopy. Furthermore, this method can indicate if the used siRNA are working well under the used conditions. Nevertheless, the Operetta screens do not allow the determination of the ciliary length and therefore need to be accompanied by

classical immunostaining experiments looking to the detailed phenotype of the resulting cilia.

Therefore, IMCD3 cells were cultivated on coverslips, transfected with siRNA, subsequently stained using different IFT-antibodies and visualized using confocal microscopy. For the knockdown studies the proteins *Ift88*, *Ift52*, *Ttc30a1*, *Ttc30b* and an additional non-IFT protein that is known to have a great effect on the intraflagellar transport, *Arl13b* (203) were chosen. In the control experiments the staining pattern for the IFT-antibodies showed a slight accumulation of the proteins *Ift52*, *Ift88* and *TRAF3IP1* at the ciliary base and the tip as well as dots along the ciliary axoneme, indicating the active IFT by trains travelling along the axoneme. For all knockdowns an effect on the cilia could be observed. Except for *Ttc30a1* all knockdowns resulted in a malformation and shortening of the analysed cilia. The double knockdown of *Ift52* and *Ift88* did not lead to a stronger phenotype than the two single knockdowns. Furthermore, for all knockdowns an accumulation of the IFT-marker proteins was observed at the ciliary base whereas no accumulation at the tip was seen, indicating a reduced activity of IFT within those cells. The knockdown of *Ttc30a1* led to the elongation of the cilia and less IFT trains were observed along the cilium as well as a reduced staining of IFT proteins at the ciliary tip. The reduced staining intensity of the IFT might be explained by the longer distance that the IFT had to travel along the cilia. Nevertheless, the activity of the IFT could be the same or even higher than in the control cells. Taken together, these results indicate that the proteins that were chosen for these knockdown studies seem to play an important role for the correct function of the IFT and therefore the whole cilium.

The intention of knocking down selected components of the IFT-B was to monitor alterations in the localization of the IFT-B. Even, and if possible to see a difference in cilium architecture and IFT when knocking down components of the different sub-complexes. The experimental setup turned out not to be the perfect tool for this purpose. This is mainly a result of the strong phenotypes, resulting from their knockdowns. If the phenotype would be more subtle and the cilia would have a normal length it would maybe be possible to observe a shift in localization by disturbing the architecture of the IFT-B within these studies. But as the localization is reduced to a very small spot on the cilium the resolution of the confocal microscope

reaches its limits. Nevertheless, the results of these knockdown studies show the importance of the targeted genes for the function of the IFT and the cilium itself.

The generated interaction data by SF-TAP as well as the data from sucrose density centrifugation allowed the generation of a predicted network for the IFT-B. The network shows the organisation of the complex as two distinct sub-complexes with central components that might play a special role in linking the two modules or stabilizing their interaction. It needs to be mentioned that the organisation of this network does not necessarily represent the right stoichiometry of the complex. It might be possible that one or more of the components are present with multiple copies within the complex. To gain more information about the IFT-B, absolute quantification (141) would be a possible strategy to follow. Thus, the exact stoichiometry of the complex components could be determined allowing generating a better model of the complex architecture.

3. Characterization of CEP170 and its association to the IFT-B

In this study the centrosomal protein 170 (CEP170) is described to be associated to the IFT-B for the first time. The localization of CEP170 to the mature centriole was previously described in the literature (204). A very recent study describes the interaction of CEP170 with the protein kinesin 2b (Kif2b (219)). Still, CEP170 was never associated with the IFT or other components of the cilium before. Using immunofluorescence it was possible to show that CEP170 localizes to the base of the primary cilium in hTERT-RPE1 cells. Additionally, monitoring the localization during ciliogenesis revealed a temporal co-localization of CEP170 with a member of the IFT-B, TRAF3IP1. To further analyse the interactions of CEP170 with the IFT-B, the DNA sequence of CEP170 was cloned into the SF-TAP vector to perform affinity purification experiments in HEK293-T cells. The two-step affinity purification strategy SF-TAP did not show any interaction with the IFT-B. The published interaction with KIF2B could not be confirmed but the protein KIF2A was detected, indeed indicating a possible interaction with a motor protein of the ciliary machinery. Furthermore, the interaction with several casein-kinases and some serine/threonine phosphatases corresponds with the hypothesis that CEP170 has a different phosphorylation state during mitosis (204). Interestingly, the specific interaction of CEP170 with the protein WD repeat-containing protein 62 (WDR62) was determined, a protein that is

associated to the spindle pole and whose mutation leads to primary microcephaly (220, 221).

To determine whether the interaction of the IFT-B was not detected due to the stringent washing conditions of the SF-TAP method, one-step affinity purification of SILAC-labelled cell lysate combined with quantitative LC-MS/MS analysis was performed. The data from this experiment again showed the interaction of CEP170 to WDR62 but no interaction to the IFT-B was detectable. This might indicate that the interaction to the IFT-B is indeed only a spatio-temporal interaction that is restricted to a short time period during ciliogenesis as indicated by the data from Figure 32. Nevertheless, in some cases the interaction of specific proteins is not detectable by mass spectrometry, even if it would occur under physiological conditions. This can for example be explained by steric inhibitions by the fusion tag. The introduction of a fusion tag can lead to a difference in protein folding and therefore to a loss of interaction to other proteins. In this case, this is however unlikely because N- and C-terminal tagging was applied to circumvent this potential issue. Another explanation is the formation of artificial protein complexes with wrong stoichiometry due to the strong overexpression of the bait protein. To circumvent these difficulties it is normally the best way to use baits for the affinity purification that do not belong to the complex that is being analysed. This approach could for example be used in the case of IFT-B by using Lebercilin as bait. Indeed, this was the way by which first indications of the interaction of CEP170 with the IFT-B were attained, the destabilization of the Lebercilin complex by SDS-AP (Figure 21). The direct interaction of CEP170 with components of the IFT-B could finally be shown by detecting it as a prey protein. In a mass spectrometric experiment, with IFT57 as bait in a one-step SILAC approach (Figure 29) as well as in a western blot analysis of SF-TAP eluates from experiments with the bait proteins Lebercilin, IFT57 and CLUAP1 (Figure 30), CEP170 could be detected as interaction partner of the IFT-B.

Additional to the characterization of the interactome of CEP170, functional studies in IMCD3 cells were performed using the siRNA technique. Therefore, CEP170 was knocked down by siRNA to a level of 40% and the effect of the knockdown on the amount of cells with a single cilium as well as the ciliary phenotype were analysed. The number of cells with a single cilium was reduced to 80% compared to the amount in the control experiment, indicating that the knockdown of CEP170 might

have a moderate effect on the ciliogenesis. In contrast to the Operetta results, the data from confocal microscopy showed a very severe phenotype for the intraflagellar transport. The knockdown of CEP170 resulted in an impaired IFT and therefore no accumulation of the IFT proteins at the ciliary tip was visible anymore. These results indicate that CEP170 is important for the IFT and its loss reduces the transport along the axoneme. Interestingly, already low amounts of CEP170 seem to be enough to maintain basal IFT activity which is needed during ciliogenesis to elongate the axoneme.

The here presented data suggest that CEP170 is an essential component of the IFT machinery that interacts with the IFT-B. Still, CEP170 does seem to be a transient interaction partner that is not a stable component of the IFT-B. This can be demonstrated by its loss due to slightly more stringent washing conditions during affinity purification. Furthermore, this hypothesis is strengthened by the observation of a slightly different elution profile compared to the other IFT-B members when destabilizing the Lebercilin protein complex by SDS (Figure 21).

4. Perspectives

Within this dissertation different qualitative and quantitative methods to analyse native protein complexes are described and applied. Protein complex analysis is a steadily emerging field and its success is coupled to the development of new methods, improving the outcome and the data quality deriving from the studies performed. Here, a new combination of methods is described, combining the advantages of recently invented techniques in modern mass spectrometry with the classical methods blue native PAGE and affinity purification. SDS-AP allows collecting more information from a single experiment to gain deeper understanding of the sub-structure of the purified protein complexes. The determination of the sub-modules of the Lebercilin complex revealed new complex components with a high sensitivity which allowed focusing on specific targets for closer characterization like CEP170 within the IFT-B. Together with classical approaches for protein complex analysis, like SF-TAP and quantitative approaches like one-step affinity purification from SILAC-labelled cells, the resulting information about the protein complex of Lebercilin were ameliorated greatly. The development of a standardized protocol for the determination of the optimal SDS-concentrations and -profiles for the corresponding protein complex in combination with an automated system for the

analysis of the generated raw-data could reduce the investment of time for a single experiment even further and make the method more applicable for external users. This task will be approached in the near future since the method is being applied for several collaborative projects with different target proteins. One example is the LisH-CTLH sub-module that was found in the present study and is now analysed in detail by Ronald Roepman (Nijmegen, the Netherlands).

The detailed characterization of the IFT-B showed that the complex is divided into two distinct sub-modules. This hypothesis already was validated using different methods. The application of the SDS-AP to further dissociate the IFT-B was not successful until now. A possible approach for tackling the problem of single dissociating proteins from the IFT-B might be to use the IFT-B fraction from the destabilization of the Lebercilin complex as a starting material for further destabilization. Thus, the problem of steric inhibition by the fusion tag, as well as artificial complex composition, derived from overexpression is circumvented. The complex destabilization could be performed in-solution and separated by molecular weight cut-off spin columns for further analysis. A further limitation for validation of the two sub-complex hypothesis is the lack of commercially available antibodies to distinguish the exact localization of the two sub-complexes. First attempts in generating monoclonal antibodies against whole fusion-proteins derived from bacteria failed due to degradation of the proteins, which also was described in the literature as being a challenge (47). The generation of antibodies against synthetic peptides is now in progress and will hopefully give better results in the near future. Using these antibodies for immuno-gold microscopy with gold particles of different sizes for differentiation will improve the resolution and thus hopefully reveal the exact localization of the two sub-complexes at the cilium.

The analysis of CEP170 showed its association to the IFT-B and its importance for the function of the intraflagellar transport along the ciliary axoneme. An additional interesting experiment would be to perform a time course observing an IFT protein during ciliogenesis when CEP170 is knocked down. Thus, it would be possible to determine at which point the IFT is impaired. This in combination with affinity purification of CEP170, at the time point where CEP170 and TRAF3IP1 are interacting during ciliogenesis, could gain further insight into the function of the protein. Additionally, the sequencing of ciliopathy patient cohorts might reveal some

mutations within the gene and thus allow to characterize the function of those mutations by comparative SILAC approaches between mutant and wild type interactome. Another approach could be to test those mutations in the zebrafish system. Since the cells had visually normal cilia after knockdown, the mutations should not be lethal and therefore the phenotypes could be characterized in detail.

VI. References

1. Dobell, C., and Leeuwenhoek, A.v. 1932. *Antony van Leeuwenhoek and his "Little animals"; being some account of the father of protozoology and bacteriology and his multifarious discoveries in these disciplines*. New York,: Harcourt, Brace and company. vii, 435, 431 p. pp.
2. Gibbons, I.R. 1981. Cilia and flagella of eukaryotes. *J Cell Biol* 91:107s-124s.
3. Zimmermann, K.W. 1898. Beitrage zur Kenntniss einiger Drusen und Epithelien. *Arch. Mikrosk. Anat.* 52:552–706.
4. Sorokin, S.P. 1968. Reconstructions of centriole formation and ciliogenesis in mammalian lungs. *J Cell Sci* 3:207-230.
5. Badano, J.L., Mitsuma, N., Beales, P.L., and Katsanis, N. 2006. The ciliopathies: an emerging class of human genetic disorders. *Annu Rev Genomics Hum Genet* 7:125-148.
6. Wheatley, D.N. 2005. Landmarks in the first hundred years of primary (9+0) cilium research. *Cell Biol Int* 29:333-339.
7. Cavalier-Smith, T. 2002. The phagotrophic origin of eukaryotes and phylogenetic classification of Protozoa. *Int J Syst Evol Microbiol* 52:297-354.
8. Fawcett, D.W. 1981. *The cell*. Philadelphia: W. B. Saunders Co. viii, 862 p. pp.
9. Beales, P., and Jackson, P.K. 2012. Cilia - the prodigal organelle. *Cilia* 1:1.
10. Toremalm, N.G., Hakansson, C.H., Mercke, U., Dahlerus, B., and Huberman, D. 1975. Mucociliary wave pattern. A comparative analysis of extracellular and intracellular activities. *Acta Otolaryngol* 79:436-441.
11. Ashton Acton, Q. 2012. *Cell Surface Extensions: Advances in Research and Application: 2011 Edition*: Scholarly Editions.
12. Becker-Heck, A., Zohn, I.E., Okabe, N., Pollock, A., Lenhart, K.B., Sullivan-Brown, J., McSheene, J., Loges, N.T., Olbrich, H., Haeffner, K., et al. 2011. The coiled-coil domain containing protein CCDC40 is essential for motile cilia function and left-right axis formation. *Nat Genet* 43:79-84.
13. Gate, D., Danielpour, M., Levy, R., Breunig, J.J., and Town, T. 2012. Basic biology and mechanisms of neural ciliogenesis and the B9 family. *Mol Neurobiol* 45:564-570.
14. Resnick, A., and Hopfer, U. 2007. Force-response considerations in ciliary mechanosensation. *Biophys J* 93:1380-1390.
15. Praetorius, H.A., and Spring, K.R. 2001. Bending the MDCK cell primary cilium increases intracellular calcium. *J Membr Biol* 184:71-79.
16. Praetorius, H.A., and Spring, K.R. 2003. Removal of the MDCK cell primary cilium abolishes flow sensing. *J Membr Biol* 191:69-76.
17. Rash, J.E., Shay, J.W., and Biesele, J.J. 1969. Cilia in cardiac differentiation. *J Ultrastruct Res* 29:470-484.
18. Dingemans, K.P. 1969. The relation between cilia and mitoses in the mouse adenohypophysis. *J Cell Biol* 43:361-367.
19. Tucker, R.W., Pardee, A.B., and Fujiwara, K. 1979. Centriole ciliation is related to quiescence and DNA synthesis in 3T3 cells. *Cell* 17:527-535.
20. Barnes, B.G. 1961. Ciliated secretory cells in the pars distalis of the mouse hypophysis. *J Ultrastruct Res* 5:453-467.

21. Berbari, N.F., O'Connor, A.K., Haycraft, C.J., and Yoder, B.K. 2009. The primary cilium as a complex signaling center. *Curr Biol* 19:R526-535.
22. Kee, H.L., Dishinger, J.F., Blasius, T.L., Liu, C.J., Margolis, B., and Verhey, K.J. 2012. A size-exclusion permeability barrier and nucleoporins characterize a ciliary pore complex that regulates transport into cilia. *Nat Cell Biol* 14:431-437.
23. Afzelius, B.A. 2004. Cilia-related diseases. *J Pathol* 204:470-477.
24. Hidaka, K., Ashizawa, N., Endoh, H., Watanabe, M., and Fukumoto, S. 1995. Fine structure of the cilia in the pancreatic duct of WBN/Kob rat. *Int J Pancreatol* 18:207-213.
25. Gibbons, B.H., Gibbons, I.R., and Baccetti, B. 1983. Structure and motility of the 9 + 0 flagellum of eel spermatozoa. *J Submicrosc Cytol* 15:15-20.
26. Flock, A., and Duvall, A.J., 3rd. 1965. The Ultrastructure of the Kinocilium of the Sensory Cells in the Inner Ear and Lateral Line Organs. *J Cell Biol* 25:1-8.
27. Feistel, K., and Blum, M. 2006. Three types of cilia including a novel 9+4 axoneme on the notochordal plate of the rabbit embryo. *Dev Dyn* 235:3348-3358.
28. Schwartz, E.A., Leonard, M.L., Bizios, R., and Bowser, S.S. 1997. Analysis and modeling of the primary cilium bending response to fluid shear. *Am J Physiol* 272:F132-138.
29. Afzelius, B.A., Eliasson, R., Johnsen, O., and Lindholmer, C. 1975. Lack of dynein arms in immotile human spermatozoa. *J Cell Biol* 66:225-232.
30. Pedersen, H., and Rebbe, H. 1975. Absence of arms in the axoneme of immobile human spermatozoa. *Biol Reprod* 12:541-544.
31. Stephens, R.E. 1997. Synthesis and turnover of embryonic sea urchin ciliary proteins during selective inhibition of tubulin synthesis and assembly. *Mol Biol Cell* 8:2187-2198.
32. Kozminski, K.G., Johnson, K.A., Forscher, P., and Rosenbaum, J.L. 1993. A motility in the eukaryotic flagellum unrelated to flagellar beating. *Proc Natl Acad Sci U S A* 90:5519-5523.
33. Behal, R.H., Bettleja, E., and Cole, D.G. 2009. Purification of IFT particle proteins and preparation of recombinant proteins for structural and functional analysis. *Methods Cell Biol* 93:179-196.
34. Pedersen, L.B., Veland, I.R., Schroder, J.M., and Christensen, S.T. 2008. Assembly of primary cilia. *Dev Dyn* 237:1993-2006.
35. Cole, D.G., Diener, D.R., Himelblau, A.L., Beech, P.L., Fuster, J.C., and Rosenbaum, J.L. 1998. Chlamydomonas kinesin-II-dependent intraflagellar transport (IFT): IFT particles contain proteins required for ciliary assembly in *Caenorhabditis elegans* sensory neurons. *J Cell Biol* 141:993-1008.
36. Taschner, M., Bhogaraju, S., and Lorentzen, E. 2012. Architecture and function of IFT complex proteins in ciliogenesis. *Differentiation* 83:S12-22.
37. Avidor-Reiss, T., Maer, A.M., Koundakjian, E., Polyanovsky, A., Keil, T., Subramaniam, S., and Zuker, C.S. 2004. Decoding cilia function: defining specialized genes required for compartmentalized cilia biogenesis. *Cell* 117:527-539.
38. Jekely, G., and Arendt, D. 2006. Evolution of intraflagellar transport from coated vesicles and autogenous origin of the eukaryotic cilium. *Bioessays* 28:191-198.

39. van Dam, T.J., Townsend, M.J., Turk, M., Schlessinger, A., Sali, A., Field, M.C., and Huynen, M.A. 2013. Evolution of modular intraflagellar transport from a coatomer-like progenitor. *Proc Natl Acad Sci U S A* 110:6943-6948.
40. Sukumaran, S., and Perkins, B.D. 2009. Early defects in photoreceptor outer segment morphogenesis in zebrafish *ift57*, *ift88* and *ift172* Intraflagellar Transport mutants. *Vision Res* 49:479-489.
41. Beales, P.L., Bland, E., Tobin, J.L., Bacchelli, C., Tuysuz, B., Hill, J., Rix, S., Pearson, C.G., Kai, M., Hartley, J., et al. 2007. IFT80, which encodes a conserved intraflagellar transport protein, is mutated in Jeune asphyxiating thoracic dystrophy. *Nat Genet* 39:727-729.
42. Tran, P.V., Haycraft, C.J., Besschetnova, T.Y., Turbe-Doan, A., Stottmann, R.W., Herron, B.J., Chesebro, A.L., Qiu, H., Scherz, P.J., Shah, J.V., et al. 2008. THM1 negatively modulates mouse sonic hedgehog signal transduction and affects retrograde intraflagellar transport in cilia. *Nat Genet* 40:403-410.
43. Walczak-Sztulpa, J., Eggenschwiler, J., Osborn, D., Brown, D.A., Emma, F., Klingenberg, C., Hennekam, R.C., Torre, G., Garshasbi, M., Tzschach, A., et al. 2010. Cranioectodermal Dysplasia, Sensenbrenner syndrome, is a ciliopathy caused by mutations in the IFT122 gene. *Am J Hum Genet* 86:949-956.
44. Pigino, G., Geimer, S., Lanzavecchia, S., Paccagnini, E., Cantele, F., Diener, D.R., Rosenbaum, J.L., and Lupetti, P. 2009. Electron-tomographic analysis of intraflagellar transport particle trains in situ. *J Cell Biol* 187:135-148.
45. Lucker, B.F., Behal, R.H., Qin, H., Siron, L.C., Taggart, W.D., Rosenbaum, J.L., and Cole, D.G. 2005. Characterization of the intraflagellar transport complex B core: direct interaction of the IFT81 and IFT74/72 subunits. *J Biol Chem* 280:27688-27696.
46. Richey, E.A., and Qin, H. 2012. Dissecting the sequential assembly and localization of intraflagellar transport particle complex B in *Chlamydomonas*. *PLoS One* 7:e43118.
47. Taschner, M., Bhogaraju, S., Vetter, M., Morawetz, M., and Lorentzen, E. 2011. Biochemical mapping of interactions within the intraflagellar transport (IFT) B core complex: IFT52 binds directly to four other IFT-B subunits. *J Biol Chem* 286:26344-26352.
48. Bhogaraju, S., Taschner, M., Morawetz, M., Basquin, C., and Lorentzen, E. 2011. Crystal structure of the intraflagellar transport complex 25/27. *Embo J* 30:1907-1918.
49. Blacque, O.E., Cevik, S., and Kaplan, O.I. 2008. Intraflagellar transport: from molecular characterisation to mechanism. *Front Biosci* 13:2633-2652.
50. Boldt, K., Mans, D.A., Won, J., van Reeuwijk, J., Vogt, A., Kinkl, N., Letteboer, S.J., Hicks, W.L., Hurd, R.E., Naggert, J.K., et al. 2011. Disruption of intraflagellar protein transport in photoreceptor cilia causes Leber congenital amaurosis in humans and mice. *J Clin Invest* 121:2169-2180.
51. Bernhard, W., and De Harven, E. 1956. [Electron microscopic study of the ultrastructure of centrioles in vertebra]. *Z Zellforsch Mikrosk Anat* 45:378-398.
52. Moser, J.J., Fritzler, M.J., and Rattner, J.B. 2009. Primary ciliogenesis defects are associated with human astrocytoma/glioblastoma cells. *BMC Cancer* 9:448.
53. Reiter, J.F., Blacque, O.E., and Leroux, M.R. 2012. The base of the cilium: roles for transition fibres and the transition zone in ciliary formation, maintenance and compartmentalization. *EMBO Rep* 13:608-618.

54. Wheatley, D.N. 1969. Cilia in cell-cultured fibroblasts. I. On their occurrence and relative frequencies in primary cultures and established cell lines. *J Anat* 105:351-362.
55. Sorokin, S. 1962. Centrioles and the formation of rudimentary cilia by fibroblasts and smooth muscle cells. *J Cell Biol* 15:363-377.
56. Anderson, R.G. 1972. The three-dimensional structure of the basal body from the rhesus monkey oviduct. *J Cell Biol* 54:246-265.
57. Sotelo, J.R., and Trujillo-Cenoz, O. 1958. Electron microscope study on the development of ciliary components of the neural epithelium of the chick embryo. *Z Zellforsch Mikrosk Anat* 49:1-12.
58. Gilula, N.B., and Satir, P. 1972. The ciliary necklace. A ciliary membrane specialization. *J Cell Biol* 53:494-509.
59. Rieder, C.L., Jensen, C.G., and Jensen, L.C. 1979. The resorption of primary cilia during mitosis in a vertebrate (PtK1) cell line. *J Ultrastruct Res* 68:173-185.
60. Pugacheva, E.N., Jablonski, S.A., Hartman, T.R., Henske, E.P., and Golemis, E.A. 2007. HEF1-dependent Aurora A activation induces disassembly of the primary cilium. *Cell* 129:1351-1363.
61. Mustafi, D., Engel, A.H., and Palczewski, K. 2009. Structure of cone photoreceptors. *Prog Retin Eye Res* 28:289-302.
62. Hoke, K.L., and Fernald, R.D. 1997. Rod photoreceptor neurogenesis. *Progress in Retinal and Eye Research* 16:31-49.
63. Young, R.W. 1967. The renewal of photoreceptor cell outer segments. *J Cell Biol* 33:61-72.
64. Sedmak, T., and Wolfrum, U. 2010. Intraflagellar transport molecules in ciliary and nonciliary cells of the retina. *J Cell Biol* 189:171-186.
65. Liu, Q., Zuo, J., and Pierce, E.A. 2004. The retinitis pigmentosa 1 protein is a photoreceptor microtubule-associated protein. *J Neurosci* 24:6427-6436.
66. Li, L., Yildiz, O., Anand, M., and Khanna, H. 2012. Photoreceptor Sensory Cilium and Associated Disorders. In *Ocular Diseases*. D.A. Adio, editor: InTech. 43-60.
67. Anand, M., and Khanna, H. 2012. Ciliary transition zone (TZ) proteins RPGR and CEP290: role in photoreceptor cilia and degenerative diseases. *Expert Opin Ther Targets* 16:541-551.
68. Ramamurthy, V., and Cayouette, M. 2009. Development and disease of the photoreceptor cilium. *Clin Genet* 76:137-145.
69. Roepman, R., and Wolfrum, U. 2007. Protein networks and complexes in photoreceptor cilia. *Subcell Biochem* 43:209-235.
70. Insinna, C., and Besharse, J.C. 2008. Intraflagellar transport and the sensory outer segment of vertebrate photoreceptors. *Dev Dyn* 237:1982-1992.
71. Fliegau, M., Benzing, T., and Omran, H. 2007. When cilia go bad: cilia defects and ciliopathies. *Nat Rev Mol Cell Biol* 8:880-893.
72. den Hollander, A.I., Koeneke, R.K., Mohamed, M.D., Arts, H.H., Boldt, K., Towns, K.V., Sedmak, T., Beer, M., Nagel-Wolfrum, K., McKibbin, M., et al. 2007. Mutations in LCA5, encoding the ciliary protein lebercilin, cause Leber congenital amaurosis. *Nat Genet* 39:889-895.
73. Ansley, S.J., Badano, J.L., Blacque, O.E., Hill, J., Hoskins, B.E., Leitch, C.C., Kim, J.C., Ross, A.J., Eichers, E.R., Teslovich, T.M., et al. 2003. Basal body dysfunction is a likely cause of pleiotropic Bardet-Biedl syndrome. *Nature* 425:628-633.

-
74. Zaghoul, N.A., and Katsanis, N. 2009. Mechanistic insights into Bardet-Biedl syndrome, a model ciliopathy. *J Clin Invest* 119:428-437.
 75. Garcia-Gonzalo, F.R., Corbit, K.C., Simerly-Piquer, M.S., Ramaswami, G., Otto, E.A., Noriega, T.R., Seol, A.D., Robinson, J.F., Bennett, C.L., Josifova, D.J., et al. 2011. A transition zone complex regulates mammalian ciliogenesis and ciliary membrane composition. *Nat Genet* 43:776-784.
 76. Cao, J., Shen, Y., Zhu, L., Xu, Y., Zhou, Y., Wu, Z., Li, Y., Yan, X., and Zhu, X. 2012. miR-129-3p controls cilia assembly by regulating CP110 and actin dynamics. *Nat Cell Biol* 14:697-706.
 77. Merbs, S.L., Khan, M.A., Hackler, L., Jr., Oliver, V.F., Wan, J., Qian, J., and Zack, D.J. 2012. Cell-specific DNA methylation patterns of retina-specific genes. *PLoS One* 7:e32602.
 78. Jenkins, P.M., Zhang, L., Thomas, G., and Martens, J.R. 2009. PACS-1 mediates phosphorylation-dependent ciliary trafficking of the cyclic-nucleotide-gated channel in olfactory sensory neurons. *J Neurosci* 29:10541-10551.
 79. Lancaster, M.A., Schroth, J., and Gleeson, J.G. 2011. Subcellular spatial regulation of canonical Wnt signalling at the primary cilium. *Nat Cell Biol* 13:700-707.
 80. Zhang, Q., Acland, G.M., Wu, W.X., Johnson, J.L., Pearce-Kelling, S., Tulloch, B., Vervoort, R., Wright, A.F., and Aguirre, G.D. 2002. Different RPGR exon ORF15 mutations in Canids provide insights into photoreceptor cell degeneration. *Hum Mol Genet* 11:993-1003.
 81. Waters, A.M., and Beales, P.L. 2011. Ciliopathies: an expanding disease spectrum. *Pediatr Nephrol* 26:1039-1056.
 82. Kobayashi, D., and Takeda, H. 2012. Ciliary motility: the components and cytoplasmic preassembly mechanisms of the axonemal dyneins. *Differentiation* 83:S23-29.
 83. Takeda, S., and Narita, K. 2012. Structure and function of vertebrate cilia, towards a new taxonomy. *Differentiation* 83:S4-11.
 84. Alberts, B. 1998. The cell as a collection of protein machines: preparing the next generation of molecular biologists. *Cell* 92:291-294.
 85. Hartwell, L.H., Hopfield, J.J., Leibler, S., and Murray, A.W. 1999. From molecular to modular cell biology. *Nature* 402:C47-52.
 86. Pereira-Leal, J.B., Levy, E.D., and Teichmann, S.A. 2006. The origins and evolution of functional modules: lessons from protein complexes. *Philos Trans R Soc Lond B Biol Sci* 361:507-517.
 87. Nooren, I.M., and Thornton, J.M. 2003. Diversity of protein-protein interactions. *Embo J* 22:3486-3492.
 88. Caetano-Anollés, G. 2010. *Evolutionary genomics and systems biology*. Hoboken, N.J.: Wiley-Blackwell. xix, 465 p., 440 p. of plates pp.
 89. Kolch, W. 2005. Coordinating ERK/MAPK signalling through scaffolds and inhibitors. *Nat Rev Mol Cell Biol* 6:827-837.
 90. O'Neill, E., and Kolch, W. 2004. Conferring specificity on the ubiquitous Raf/MEK signalling pathway. *Br J Cancer* 90:283-288.
 91. McCammon, J.A., Gelin, B.R., and Karplus, M. 1977. Dynamics of folded proteins. *Nature* 267:585-590.
 92. Levitt, M., and Sharon, R. 1988. Accurate simulation of protein dynamics in solution. *Proc Natl Acad Sci U S A* 85:7557-7561.
-

93. Deng, X., Gao, F., and May, W.S. 2009. Protein phosphatase 2A inactivates Bcl2's antiapoptotic function by dephosphorylation and up-regulation of Bcl2-p53 binding. *Blood* 113:422-428.
94. de Lichtenberg, U., Jensen, L.J., Brunak, S., and Bork, P. 2005. Dynamic complex formation during the yeast cell cycle. *Science* 307:724-727.
95. Hashimoto, K., Nishi, H., Bryant, S., and Panchenko, A.R. 2011. Caught in self-interaction: evolutionary and functional mechanisms of protein homooligomerization. *Phys Biol* 8:035007.
96. Mittag, T., Kay, L.E., and Forman-Kay, J.D. 2010. Protein dynamics and conformational disorder in molecular recognition. *J Mol Recognit* 23:105-116.
97. Braun, P., and Gingras, A.C. 2012. History of protein-protein interactions: from egg-white to complex networks. *Proteomics* 12:1478-1498.
98. Kuhner, S., van Noort, V., Betts, M.J., Leo-Macias, A., Batisse, C., Rode, M., Yamada, T., Maier, T., Bader, S., Beltran-Alvarez, P., et al. 2009. Proteome organization in a genome-reduced bacterium. *Science* 326:1235-1240.
99. Hyung, S.J., and Ruotolo, B.T. 2012. Integrating mass spectrometry of intact protein complexes into structural proteomics. *Proteomics* 12:1547-1564.
100. Kocher, T., and Superti-Furga, G. 2007. Mass spectrometry-based functional proteomics: from molecular machines to protein networks. *Nat Methods* 4:807-815.
101. Braun, P. 2012. Interactome mapping for analysis of complex phenotypes: insights from benchmarking binary interaction assays. *Proteomics* 12:1499-1518.
102. Kiel, C., Vogt, A., Campagna, A., Chatr-aryamontri, A., Swiatek-de Lange, M., Beer, M., Bolz, S., Mack, A.F., Kinkl, N., Cesareni, G., et al. 2011. Structural and functional protein network analyses predict novel signaling functions for rhodopsin. *Mol Syst Biol* 7:551.
103. Janson, J.-C. 2011. *Protein purification : principles, high resolution methods, and applications*. Hoboken, N.J.: John Wiley & Sons. xiv, 517 p. pp.
104. Fang, X., and Zhang, W.W. 2008. Affinity separation and enrichment methods in proteomic analysis. *J Proteomics* 71:284-303.
105. Bildl, W., Haupt, A., Muller, C.S., Biniossek, M.L., Thumfart, J.O., Huber, B., Fakler, B., and Schulte, U. 2012. Extending the dynamic range of label-free mass spectrometric quantification of affinity purifications. *Mol Cell Proteomics* 11:M111 007955.
106. Lin, S.H., and Guidotti, G. 2009. Purification of membrane proteins. *Methods Enzymol* 463:619-629.
107. Rosenberg, I.M. 2005. *Protein analysis and purification : benchtop techniques*. Boston: Birkhäuser. xxvi, 520 p. pp.
108. Hopp, T.P., Prickett, K.S., Price, V.L., Libby, R.T., March, C.J., Pat Cerretti, D., Urdal, D.L., and Conlon, P.J. 1988. A Short Polypeptide Marker Sequence Useful for Recombinant Protein Identification and Purification. *Nat Biotech* 6:1204-1210.
109. Li, Y. 2010. Commonly used tag combinations for tandem affinity purification. *Biotechnol Appl Biochem* 55:73-83.
110. Gavin, A.C., Bosche, M., Krause, R., Grandi, P., Marzioch, M., Bauer, A., Schultz, J., Rick, J.M., Michon, A.M., Cruciat, C.M., et al. 2002. Functional organization of the yeast proteome by systematic analysis of protein complexes. *Nature* 415:141-147.

111. Kimple, M.E., and Sondek, J. 2004. Overview of affinity tags for protein purification. *Curr Protoc Protein Sci* Chapter 9:Unit 9 9.
112. Rigaut, G., Shevchenko, A., Rutz, B., Wilm, M., Mann, M., and Seraphin, B. 1999. A generic protein purification method for protein complex characterization and proteome exploration. *Nat Biotechnol* 17:1030-1032.
113. Puig, O., Caspary, F., Rigaut, G., Rutz, B., Bouveret, E., Bragado-Nilsson, E., Wilm, M., and Seraphin, B. 2001. The tandem affinity purification (TAP) method: a general procedure of protein complex purification. *Methods* 24:218-229.
114. Xu, X., Song, Y., Li, Y., Chang, J., Zhang, H., and An, L. 2010. The tandem affinity purification method: an efficient system for protein complex purification and protein interaction identification. *Protein Expr Purif* 72:149-156.
115. Gloeckner, C.J., Boldt, K., Schumacher, A., Roepman, R., and Ueffing, M. 2007. A novel tandem affinity purification strategy for the efficient isolation and characterisation of native protein complexes. *Proteomics* 7:4228-4234.
116. Gloeckner, C.J., Boldt, K., and Ueffing, M. 2009. Strep/FLAG tandem affinity purification (SF-TAP) to study protein interactions. *Curr Protoc Protein Sci* Chapter 19:Unit19 20.
117. Bornens, M., and Moudjou, M. 1999. Studying the composition and function of centrosomes in vertebrates. *Methods Cell Biol* 61:13-34.
118. Fleischman, D., Denisevich, M., Raveed, D., and Pannbacker, R.G. 1980. Association of guanylate cyclase with the axoneme of retinal rods. *Biochim Biophys Acta* 630:176-186.
119. Raychowdhury, M.K., McLaughlin, M., Ramos, A.J., Montalbetti, N., Bouley, R., Ausiello, D.A., and Cantiello, H.F. 2005. Characterization of single channel currents from primary cilia of renal epithelial cells. *J Biol Chem* 280:34718-34722.
120. Pagh-Roehl, K., and Burnside, B. 1995. Preparation of teleost rod inner and outer segments. *Methods Cell Biol* 47:83-92.
121. Pertoft, H. 2000. Fractionation of cells and subcellular particles with Percoll. *J Biochem Biophys Methods* 44:1-30.
122. Tanese, N. 1997. Small-scale density gradient sedimentation to separate and analyze multiprotein complexes. *Methods* 12:224-234.
123. de Araujo, M.E., Huber, L.A., and Stasyk, T. 2008. Isolation of endocytic organelles by density gradient centrifugation. *Methods Mol Biol* 424:317-331.
124. Volk, S., Schreiber, T.D., Eisen, D., Wiese, C., Planatscher, H., Pynn, C.J., Stoll, D., Templin, M.F., Joos, T.O., and Potz, O. 2012. Combining ultracentrifugation and peptide termini group-specific immunoprecipitation for multiplex plasma protein analysis. *Mol Cell Proteomics* 11:O111 015438.
125. Steen, H., and Mann, M. 2004. The ABC's (and XYZ's) of peptide sequencing. *Nat Rev Mol Cell Biol* 5:699-711.
126. Gingras, A.C., Aebersold, R., and Raught, B. 2005. Advances in protein complex analysis using mass spectrometry. *J Physiol* 563:11-21.
127. Kumar, C., and Mann, M. 2009. Bioinformatics analysis of mass spectrometry-based proteomics data sets. *FEBS Lett* 583:1703-1712.
128. Walther, T.C., and Mann, M. 2010. Mass spectrometry-based proteomics in cell biology. *J Cell Biol* 190:491-500.
129. Ong, S.E., Blagoev, B., Kratchmarova, I., Kristensen, D.B., Steen, H., Pandey, A., and Mann, M. 2002. Stable isotope labeling by amino acids in cell culture,

- SILAC, as a simple and accurate approach to expression proteomics. *Mol Cell Proteomics* 1:376-386.
130. Vermeulen, M., Hubner, N.C., and Mann, M. 2008. High confidence determination of specific protein-protein interactions using quantitative mass spectrometry. *Curr Opin Biotechnol* 19:331-337.
 131. Cox, J., and Mann, M. 2008. MaxQuant enables high peptide identification rates, individualized p.p.b.-range mass accuracies and proteome-wide protein quantification. *Nat Biotechnol* 26:1367-1372.
 132. Bantscheff, M., Lemeer, S., Savitski, M.M., and Kuster, B. 2012. Quantitative mass spectrometry in proteomics: critical review update from 2007 to the present. *Anal Bioanal Chem* 404:939-965.
 133. Elliott, M.H., Smith, D.S., Parker, C.E., and Borchers, C. 2009. Current trends in quantitative proteomics. *J Mass Spectrom* 44:1637-1660.
 134. Bantscheff, M., Schirle, M., Sweetman, G., Rick, J., and Kuster, B. 2007. Quantitative mass spectrometry in proteomics: a critical review. *Anal Bioanal Chem* 389:1017-1031.
 135. Coombs, K.M. 2011. Quantitative proteomics of complex mixtures. *Expert Rev Proteomics* 8:659-677.
 136. Schmidt, A., Kellermann, J., and Lottspeich, F. 2005. A novel strategy for quantitative proteomics using isotope-coded protein labels. *Proteomics* 5:4-15.
 137. Kellermann, J. 2008. ICPL--isotope-coded protein label. *Methods Mol Biol* 424:113-123.
 138. Ross, P.L., Huang, Y.N., Marchese, J.N., Williamson, B., Parker, K., Hattan, S., Khainovski, N., Pillai, S., Dey, S., Daniels, S., et al. 2004. Multiplexed protein quantitation in *Saccharomyces cerevisiae* using amine-reactive isobaric tagging reagents. *Mol Cell Proteomics* 3:1154-1169.
 139. Pierce, A., Unwin, R.D., Evans, C.A., Griffiths, S., Carney, L., Zhang, L., Jaworska, E., Lee, C.F., Blinco, D., Okoniewski, M.J., et al. 2008. Eight-channel iTRAQ enables comparison of the activity of six leukemogenic tyrosine kinases. *Mol Cell Proteomics* 7:853-863.
 140. Lange, V., Picotti, P., Domon, B., and Aebersold, R. 2008. Selected reaction monitoring for quantitative proteomics: a tutorial. *Mol Syst Biol* 4:222.
 141. Gerber, S.A., Rush, J., Stemman, O., Kirschner, M.W., and Gygi, S.P. 2003. Absolute quantification of proteins and phosphoproteins from cell lysates by tandem MS. *Proc Natl Acad Sci U S A* 100:6940-6945.
 142. Kirkpatrick, D.S., Gerber, S.A., and Gygi, S.P. 2005. The absolute quantification strategy: a general procedure for the quantification of proteins and post-translational modifications. *Methods* 35:265-273.
 143. Schmidt, C., Lenz, C., Grote, M., Luhrmann, R., and Urlaub, H. 2010. Determination of protein stoichiometry within protein complexes using absolute quantification and multiple reaction monitoring. *Anal Chem* 82:2784-2796.
 144. King, R., Bonfiglio, R., Fernandez-Metzler, C., Miller-Stein, C., and Olah, T. 2000. Mechanistic investigation of ionization suppression in electrospray ionization. *J Am Soc Mass Spectrom* 11:942-950.
 145. Nahnsen, S., Bielow, C., Reinert, K., and Kohlbacher, O. 2012. Tools for label-free peptide quantification. *Mol Cell Proteomics*.
 146. Chelius, D., and Bondarenko, P.V. 2002. Quantitative profiling of proteins in complex mixtures using liquid chromatography and mass spectrometry. *J Proteome Res* 1:317-323.

147. Liu, H., Sadygov, R.G., and Yates, J.R., 3rd. 2004. A model for random sampling and estimation of relative protein abundance in shotgun proteomics. *Anal Chem* 76:4193-4201.
148. Saiki, R.K., Gelfand, D.H., Stoffel, S., Scharf, S.J., Higuchi, R., Horn, G.T., Mullis, K.B., and Erlich, H.A. 1988. Primer-directed enzymatic amplification of DNA with a thermostable DNA polymerase. *Science* 239:487-491.
149. Hartley, J.L., Temple, G.F., and Brasch, M.A. 2000. DNA cloning using in vitro site-specific recombination. *Genome Res* 10:1788-1795.
150. Gloeckner, C.J., Boldt, K., Schumacher, A., and Ueffing, M. 2009. Tandem affinity purification of protein complexes from mammalian cells by the Strep/FLAG (SF)-TAP tag. *Methods Mol Biol* 564:359-372.
151. Pfaffl, M.W. 2004. Real-time RT-PCR: Neue Ansätze zur exakten mRNA Quantifizierung. *BIOspektrum* 10:92-95.
152. Pfaffl, M.W., Horgan, G.W., and Dempfle, L. 2002. Relative expression software tool (REST) for group-wise comparison and statistical analysis of relative expression results in real-time PCR. *Nucleic Acids Res* 30:e36.
153. Bradford, M.M. 1976. A rapid and sensitive method for the quantitation of microgram quantities of protein utilizing the principle of protein-dye binding. *Anal Biochem* 72:248-254.
154. Splittgerber, A.G., and Sohl, J. 1989. Nonlinearity in protein assays by the Coomassie blue dye-binding method. *Anal Biochem* 179:198-201.
155. Peterson, G.L. 1983. Determination of total protein. *Methods Enzymol* 91:95-119.
156. Wessel, D., and Flugge, U.I. 1984. A method for the quantitative recovery of protein in dilute solution in the presence of detergents and lipids. *Anal Biochem* 138:141-143.
157. Laemmli, U.K. 1970. Cleavage of structural proteins during the assembly of the head of bacteriophage T4. *Nature* 227:680-685.
158. Fazekas de St Groth, S., Webster, R.G., and Datyner, A. 1963. Two new staining procedures for quantitative estimation of proteins on electrophoretic strips. *Biochim Biophys Acta* 71:377-391.
159. Candiano, G., Bruschi, M., Musante, L., Santucci, L., Ghiggeri, G.M., Carnemolla, B., Orecchia, P., Zardi, L., and Righetti, P.G. 2004. Blue silver: a very sensitive colloidal Coomassie G-250 staining for proteome analysis. *Electrophoresis* 25:1327-1333.
160. Neuhoff, V., Arold, N., Taube, D., and Ehrhardt, W. 1988. Improved staining of proteins in polyacrylamide gels including isoelectric focusing gels with clear background at nanogram sensitivity using Coomassie Brilliant Blue G-250 and R-250. *Electrophoresis* 9:255-262.
161. Kang, D., Gho, Y.S., Suh, M., and Kang, C. 2002. Highly Sensitive and Fast Protein Detection with Coomassie Brilliant Blue in Sodium Dodecyl Sulfate-Polyacrylamide Gel Electrophoresis. *Bull. Korean Chem. Soc.* 23:1511-1512.
162. Shevchenko, A., Wilm, M., Vorm, O., and Mann, M. 1996. Mass spectrometric sequencing of proteins silver-stained polyacrylamide gels. *Anal Chem* 68:850-858.
163. Switzer, R.C., 3rd, Merrill, C.R., and Shifrin, S. 1979. A highly sensitive silver stain for detecting proteins and peptides in polyacrylamide gels. *Anal Biochem* 98:231-237.

164. Towbin, H., Staehelin, T., and Gordon, J. 1979. Electrophoretic transfer of proteins from polyacrylamide gels to nitrocellulose sheets: procedure and some applications. *Proc Natl Acad Sci U S A* 76:4350-4354.
165. Stochaj, W.R., Berkelman, T., and Laird, N. 2006. Staining membrane-bound proteins with ponceau s. *CSH Protoc* 2006.
166. Kaufmann, S.H., Ewing, C.M., and Shaper, J.H. 1987. The erasable Western blot. *Anal Biochem* 161:89-95.
167. Schmidt, T.G., and Skerra, A. 1994. One-step affinity purification of bacterially produced proteins by means of the "Strep tag" and immobilized recombinant core streptavidin. *J Chromatogr A* 676:337-345.
168. Schmidt, T.G., and Skerra, A. 1993. The random peptide library-assisted engineering of a C-terminal affinity peptide, useful for the detection and purification of a functional Ig Fv fragment. *Protein Eng* 6:109-122.
169. Schmidt, T.G., Koepke, J., Frank, R., and Skerra, A. 1996. Molecular interaction between the Strep-tag affinity peptide and its cognate target, streptavidin. *J Mol Biol* 255:753-766.
170. Voss, S., and Skerra, A. 1997. Mutagenesis of a flexible loop in streptavidin leads to higher affinity for the Strep-tag II peptide and improved performance in recombinant protein purification. *Protein Eng* 10:975-982.
171. Schmidt, T.G., and Skerra, A. 2007. The Strep-tag system for one-step purification and high-affinity detection or capturing of proteins. *Nat Protoc* 2:1528-1535.
172. Lichty, J.J., Malecki, J.L., Agnew, H.D., Michelson-Horowitz, D.J., and Tan, S. 2005. Comparison of affinity tags for protein purification. *Protein Expr Purif* 41:98-105.
173. Brizzard, B.L., Chubet, R.G., and Vizard, D.L. 1994. Immunoaffinity purification of FLAG epitope-tagged bacterial alkaline phosphatase using a novel monoclonal antibody and peptide elution. *Biotechniques* 16:730-735.
174. Shapiro, A.L., Vinuela, E., and Maizel, J.V., Jr. 1967. Molecular weight estimation of polypeptide chains by electrophoresis in SDS-polyacrylamide gels. *Biochem Biophys Res Commun* 28:815-820.
175. Weber, K., and Osborn, M. 1969. The reliability of molecular weight determinations by dodecyl sulfate-polyacrylamide gel electrophoresis. *J Biol Chem* 244:4406-4412.
176. Shirahama, K., Tsujii, K., and Takagi, T. 1974. Free-boundary electrophoresis of sodium dodecyl sulfate-protein polypeptide complexes with special reference to SDS-polyacrylamide gel electrophoresis. *J Biochem* 75:309-319.
177. Klodmann, J., Sunderhaus, S., Nimtz, M., Jansch, L., and Braun, H.P. 2010. Internal architecture of mitochondrial complex I from *Arabidopsis thaliana*. *Plant Cell* 22:797-810.
178. Burck, C.H. 1988. *Histologische Technik*. Stuttgart: Thieme.
179. Shi, S.R., Cote, R.J., and Taylor, C.R. 1997. Antigen retrieval immunohistochemistry: past, present, and future. *J Histochem Cytochem* 45:327-343.
180. Vekemans, K., Rosseel, L., Wisse, E., and Braet, F. 2004. Immunolocalization of Fas and FasL in rat hepatic endothelial cells: influence of different fixation protocols. *Micron* 35:303-306.
181. Brouns, I., Van Nassauw, L., Van Genechten, J., Majewski, M., Scheuermann, D.W., Timmermans, J.P., and Adriaensen, D. 2002. Triple immunofluorescence staining with antibodies raised in the same species to

- study the complex innervation pattern of intrapulmonary chemoreceptors. *J Histochem Cytochem* 50:575-582.
182. Rosenfeld, J., Capdevielle, J., Guillemot, J.C., and Ferrara, P. 1992. In-gel digestion of proteins for internal sequence analysis after one- or two-dimensional gel electrophoresis. *Anal Biochem* 203:173-179.
 183. Hu, Q., Noll, R.J., Li, H., Makarov, A., Hardman, M., and Graham Cooks, R. 2005. The Orbitrap: a new mass spectrometer. *J Mass Spectrom* 40:430-443.
 184. Rehm, H., and Letzel, T. 2010. *Der Experimentator: Proteinbiochemie/Proteomics (German Edition)*: Spektrum Akademischer Verlag.
 185. Makarov, A., Denisov, E., Lange, O., and Horning, S. 2006. Dynamic range of mass accuracy in LTQ Orbitrap hybrid mass spectrometer. *J Am Soc Mass Spectrom* 17:977-982.
 186. Scigelova, M., and Makarov, A. 2006. Orbitrap mass analyzer--overview and applications in proteomics. *Proteomics* 6 Suppl 2:16-21.
 187. Makarov, A. 2000. Electrostatic axially harmonic orbital trapping: a high-performance technique of mass analysis. *Anal Chem* 72:1156-1162.
 188. Jedrychowski, M.P., Huttlin, E.L., Haas, W., Sowa, M.E., Rad, R., and Gygi, S.P. 2011. Evaluation of HCD- and CID-type fragmentation within their respective detection platforms for murine phosphoproteomics. *Mol Cell Proteomics* 10:M111 009910.
 189. Olsen, J.V., Schwartz, J.C., Griep-Raming, J., Nielsen, M.L., Damoc, E., Denisov, E., Lange, O., Remes, P., Taylor, D., Splendore, M., et al. 2009. A dual pressure linear ion trap Orbitrap instrument with very high sequencing speed. *Mol Cell Proteomics* 8:2759-2769.
 190. Egas, D.A., and Wirth, M.J. 2008. Fundamentals of protein separations: 50 years of nanotechnology, and growing. *Annu Rev Anal Chem (Palo Alto Calif)* 1:833-855.
 191. Olsen, J.V., de Godoy, L.M., Li, G., Macek, B., Mortensen, P., Pesch, R., Makarov, A., Lange, O., Horning, S., and Mann, M. 2005. Parts per million mass accuracy on an Orbitrap mass spectrometer via lock mass injection into a C-trap. *Mol Cell Proteomics* 4:2010-2021.
 192. Nesvizhskii, A.I., and Aebersold, R. 2004. Analysis, statistical validation and dissemination of large-scale proteomics datasets generated by tandem MS. *Drug Discov Today* 9:173-181.
 193. Andersen, J.S., Wilkinson, C.J., Mayor, T., Mortensen, P., Nigg, E.A., and Mann, M. 2003. Proteomic characterization of the human centrosome by protein correlation profiling. *Nature* 426:570-574.
 194. Yan, W., Aebersold, R., and Raines, E.W. 2009. Evolution of organelle-associated protein profiling. *J Proteomics* 72:4-11.
 195. Lubber, C.A., Cox, J., Lauterbach, H., Fancke, B., Selbach, M., Tschopp, J., Akira, S., Wiegand, M., Hochrein, H., O'Keeffe, M., et al. 2010. Quantitative proteomics reveals subset-specific viral recognition in dendritic cells. *Immunity* 32:279-289.
 196. Ishikawa, H., Thompson, J., Yates, J.R., 3rd, and Marshall, W.F. 2012. Proteomic analysis of mammalian primary cilia. *Curr Biol* 22:414-419.
 197. Mukhopadhyay, S., Wen, X., Chih, B., Nelson, C.D., Lane, W.S., Scales, S.J., and Jackson, P.K. 2010. TULP3 bridges the IFT-A complex and membrane phosphoinositides to promote trafficking of G protein-coupled receptors into primary cilia. *Genes Dev* 24:2180-2193.

198. Obsil, T., and Obsilova, V. 2011. Structural basis of 14-3-3 protein functions. *Semin Cell Dev Biol* 22:663-672.
199. Tomastikova, E., Cenklova, V., Kohoutova, L., Petrovska, B., Vachova, L., Halada, P., Kocarova, G., and Binarova, P. 2012. Interactions of an Arabidopsis RanBPM homologue with LisH-CTLH domain proteins revealed high conservation of CTLH complexes in eukaryotes. *BMC Plant Biol* 12:83.
200. Schultz, J., Milpetz, F., Bork, P., and Ponting, C.P. 1998. SMART, a simple modular architecture research tool: identification of signaling domains. *Proc Natl Acad Sci U S A* 95:5857-5864.
201. Kobayashi, N., Yang, J., Ueda, A., Suzuki, T., Tomaru, K., Takeno, M., Okuda, K., and Ishigatsubo, Y. 2007. RanBPM, Muskelin, p48EMLP, p44CTLH, and the armadillo-repeat proteins ARMC8alpha and ARMC8beta are components of the CTLH complex. *Gene* 396:236-247.
202. Lo, K.W., Kogoy, J.M., Rasoul, B.A., King, S.M., and Pfister, K.K. 2007. Interaction of the DYNLT (TCTEX1/RP3) light chains and the intermediate chains reveals novel intersubunit regulation during assembly of the dynein complex. *J Biol Chem* 282:36871-36878.
203. Cevik, S., Hori, Y., Kaplan, O.I., Kida, K., Toivenon, T., Foley-Fisher, C., Cottell, D., Katada, T., Kontani, K., and Blacque, O.E. 2010. Joubert syndrome Arl13b functions at ciliary membranes and stabilizes protein transport in *Caenorhabditis elegans*. *J Cell Biol* 188:953-969.
204. Guarguaglini, G., Duncan, P.I., Stierhof, Y.D., Holmstrom, T., Duensing, S., and Nigg, E.A. 2005. The forkhead-associated domain protein Cep170 interacts with Polo-like kinase 1 and serves as a marker for mature centrioles. *Mol Biol Cell* 16:1095-1107.
205. Denison, F.C., Paul, A.L., Zupanska, A.K., and Ferl, R.J. 2011. 14-3-3 proteins in plant physiology. *Semin Cell Dev Biol* 22:720-727.
206. Kleppe, R., Martinez, A., Doskeland, S.O., and Haavik, J. 2011. The 14-3-3 proteins in regulation of cellular metabolism. *Semin Cell Dev Biol* 22:713-719.
207. Mrowiec, T., and Schwappach, B. 2006. 14-3-3 proteins in membrane protein transport. *Biol Chem* 387:1227-1236.
208. Bustos, D.M. 2012. The role of protein disorder in the 14-3-3 interaction network. *Mol Biosyst* 8:178-184.
209. Heisler, F.F., Loebrich, S., Pechmann, Y., Maier, N., Zivkovic, A.R., Tokito, M., Hausrat, T.J., Schweizer, M., Bähring, R., Holzbaur, E.L., et al. 2011. Muskelin regulates actin filament- and microtubule-based GABA(A) receptor transport in neurons. *Neuron* 70:66-81.
210. Hao, L., Efimenko, E., Swoboda, P., and Scholey, J.M. 2011. The retrograde IFT machinery of *C. elegans* cilia: two IFT dynein complexes? *PLoS One* 6:e20995.
211. Pathak, N., Obara, T., Mangos, S., Liu, Y., and Drummond, I.A. 2007. The zebrafish fleer gene encodes an essential regulator of cilia tubulin polyglutamylation. *Mol Biol Cell* 18:4353-4364.
212. Sloboda, R.D. 2005. Intraflagellar transport and the flagellar tip complex. *J Cell Biochem* 94:266-272.
213. Follit, J.A., Li, L., Vucica, Y., and Pazour, G.J. 2010. The cytoplasmic tail of fibrocystin contains a ciliary targeting sequence. *J Cell Biol* 188:21-28.
214. Tam, B.M., Moritz, O.L., Hurd, L.B., and Papermaster, D.S. 2000. Identification of an outer segment targeting signal in the COOH terminus of rhodopsin using transgenic *Xenopus laevis*. *J Cell Biol* 151:1369-1380.

-
215. Ismail, S.A., Chen, Y.X., Miertzschke, M., Vetter, I.R., Koerner, C., and Wittinghofer, A. 2012. Structural basis for Arl3-specific release of myristoylated ciliary cargo from UNC119. *EMBO J* 31:4085-4094.
 216. Watzlich, D., Vetter, I., Gotthardt, K., Miertzschke, M., Chen, Y.X., Wittinghofer, A., and Ismail, S. 2013. The interplay between RPGR, PDEdelta and Arl2/3 regulate the ciliary targeting of farnesylated cargo. *EMBO Rep.*
 217. Fan, Z.C., Behal, R.H., Geimer, S., Wang, Z., Williamson, S.M., Zhang, H., Cole, D.G., and Qin, H. 2010. Chlamydomonas IFT70/CrDYF-1 is a core component of IFT particle complex B and is required for flagellar assembly. *Mol Biol Cell* 21:2696-2706.
 218. Li, J., and Sun, Z. 2011. Qilin is essential for cilia assembly and normal kidney development in zebrafish. *PLoS One* 6:e27365.
 219. Welburn, J.P., and Cheeseman, I.M. 2012. The microtubule-binding protein Cep170 promotes the targeting of the kinesin-13 depolymerase Kif2b to the mitotic spindle. *Mol Biol Cell* 23:4786-4795.
 220. Nicholas, A.K., Khurshid, M., Desir, J., Carvalho, O.P., Cox, J.J., Thornton, G., Kausar, R., Ansar, M., Ahmad, W., Verloes, A., et al. 2010. WDR62 is associated with the spindle pole and is mutated in human microcephaly. *Nat Genet* 42:1010-1014.
 221. Yu, T.W., Mochida, G.H., Tischfield, D.J., Sgaier, S.K., Flores-Sarnat, L., Sergi, C.M., Topcu, M., McDonald, M.T., Barry, B.J., Felie, J.M., et al. 2010. Mutations in WDR62, encoding a centrosome-associated protein, cause microcephaly with simplified gyri and abnormal cortical architecture. *Nat Genet* 42:1015-1020.

VII. Annex

1. Figure index

Figure 1: Number of publications on primary cilia.....	19
Figure 2: Formation and resorption of the primary cilium.	20
Figure 3: Structure of the cilium.....	21
Figure 4: Cross section of the cilium.....	22
Figure 5: Schematic illustration of the IFT and its components.	23
Figure 6: Dissociation of the IFT-B by ionic strength.	25
Figure 7: Ciliogenesis.....	27
Figure 8: Schematic overview of the retinal photoreceptor cell.....	29
Figure 9: Clinical phenotypes associated with ciliopathies.	30
Figure 10: Timeline of protein-protein interaction research.....	33
Figure 11: SF-TAP workflow.....	36
Figure 12: Typical workflow of a mass spectrometry approach.	39
Figure 13: Three dimensional peak detection by the MaxQuant software.	41
Figure 14: Workflows of commonly used proteomic labelling techniques.....	42
Figure 15: Overview of the GATEWAY cloning strategy.....	63
Figure 16: Scheme of the LTQ-Orbitrap XL and the LTQ-Orbitrap Velos mass spectrometer.....	89
Figure 17: Schematic overview of the Dionex Ultimate 3000 Nano RSLC HPLC system.	92
Figure 18: Gradient of an LC run.	93
Figure 19: Workflow of the SDS-AP.	99
Figure 20: Optimization SDS-concentration.....	100
Figure 21: SDS destabilization of the Lebercilin protein complex.	102
Figure 22: Western blot of the proteins eluted by SDS destabilization of the Lebercilin protein complex.	105
Figure 23: Isolation of IFT-B sub-complexes by sucrose density centrifugation.	109
Figure 24: Knockdown of several IFT proteins in IMCD3 cells.	111
Figure 25: Localization of IFT particle during knockdown of different IFT proteins.	112
Figure 26: Control experiment for the knockdown of IFT proteins by siRNA in IMCD3 cells.	113

Figure 27: predicted network for the IFT-B.	116
Figure 28: Scatter plot of the STREP-SILAC analysis of CEP170-N-SF-TAP.	120
Figure 29: Scatter plot of the STREP-SILAC analysis of the interactome of IFT57.	120
Figure 30: Western Blot experiments with anti-CEP170.	121
Figure 31: Immunofluorescence of CEP170 and TRAF3IP1 in hTERT RPE1 cells.	122
Figure 32: Immunofluorescence of TRAF3IP1 and CEP170 during ciliogenesis.	123
Figure 33: Knockdown of <i>Cep170</i> in IMCD3 cells.	124
Figure 34: Localization of the IFT-B during <i>Cep170</i> knockdown in IMCD3 cells. ...	126
Figure 35: Concentration profile SDS-finemapping.	130

2. Table index

Table 1: Overview of the components of the IFT particle.	26
Table 2: Overview of commonly used affinity tags for protein purification.	34
Table 3: Oligonucleotides.	49
Table 4: qPCR primer.	50
Table 5: DNA constructs.	50
Table 6: DNA plasmids.	51
Table 7: siRNA sequences.	52
Table 8: Mammalian cell lines.	54
Table 9: Primary antibodies.	56
Table 10: Secondary antibodies.	57
Table 11: PEI transfection.	69
Table 12: Reagents and volumes for SDS-PAGE gels.	73
Table 13: SF-TAP-analysis of TULP3-N-SF-TAP.	103
Table 14: SF-TAP analysis of RANBP9.	104
Table 15: SF-TAP experiment of IFT88-SF-TAP in HEK293-T cells.	106
Table 16: SF-TAP experiment with a stable IFT88-SF-TAP HEK293 cell line.	107
Table 17: SF-TAP experiments with different baits.	108
Table 18: Knockdown efficiency of IFT proteins in IMCD3 cells.	115
Table 19: SF-TAP analysis of CEP170-SF-TAP.	118
Table 20: STREP-SILAC analysis of the CEP170 interactome.	119
Table 21: Knockdown efficiency of <i>Cep170</i> in IMCD3 cells.	125

3. Publications and poster presentations

3.1. Peer-reviewed publications

- Castaings L, Camargo A, Pocholle D, Gaudon V, Texier Y, Boutet-Mercey S, Taconnat L, Renou JP, Daniel-Vedele F, Fernandez E, Meyer C, Krapp A. “The nodule inception-like protein 7 modulates nitrate sensing and metabolism in Arabidopsis.” *Plant J.* 2009 Feb;57(3):426-35.
- Boldt K, Mans DA, Won J, van Reeuwijk J, Vogt A, Kinkl N, Letteboer SJ, Hicks WL, Hurd RE, Naggert JK, Texier Y, den Hollander AI, Koenekoop RK, Bennett J, Cremers FP, Gloeckner CJ, Nishina PM, Roepman R, Ueffing M. “Disruption of intraflagellar protein transport in photoreceptor cilia causes Leber congenital amaurosis in humans and mice.” *J Clin Invest.* 2011 Jun;121(6):2169-80.
- Texier Y, Kinkl N, Boldt K, Ueffing M. “From quantitative protein complex analysis to disease mechanism.” *Vision Res.* 2012 Dec 15; 75:108-11.
- Texier Y, Toedt G, Gorza M, Mans DA, Horn N, Katsanis N, van Reeuwijk J, Bolz S, Roepmann R, Gibson TJ, Ueffing M, Boldt K. “EPASIS: Elution profile analysis of SDS-induced sub-complexes by quantitative mass spectrometry” manuscript in preparation
- Texier Y, Bolz S, Wheway G, Reuter P, Horn N, Pazour GJ, Wissinger B, Johnson CA, Ueffing M, Boldt K. “Centrosomal protein 170 (CEP170) is associated to the intraflagellar transport complex B.” manuscript in preparation
- Texier Y, Mans DA, Toedt G, Wheway G, Koutroumpas K, Reuter P, Pazour GJ, van Reeuwijk J, Bolz S, Horn N, Helm S, Wissinger B, Johnson CA, Roepmann R, Boldt K, Ueffing M. “The intraflagellar transport complex B is divided into two distinct sub-complexes” manuscript in preparation

3.2. Poster presentations

- Texier Y, Mans DA, van Reeuwijk J, Roepman R, Boldt K, Ueffing M. “Dissecting the sub-structure of the intraflagellar transport complex B” *Cilia* 2012, London UK

4. Acknowledgements

Ich möchte mich noch bei Allen bedanken die zum erfolgreichen Gelingen dieser Arbeit beigetragen haben.

Mein besonderer Dank gilt Marius, der mir die Möglichkeit gegeben hat diese Doktorarbeit in seiner Abteilung durchführen zu können. Ich danke ihm für sein Vertrauen, die Freiheiten bei der Bearbeitung meines Themas und die Unterstützung die ich während dieser Zeit von ihm bekommen habe. Ich habe gemerkt wie wichtig es ist eine gute Infrastruktur am Arbeitsplatz zu haben in der man die besten Voraussetzungen für wissenschaftliches Arbeiten genießen kann. Des Weiteren danke ich ihm für die Förderung in Form von Diskussionen, Kritik, Fortbildung und der Teilnahme an internationalen Kongressen, die mir die Möglichkeiten gegeben haben über den Tellerrand hinauszuschauen. Außerdem möchte ich ihm für die Möglichkeit danken meine Doktorarbeit nach dem Umzug nach Tübingen weiterführen zu können, die neue Umgebung und die erweiterten Möglichkeiten am neuen Standort haben mir großen Auftrieb bei der Bearbeitung meiner Arbeit gegeben.

Bei Prof. Martin Hrabé de Angelis möchte ich mich für das Interesse an meiner Arbeit und die Betreuung der Arbeit an der Universität danken.

Ebenso möchte ich mich bei Prof. Jerzy Adamski für die Bereitschaft bedanken, das Zweitgutachten dieser Arbeit zu übernehmen.

Mein Dank gilt auch Prof. Bernhard Küster für die Übernahme des Prüfungsvorsitzes dieser Arbeit.

Ich möchte mich insbesondere bei Karsten für die Betreuung meiner Arbeit bedanken. Dafür dass ich sein erster Doktorand war und er meine Betreuung noch zu seiner eigenen Doktorandenzeit übernommen hat, hat er die Betreuung bereits von Anfang an sehr gut gemacht und es hat sehr viel Spaß gemacht ihn beim Chefwerden zu begleiten. Bereits zu Beginn dieser Arbeit hat er alle meine Fragen geduldig über sich ergehen lassen und stand mir immer mit Rat und Tat zur Seite. Ich möchte ihm für das Vertrauen und die Freiheiten danken die er mir bei der Bearbeitung meiner Arbeit gelassen hat und trotzdem stets Interesse an den Fortschritten gezeigt hat. Ich bin ihm außerdem sehr dankbar dass er mir die Möglichkeit gegeben hat in Tübingen direkt an den Massenspektrometern zu arbeiten und dass er mir so viel von seinem Fachwissen über die, manchmal so zickigen, Geräte weitergegeben hat. Ich möchte ihm außerdem dafür danken, dass wir stets sehr direkt und unproblematisch miteinander kommunizieren konnten was so vieles im Alltag leichter gemacht hat.

Des Weiteren möchte ich mich bei Norbert bedanken dass er mir mit seiner stets freundlichen und hilfsbereiten Art bei vielen Dingen des Laboralltags, sowie dem Korrekturlesen meines ersten Papers geholfen hat.

Bei Andreas möchte ich mich für die Unterstützung und Einführung in die Welt der Sucrosegradienten, Augen und des ICPL bedanken. Auch die vielen gemeinsamen Begegnungen mit dem skurilen Personal der Schlachthöfe in Rottenburg und Balingen werden mir sicher lange in Erinnerung bleiben.

Ich möchte mich bei Johannes für viele interessante Unterhaltungen bedanken. Außerdem für die Hilfe bei Primerdesign, Klonierungen und IT-Problemen.

Bei Silke möchte ich mich für die viele gemeinsame Zeit bedanken, die sie investiert hat um mir die QTrap näher zu bringen.

Bei den unersetzlichen Helfern unserer Labore in München und Tübingen, Felix, Jen, Caro, Sandra, Hakan, Nicola und Jenni möchte ich mich für die Unterstützung im Laboralltag sowie für die vielen Bestellungen und den ganzen Papierkram bedanken mit dem sie mir in der Zeit meiner Arbeit geholfen haben. Außerdem möchte ich mich bei allen anderen Kollegen meiner Arbeitsgruppe für die stets freundliche und reibungslose Zusammenarbeit bedanken.

Bei Grischa Toedt möchte ich mich für die bioinformatische Unterstützung meiner Experimente bedanken. Außerdem danke ich ihm für die vielen guten fachlichen und privaten Gespräche die wir bei unseren vielen Treffen und gemeinsamen Tagungen miteinander geführt haben. Außerdem möchte ich ihm für die exzellente Statistik bedanken die in das SDS-Paper mit einfließen wird.

Ich möchte mich auch bei Ludwig und Marcel für die informatische Unterstützung meiner Arbeit in München bedanken.

Ich möchte mich außerdem bei Sylvi für die viele Unterstützung und Hilfe bei den Immunofärbungen bedanken. Ihre stets freundliche Art und gute Laune hat mir ganz oft die gute Laune zurückgebracht.

Bei Peggy Reuter möchte ich mich für die Unterstützung bei meinen qPCR-Experimenten bedanken. Bei Bernd Wissinger möchte ich mich dafür bedanken dass er mir die Möglichkeit gegeben hat die qPCR-Experimente in seinem Labor durchführen zu können.

Bei Matteo möchte ich mich für die netten Gespräche und die große Hilfsbereitschaft bedanken. Außerdem danke ich ihm für die grundlegende Idee bei der Entwicklung der SDS-Destabilisierung.

Mein ganz besonderer Dank gilt Elisabeth Kremmer, die mir bei der Suche nach meiner Doktorandenstelle geholfen und mich stets unterstützt hat. Ich danke ihr für das in mich gesetzte Vertrauen, die vielen Anregungen und guten Gespräche sowie ihre herzliche Art mit der sie mich stets empfangen hat. Ich möchte auch ihrem Mann Klaus für die vielen guten und motivierenden Gespräche sowie die vielen netten Abende danken die wir gemeinsam verbracht haben.

Bei Saskia Hanf, Barbara Huth und Christine Augustin möchte ich mich für die Unterstützung bei allen administrativen Dingen bedanken.

Bei Herrn Sintakis von der Firma Dionex möchte ich mich für die vielen Informationen zu Nano-HPLC und das gemeinsame Schrauben an den Geräten bedanken.

Herrn Vollmer von der Feinwerkstatt in Tübingen möchte ich für das Bauen der Coverslip-Halter der Ultrazentrifugenröhrchen sowie für das Bauen und Optimieren der Multiarray-Blotter danken.

Chichung Lie und Heiko Lickert möchte ich für die Teilnahme an meinem Thesis Committee und die guten Anregungen danken.

Ich möchte ferner meiner gesamten Familie für die Unterstützung während meiner Arbeit danken. Insbesondere meine Mutter und mein Vater standen stets mit Rat und Tat zur Seite und waren mir eine große Hilfe. Des Weiteren gilt mein Dank meiner verstorbenen Oma, die mir während meiner gesamten Studienzeit oft finanziell weitergeholfen hat.

Außerdem möchte ich meinem besten Freund Patric für die Freundschaft, die Unterstützung, das Interesse und die gemeinsame Zeit danken mit denen er mich durch die letzten Jahre begleitet hat.

Meinen Freunden Mike Huppert und Mike Zwoch möchte ich für ebenfalls für ihre Freundschaft und Unterstützung danken.

I want to thank Dali for his help, good idea and friendship during my time in Tübingen.

I want to thank Jeroen van Reeuwijk and Konstantinos Koutroumpas for their bioinformatic support of my work.

Furthermore I want to thank Colin Johnson for receiving me at his lab in Leeds and giving me the possibility of performing my knockdown experiments there. Gabrielle Wheway and Katarzyna Szymanska for all the hearty invitations and activities we shared during my stay in Leeds. Moreover, Gabrielle Wheway for helping me with my siRNA knockdowns and for proofreading my thesis.

Ronald Roepman, Dorus Mans, Erwin van Wijk, Hannie Kremer from Nijmegen for collaboration, support with constructs, antibodies and good discussions.

Toby Gibson for receiving me at the EMBL in Heidelberg and giving me the possibility to work there with Grischa as well as for good discussions and idea for my projects.

I also want to thank some further collaboration partners: Olliver Blacque for good discussion on the IFT sub-complex story, Greg Pazour for the IFT antibodies, Andy Gießl for the pericentrin antibody, Erich Nigg for the CEP170-GFP construct, Nico Katsanis for the TULP3 construct and Uwe Wolfrum good discussions and idea.

5. Curriculum vitae

Personal Information	
Name	Texier, Yves
Nationalities	German, French
Date of Birth	08/22/1980
Place of Birth	Bochum-Wattenscheid
Education	
Since January 2009	<p>PhD thesis at the department of protein science at the Helmholtz Zentrum München, German Research Center for Environmental Health, Munich, Germany and at the Medical Proteome Center, Centre for Ophthalmology, Eberhard Karls University Tübingen, Tübingen, Germany with Prof. Dr. Marius Ueffing. Title: "Quantitative analysis of ciliary protein networks -Characterization of the intraflagellar transport complex B"</p>
October 2007 - August 2008	<p>Master thesis at the National Institute of Agronomical Research, Versailles, France (Stipendiary of the DAAD) Title: "Function of the <i>NLP</i>-genes in <i>Arabidopsis thaliana</i>" Director: Dr. Françoise Vedele Supervising tutor: Dr. Anne Krapp</p>
October 2006 - August 2008	<p>Studies in molecular biology (Master of Science (MSc)) Accredited degree course Fachhochschule Gelsenkirchen, Abteilung Recklinghausen, Germany</p>
March 2006 - August 2006	<p>Bachelor thesis at the Ege-University, Faculty of Medicine, Molecular Medicine Research Laboratory, Izmir, Turkey (in Cooperation with Medizinisches Hochschulinstitut (M.I.T.), Recklinghausen, Germany) Title: "Genes / polymorphisms with clinical relevance for Hypertension: Diagnostic differentiation and development of risk determining PCR-systems"</p>
October 2003 - August 2006	<p>Bachelor of Science (BSc) Molecular Biology Fachhochschule Gelsenkirchen, Abteilung Recklinghausen, Germany</p>
September 2001 - July 2003	<p>Advanced technical college certificate Marian-Batko-Berufsoberschule München Ausbildungsrichtung Technik, München, Germany</p>
September 1997 – February 2001	<p>Certificate of proficiency in car mechanics Mercedes-Benz Ing. Eugen Popp GmbH, Starnberg, Germany</p>
September 1991 - July 1997	<p>High-school diploma Städt. Käthe-Kollwitz-Gymnasium München, Germany</p>

Work Experience

November 2006 - January 2007	<p>Student assistant Prof. Dr. Michael Veith Fachhochschule Gelsenkirchen, Abteilung Recklinghausen Cooperative project: "Biofunctionalized surfaces of dental implants"</p>
September 2005 - February 2006 October 2004 - June 2005	<p>Freelancer Prof. Dr. Christian Herrmann Ruhr-Universität Bochum, Physikalische Chemie I, AG Protein-Interaktionen, Bochum, Germany</p>
August 2005	<p>Internship Dr. Andreas Dessauer Roche Diagnostics GmbH, Molecular Diagnostics Oncology, Penzberg, Germany</p>
August 2004 - September 2004	<p>Internship Prof. Dr. Christian Herrmann Ruhr-Universität Bochum, Physikalische Chemie I, AG Protein-Interaktionen, Bochum, Germany</p>
August 2003 - September 2003	<p>Internship Dr. Elisabeth Kremmer GSF-Forschungszentrum für Umwelt und Gesundheit GmbH, Institut für Molekulare Immunologie, München, Germany</p>
Mars 2001 - August 2001	<p>Car mechanic Mercedes Fichtl & Popp GmbH, Starnberg, Germany</p>

Personal skills and competences

Languages German, French (Mother tongue)
English (business fluent)

Time abroad

December 2012 Section of Ophthalmology and Neurosciences, Leeds Institute of Molecular Medicine, Leeds, UK in the group of Colin A Johnson

Publications

Castaings L, Camargo A, Pocholle D, Gaudon V, Texier Y, Boutet-Mercey S, Taconnat L, Renou JP, Daniel-Vedele F, Fernandez E, Meyer C, Krapp A. "The nodule inception-like protein 7 modulates nitrate sensing and metabolism in Arabidopsis." Plant J. 2009 Feb;57(3):426-35.

Boldt K, Mans DA, Won J, van Reeuwijk J, Vogt A, Kinkl N, Letteboer SJ, Hicks WL, Hurd RE, Naggert JK, Texier Y, den Hollander AI, Koenekoop RK, Bennett J, Cremers FP, Gloeckner CJ, Nishina PM, Roepman R, Ueffing M. "Disruption of intraflagellar protein transport in photoreceptor cilia causes Leber congenital amaurosis in humans and mice." J Clin Invest. 2011 Jun;121(6):2169-80.

Texier Y, Kinkl N, Boldt K, Ueffing M. "From quantitative protein complex analysis to disease mechanism." Vision Res. 2012 Dec 15;75:108-11.